DEPARTMENT OF COMMERCE
SINCLAIR WEEKS, Secretary

WEATHER BUREAU
F. W. REICHELDERFER, Chief

MONTHLY WEATHER REVIEW

JAMES E. CASKEY, JR., Editor

Volume 86
Number 8

AUGUST 1958

Closed October 15, 1958
Issued November 15, 1958

THE LATTICE STRUCTURE OF THE FINITE-DIFFERENCE PRIMITIVE AND VORTICITY EQUATIONS†

GEORGE W. PLATZMAN

The University of Chicago, Chicago, Ill.

[Manuscript Received July 28, 1958]

ABSTRACT

The use of central differences on a rectangular net, in solving the primitive or vorticity equations, produces solutions on each of two lattices. By exploring this lattice structure, a formal equivalence is established between the central-difference vorticity and primitive equations. A demonstration is given also that exponential instability previously found to result from certain types of boundary conditions is suppressed by applying these conditions in such a way as to avoid coupling the lattices.

1. INTRODUCTION

In a recent study (Platzman [7]) the primitive equations (that is, the momentum and continuity equations) were integrated numerically in an investigation of surges on Lake Michigan. It was pointed out there that, when central differences are used, the finite-difference primitive equations give rise to solutions on two independent lattices. The purpose of the present note is to demonstrate that a more satisfactory understanding of the analytical properties of these equations is provided by taking account of this lattice structure.*

2. THE WAVE EQUATION

Consider a canal of uniform depth D and uniform cross section, closed by rigid vertical walls at $x=0$ and $x=L$. The differential equation for "tidal" disturbances is the one-dimensional wave equation

$$\frac{\partial^2 u}{\partial t^2}=c^2\frac{\partial^2 u}{\partial x^2},$$

where u is the particle velocity along x, and $c\equiv\sqrt{gD}$.

Partition the axes uniformly as follows: $t/\Delta t=0, 1, 2, \ldots,$ and $x/\Delta x=0, 1, 2, \ldots, p$, so that $L=p\Delta x$. Using central differences,

$$\delta_t^2 u=\sigma^2\delta_x^2 u, \tag{2.1}$$

where $\sigma\equiv c\Delta t/\Delta x$ and δ denotes the operator

$$\delta_t u(x,t)=u(x,t+\tfrac{1}{2}\Delta t)-u(x,t-\tfrac{1}{2}\Delta t)$$

$$\delta_x u(x,t)=u(x+\tfrac{1}{2}\Delta x,t)-u(x-\tfrac{1}{2}\Delta x,t).$$

Subject to boundary conditions $u(0,t)=0$ and $u(L,t)=0$, we may represent $u(x,t)$ by the discrete Fourier series

$$u(x,t)=\sum_{l=1}^{p-1}u_l(t)\sin k_l x \tag{2.2}$$

$$k_l\equiv l\pi/L \quad (l=1, 2, \ldots, p-1)$$

where k_l is the wave number of the lth mode.

Substitution of (2.2) in (2.1) yields the following difference equation for the expansion coefficient $u_l(t)$:

$$\delta_t^2 u_l=-4\,(\sigma\sin\tfrac{1}{2}k_l\Delta x)^2 u_l.$$

The general solution of this is

$$u_l(t)=\alpha\cos\nu_l t+\beta\sin\nu_l t, \tag{2.3}$$

where α and β are constants of integration, and

† This investigation was supported by funds provided by the U. S. Weather Bureau.

* After the substance of the present work was completed, the writer's attention was called to an elegant study by A. Eliassen, in which similar ideas are involved (A. Eliassen, "A Procedure for Numerical Integration of the Primitive Equations of the Two-Parameter Model of the Atmosphere," University of California at Los Angeles, Department of Meteorology, 1956).

$$\sin \tfrac{1}{2}\nu_l \Delta t = \sigma \sin \tfrac{1}{2}k_l \Delta x \tag{2.4}$$

determines the frequency.

For initial conditions we specify u and $\partial u/\partial t$; in the finite-difference frame, this is equivalent to a specification of $u_l(0)$ and $u_l(\Delta t)$, in terms of which (2.3) becomes

$u_l(t) = (\csc \nu_l \Delta t)[-u_l(0) \sin \nu_l(t-\Delta t) + u_l(\Delta t) \sin \nu_l t]$.

If we assign to $u_l(\Delta t)$ the value

$$u_l(\Delta t) = u_l(0) + \dot{u}_l(0)\Delta t,$$

where $\dot{u}_l(0)$ is $\partial u_l/\partial t$ at $t=0$, then we get

$$u_l(t) = (\sec \tfrac{1}{2}\nu_l \Delta t)[u_l(0) \cos \nu_l(t-\tfrac{1}{2}\Delta t) + \dot{u}_l(0)(\tfrac{1}{2}\Delta t \csc \tfrac{1}{2}\nu_l \Delta t) \sin \nu_l t].$$

This form shows clearly the amplitude and phase distortion produced by truncation errors (see Platzman [5]), and expresses the solution explicitly in terms of data prescribed along the initial line.

The finite-difference system has $2(p-1)$ degrees of freedom, represented by the $p-1$ independent values of $u(x,0)$ and the $p-1$ independent values of $u(x,\Delta t)$, or by the values of the corresponding Fourier coefficients. These degrees of freedom are provided by the $2(p-1)$ distinct fundamental modes $\exp(\pm i\nu_l t)$ determined by the frequency equation (2.4), of which $p-1$ correspond to wave propagation along positive x, and $p-1$ correspond to backward propagation.

3. THE PRIMITIVE EQUATIONS

The preceding problem may be formulated in terms of the linearized primitive equations

$$\frac{\partial u}{\partial t} = -g\frac{\partial h}{\partial x}$$

$$\frac{\partial h}{\partial t} = -D\frac{\partial u}{\partial x},$$

where h is the free-surface displacement from mean level.

As before, we place u at the points $t/\tfrac{1}{2}\Delta t = 0, 2, 4, \ldots$, and $x/\tfrac{1}{2}\Delta x = 0, 2, 4, \ldots, 2p$; further, we place h at the "half-way" points $t/\tfrac{1}{2}\Delta t = 1, 3, 5, \ldots$, and $x/\tfrac{1}{2}\Delta x = 1, 3, 5, \ldots, 2p-1$ (see fig. 1a). Then the central difference equations are, in the notation of (2.1),

$$\delta_t u = -\sigma\delta_x h \tag{3.1a}$$

$$\delta_t h = -\sigma\delta_x u; \tag{3.1b}$$

in (3.1), u and h have been reduced to dimensionless form through division, respectively, by $\sqrt{gD}$ and D. If one eliminates h from (3.1), by applying δ_t to (3.1a), equation (2.1) is obtained, so that our frequency equation is again (2.4). However, instead of working with the wave-equation solutions, we will obtain the solutions of (3.1) directly without elimination.

We first represent $u(x,t)$ in the manner of (2.2), and $h(x,t)$ by the discrete series

$$h(x,t) = \sum_{l=0}^{p-1} h_l(t) \cos k_l x. \tag{3.2}$$

Substitution in (3.1) yields

$$\delta_t u_l = +2(\sigma \sin \tfrac{1}{2}k_l \Delta x)h_l$$

$$\delta_t h_l = -2(\sigma \sin \tfrac{1}{2}k_l \Delta x)u_l,$$

for which we have the general solution

$$u_l(t) = \alpha \cos \nu_l t + \beta \sin \nu_l t$$

$$h_l(t) = \beta \cos \nu_l t - \alpha \sin \nu_l t,$$

with ν_l as in (2.4). If, in addition to the initial distribution of u, one specifies the initial distribution of h (instead of the initial acceleration $\partial u/\partial t$), the solution is

$$u_l(t) = (\sec \tfrac{1}{2}\nu_l \Delta t)[u_l(0) \cos \nu_l(t-\tfrac{1}{2}\Delta t) + h_l(\tfrac{1}{2}\Delta t) \sin \nu_l t] \tag{3.3a}$$

$$h_l(t) = (\sec \tfrac{1}{2}\nu_l \Delta t)[h_l(\tfrac{1}{2}\Delta t) \cos \nu_l t - u_l(0) \sin \nu_l(t-\tfrac{1}{2}\Delta t)]. \tag{3.3b}$$

Note that the initial values of h are those assigned on the line $t=\tfrac{1}{2}\Delta t$, because in the lattice of figure 1a, values of h are not given on $t=0$.

In figure 1b is shown the lattice which is initiated by assigning h on the line $t=0$ and u on $t=\tfrac{1}{2}\Delta t$. The solution in this case is

$$u_l(t) = (\sec \tfrac{1}{2}\nu_l \Delta t)[u_l(\tfrac{1}{2}\Delta t) \cos \nu_l t + h_l(0) \sin \nu_l(t-\tfrac{1}{2}\Delta t)] \tag{3.4a}$$

$$h_l(t) = (\sec \tfrac{1}{2}\nu_l \Delta t)[h_l(0) \cos \nu_l(t-\tfrac{1}{2}\Delta t) - u_l(\tfrac{1}{2}\Delta t) \sin \nu_l t]. \tag{3.4b}$$

The lattices of figures 1a and 1b differ only by a phase shift of $\tfrac{1}{2}\Delta t$.

The equations (3.1) involve $p-1$ values of u (exclusive of the boundary values, which are fixed at zero), and p values of h; hence, there are $2p-1$ degrees of freedom in the initial conditions. In order to obtain an equal number of fundamental modes for (3.1), one must include the root $l=0$, $\nu_l=0$ of the frequency equation (2.4); the corresponding mode is $u=0$, $h=h_0=$constant, which evidently satisfies (3.1) and boundary conditions. Note also that if (3.1b) is summed over all values of x where h is defined, the right side sums to zero, with the help of the boundary conditions, so that the x-sum of h is independent of t. (This is merely a statement of the integral form of the continuity equation.) From (3.2), we see that the x-sum of h is equal to ph_0; hence, again, $h_0=$constant.

To insure that the finite-difference solution is stable, it is sufficient to choose Δt and Δx so that $\sigma \equiv c\Delta t/\Delta x < 1$, since then the frequency ν_l determined by (2.4) must be real. This is the von Neumann stability condition, and is also the well-known restriction on the difference equations for hyperbolic systems, which insures that the solu-

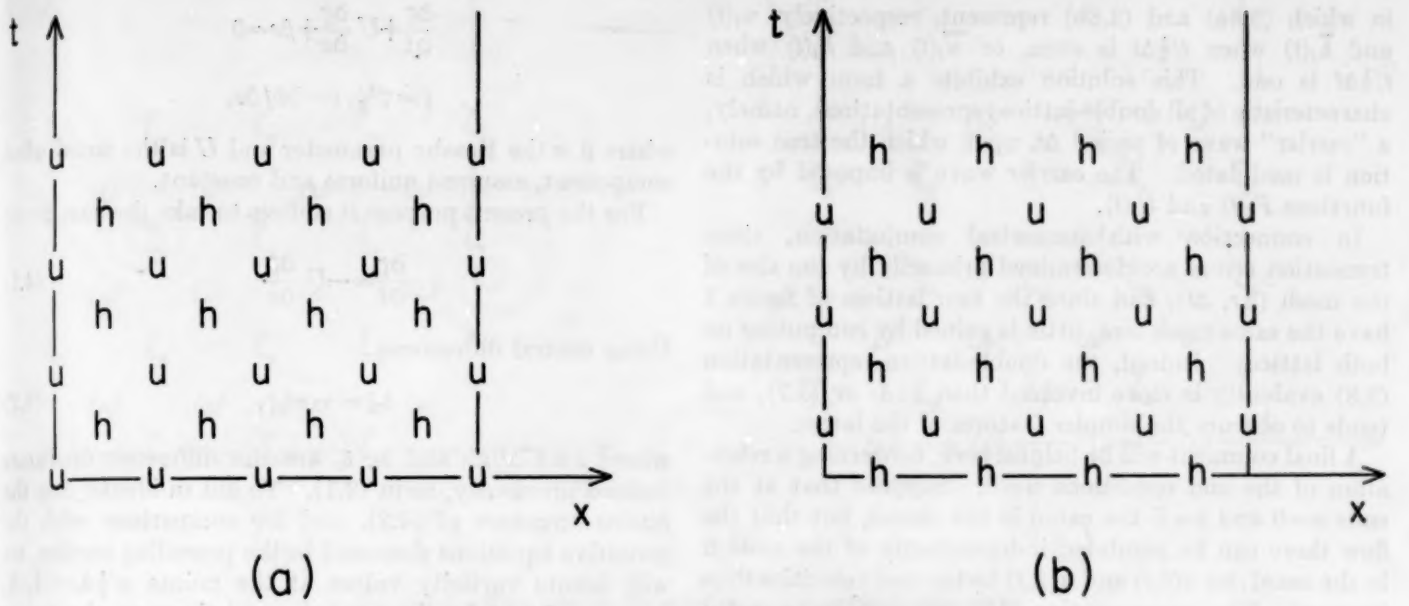

FIGURE 1.—Two lattices for solution of the primitive equations.

tions of the difference equation and the solution of the differential equation coalesce in the limit Δt, $\Delta x \to 0$.*

Taking this limit in (3.3) or (3.4)

$$u_l(t) = u_l(0) \cos \nu_l t + h_l(0) \sin \nu_l t \qquad (3.5a)$$

$$h_l(t) = h_l(0) \cos \nu_l t - u_l(0) \sin \nu_l t, \qquad (3.5b)$$

the frequency equation being simply $\nu_l = ck_l$.

Suppose now that we specify as initial conditions the values of $u(x,0)$ at $x/\Delta x = 0, 2, 4, \ldots, 2p$, and on the same line $t=0$ the values of $h(x,0)$ at the intermediate points $x/\frac{1}{2}\Delta x = 1, 3, 5, \ldots, 2p-1$. To initiate the lattice of figure 1a, we must move from $h(x,0)$ to $h(x,\frac{1}{2}\Delta t)$; if we do this by the uncentered step

$$h(x,\tfrac{1}{2}\Delta t) = \overline{h}(x,0) - \tfrac{1}{2}\sigma\delta_x u(x,0),$$

the expansion coefficients $h_l(\frac{1}{2}\Delta t)$ will be

$$h_l(\tfrac{1}{2}\Delta t) = \overline{h}_l(0) - u_l(0) \sin \tfrac{1}{2}\nu_l \Delta t.$$

(In these and in subsequent relations the bar is used to identify quantities associated with the lattice of figure 1b.) Substitution in (3.3) yields

$$u_l(t) = u_l(0) \cos \nu_l t + \overline{h}_l(0) (\sec \tfrac{1}{2}\nu_l \Delta t) \sin \nu_l t \qquad (3.6a)$$

$$h_l(t) = \overline{h}_l(0) (\sec \tfrac{1}{2}\nu_l \Delta t) \cos \nu_l t - u_l(0) \sin \nu_l t. \qquad (3.6b)$$

Similarly, to initiate the lattice of figure 1b, we must move from $u(x, 0)$ to $u(x, \frac{1}{2}\Delta t)$; proceeding as above, we find

$$\overline{u}_l(t) = u_l(0) (\sec \tfrac{1}{2}\nu_l \Delta t) \cos \nu_l t + \overline{h}_l(0) \sin \nu_l t \qquad (3.7a)$$

$$\overline{h}_l(t) = \overline{h}_l(0) \cos \nu_l t - u_l(0) (\sec \tfrac{1}{2}\nu_l \Delta t) \sin \nu_l t. \qquad (3.7b)$$

In (3.6) the initial data $u_l(0)$ are *concordant*, in the sense that they belong to the lattice on which the solution is represented; on the other hand, $\overline{h}_l(0)$ in (3.6) are *discordant* data. Similarly, with respect to the lattice on which (3.7) represents a solution, the $u_l(0)$ are discordant and $\overline{h}_l(0)$ are concordant data.

Using the exact solution (3.5) for comparison, one may characterize (3.6) and (3.7) by saying that, if all initial data originate on the same line ($t=0$), *the concordant data are propagated without distortion* (of amplitude or phase) while the discordant data suffer an amplitude distortion sec $\frac{1}{2}\nu_l \Delta t$.

It is important to bear in mind that in the solution (3.6), on the lattice of figure 1a, the values of $u_l(t)$ are to be taken only for $t/\frac{1}{2}\Delta t = 0, 2, 4, \ldots$, while the values of $h_l(t)$ are for $t/\frac{1}{2}\Delta t = 1, 3, 5, \ldots$; the converse is true of (3.7), which applies to the lattice of figure 1b. One can, of course, represent the two solutions in a single formula. This can be done with the aid of the functions

$$F_l(t) \equiv \tfrac{1}{2}[1 + (-)^n] + \tfrac{1}{2}[1 - (-)^n] \sec \tfrac{1}{2}\nu_l \Delta t$$

$$G_l(t) \equiv \tfrac{1}{2}[1 - (-)^n] + \tfrac{1}{2}[1 + (-)^n] \sec \tfrac{1}{2}\nu_l \Delta t,$$

where $n \equiv t/\frac{1}{2}\Delta t$; evidently, when n is even, $F_l = 1$ and $G_l = \sec \frac{1}{2}\nu_l \Delta t$, and when n is odd, $F_l = \sec \frac{1}{2}\nu_l \Delta t$ and $G_l = 1$. On this understanding, the solutions (3.6) and (3.7) are contained in the single representation

$$u_l(0) F_l(t) \cos \nu_l t + \overline{h}_l(0) G_l(t) \sin \nu_l t \qquad (3.8a)$$

$$\overline{h}_l(0) F_l(t) \cos \nu_l t - u_l(0) G_l(t) \sin \nu_l t, \qquad (3.8b)$$

*Convergence (coalescence) may be obtained for special choices of initial data even though $\sigma > 1$ (see, for example, Platzman [5]). This may seem paradoxical because it suggests that in the limit, the domain of dependence does not span the interval intercepted by two characteristics; but the special choices in question all involve analytic initial data, capable of continuation. On the other hand, if one adopts the definition of convergence employed by Lax and Richtmyer [3], the condition $\sigma < 1$ is also necessary (as well as sufficient), since they require convergence for *arbitrary* initial data. In their basic study, Lax and Richtmyer have established equivalence between stability and convergence, under very general conditions.

in which (3.8a) and (3.8b) represent, respectively, $u_l(t)$ and $\overline{h}_l(t)$ when $t/\frac{1}{2}\Delta t$ is even, or $\overline{u}_l(t)$ and $h_l(t)$ when $t/\frac{1}{2}\Delta t$ is odd. This solution exhibits a form which is characteristic of all double-lattice representations, namely, a "carrier" wave of period Δt, upon which the true solution is modulated. The carrier wave is imposed by the functions $F_l(t)$ and $G_l(t)$.

In connection with numerical computation, since truncation errors are determined primarily by the size of the mesh (Δx, Δt), and since the two lattices of figure 1 have the same mesh size, little is gained by computing on both lattices. Indeed, the double-lattice representation (3.8) evidently is more involved than (3.6) or (3.7), and tends to obscure the simpler features of the latter.

A final comment will be helpful here, concerning a relaxation of the end conditions $u=0$. Suppose that at the ends $x=0$ and $x=L$ the canal is not closed, but that the flow there can be regulated independently of the motion in the canal; let $u(0,t)$ and $u(L,t)$ be the end velocities thus imposed. The representation (2.2) may now be amended to read

$$u(x,t)=\sum_{l=1}^{p-1}u_l(t)\sin k_l x+u(0,t)+[u(L,t)-u(0,t)]x/L,$$

while (3.2) is unaltered. Substitution in (3.1) leads to an inhomogeneous system for $u_l(t)$ and $h_l(t)$. The fundamental modes are identical to those obtained above, but a particular solution must be added now to incorporate the forcing which comes from the ends. The integral form of the continuity equation is

$$\delta_t\sum_{x(h)}h=-\sigma[u(L,t)-u(0,t)],$$

obtained by summing (3.1b) over all x-points where h is defined. Clearly, this states merely that the change of mean level is determined by the net volume transport through the ends.

In particular, if $u(0,t)$ and $u(L,t)$ are constants (independent of t) we have the following particular solution

$$u=u(0,t)+[u(L,t)-u(0,t)]x/L$$

$$h=-[u(L,t)-u(0,t)]ct/L$$

(Since x and t enter here linearly, this is a solution with zero truncation error.) The fact that h is a linear function of t obviously results from the constant net volume transport imposed at the ends. Mathematically, this may be interpreted as a resonant solution of the inhomogeneous system for u_l and h_l coming from the mode corresponding to $l=0$, the frequency of which is zero and coincident therefore with the zero frequency inherent in the constant values of $u(0,t)$ and $u(L,t)$.*

4. THE VORTICITY EQUATION

The linearized one-dimensional vorticity equation is

$$\frac{\partial\zeta}{\partial t}+U\frac{\partial\zeta}{\partial x}+\beta v=0$$

$$\zeta=\nabla^2\psi,\ v=\partial\psi/\partial x,$$

where β is the Rossby parameter and U is the zonal wind component, assumed uniform and constant.

For the present purpose it suffices to take the case $\beta=0$:

$$\frac{\partial\zeta}{\partial t}=-U\frac{\partial\zeta}{\partial x}. \tag{4.1}$$

Using central differences

$$\delta_{tt}\zeta=-\sigma\delta_x\zeta, \tag{4.2}$$

where $\sigma\equiv U\Delta t/\Delta x$ and δ_{tt}, δ_x are the difference operators defined previously, as in (2.1). To aid in identifying the lattice structure of (4.2), and for comparison with the primitive equations discussed in the preceding section, we will denote vorticity values at the points $x/\frac{1}{2}\Delta x=1, 3, 5, \ldots, 2p-1$ by the symbol ω and those at the points $x/\frac{1}{2}\Delta x=0, 2, 4, \ldots, 2p$, by the symbol ζ. On reference to the lattices of figure 2, we find that equation (4.2) is equivalent to the system

$$\delta_{tt}\zeta=-\sigma\delta_x\omega \tag{4.3a}$$

$$\delta_{tt}\omega=-\sigma\delta_x\zeta. \tag{4.3b}$$

The structure of these equations is identical to that of the primitive equations (3.1), with ζ playing the role of u and ω that of h. The significance of this equivalence is that (4.3) must admit of both forward and backward wave propagation (as in the primitive equations), whereas the parent differential equation (the vorticity equation) permits propagation in one direction only; in other words, (4.3) has the properties of a continuous hyperbolic system with two families of characteristics, while only one family is allowed by the vorticity equation. The intrusion of this virtual set of characteristics, and the associated truncation errors, are the penalties imposed by the use of central differences.

The preceding remarks can be made more specific, as follows. If one eliminates ω from (4.3), the result is

$$\delta_{tt}^2\zeta=\sigma^2\delta_x^2\zeta, \tag{4.4}$$

which is the wave equation (2.1). In other words, the ζ-field on the lattices of figure 2 satisfies the finite-difference wave equation. The corresponding differential equation may be obtained merely by differentiating (4.1) with respect to t, and eliminating the resulting mixed derivative by using (4.1) again; one finds

$$\frac{\partial^2\zeta}{\partial t^2}=U^2\frac{\partial^2\zeta}{\partial x^2}. \tag{4.5}$$

We now ask the question: how do the solutions of (4.5) compare with those of (4.1)?

To examine this question, one must be very explicit about the boundary and initial conditions. For (4.5), we

*A thorough discussion of resonance in the application of end conditions to the finite-difference vorticity equation has been undertaken by Birchfield [1].

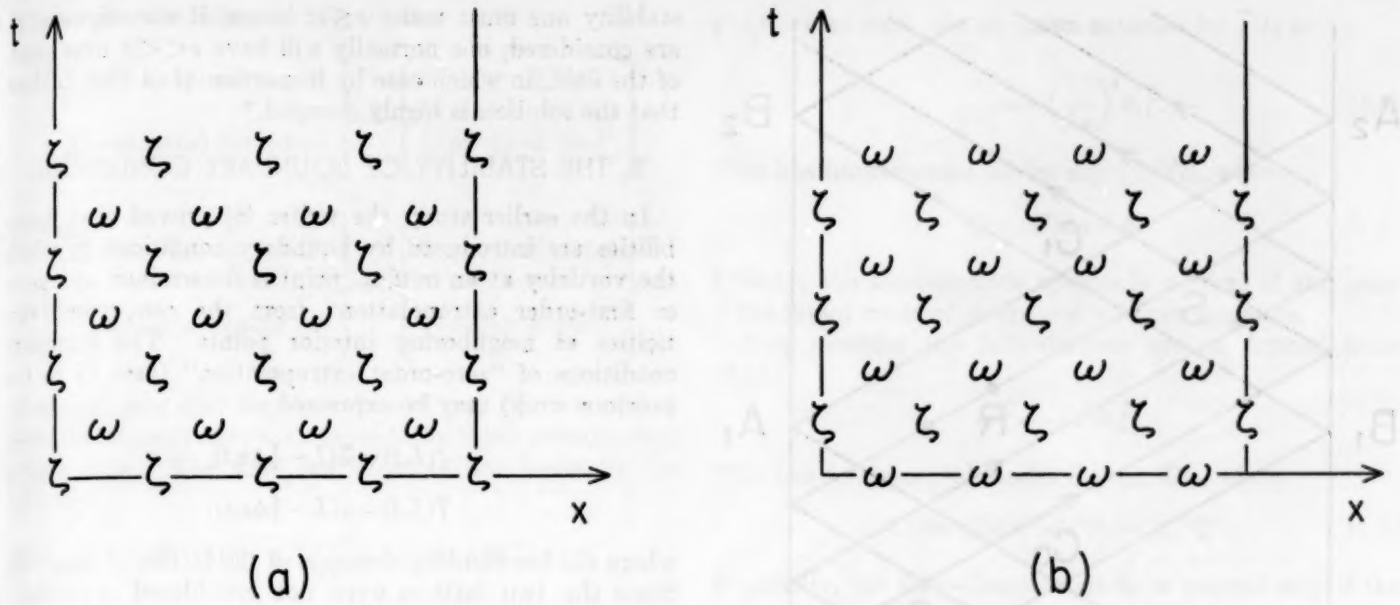

FIGURE 2.—Two lattices for solution of the vorticity equation.

impose ζ and $\partial\zeta/\partial t$ on the line $t=0$, and $\zeta=0$ on the ends $x=0$ and $x=L$ for all t; the latter condition corresponds to total reflection. For (4.1), we impose ζ on the line $t=0$ and $\zeta=0$ on the end $x=0$; the latter condition presupposes $U>0$ (which we assume henceforth), so that $x=0$ is a point of inflow for the vorticity. The solution of (4.1) is then, with reference to figure 3,

$$\zeta(x,t)=\zeta(x-Ut,0) \text{ inside } A_0B_0A_1$$

$$\zeta(x,t)=0 \text{ outside } A_0B_0A_1.$$

Thus, the initial values of ζ on A_0B_0, as well as the inflow values of ζ on the line $A_0B_1A_2$ . . . are simply propagated without change along the characteristics $x-Ut=$constant, which are the only characteristics admitted by (4.1).

To obtain an explicit and appropriate solution of (4.5), we will assume that $\partial\zeta/\partial t$ *on the initial line only* is specified in accordance with (4.1). This means that *initially*, the motion is organized strictly as a forward wave propagation. A disturbance at any point on the initial line, such as D (fig. 3), therefore moves out along the forward characteristic $x-Ut=$constant, until the boundary at $x=L$ is reached. There, total reflection occurs and the disturbance returns along the backward characteristic $x+Ut=$constant. It follows that in the triangle $A_0B_0C_0$ the solutions of (4.1) and (4.5) coincide, since no point in this triangle is accessible by reflection; in particular, $\zeta(P)=\zeta(D)$. On the other hand, every point in the triangle $C_0B_0A_1$, is accessible from two points on the initial line; for example, $\zeta(Q)=\zeta(D)-\zeta(E)$. In this triangle therefore, the solutions of (4.1) and (4.5) do not coincide, since (4.1) requires $\zeta(Q)=\zeta(D)$. Evidently, (4.5) permits the point Q to be affected by the reflected disturbance originating at E on the initial line. Similarly, in the parallelogram $C_0A_1C_1B_1$, we have $\zeta(R)=-\zeta(D)$ from (4.4) and $\zeta(R)=0$ from (4.1), while in the triangle $B_1C_1A_2$ we have $\zeta(S)=\zeta(E)-\zeta(D)$ from (4.5) and $\zeta(S)=0$ from (4.1).

The preceding discussion shows that only in the triangle $A_0B_0C_0$ do the solutions of (4.5) and (4.1) coincide.* The finite-difference equations (4.3) will, of course, exhibit the properties of (4.5). We turn now to a consideration of these equations.

In an earlier study of equation (4.2) the writer showed that an arbitrary imposition of ζ on the boundaries leads to a "neutral" prediction system; that is, a system whose modes are neither damped nor amplified, apart from resonance (Platzman [6]). In particular, if one takes $\zeta=0$ at the ends, then the problem posed by (4.3) is identical to that of "tidal" motion in a closed canal, the solutions of which have been given in detail in the preceding sections; hence, if in the latter solutions we replace u by ζ and h by ω, we obtain the solution of (4.3). From (2.2) and (3.2) we have

$$\zeta(x,t)=\sum_{l=1}^{p-1}\zeta_l(t)\sin k_l x \qquad (4.6a)$$

$$\omega(x,t)=\sum_{l=0}^{p-1}\omega_l(t)\cos k_l x; \qquad (4.6b)$$

if all initial conditions are specified on the line $t=0$, we get solutions of the form (3.6a) and (3.6b), or (3.7a) and (3.7b), for the coefficients $\zeta_l(t)$ and $\omega_l(t)$, respectively.

It is pertinent to note that in the limit Δx, $\Delta t\to 0$ the finite-difference solutions ζ and ω determined in the manner just described will coalesce with the continuous solutions of the equivalent primitive (or wave) equations,

*In the particular case considered, with $\zeta=0$ on the inflow boundary, we have coincidence of the two solutions also in the triangles $A_2C_1B_1$, $C_1A_1B_1$, and so on, where both solutions give $\zeta=0$.

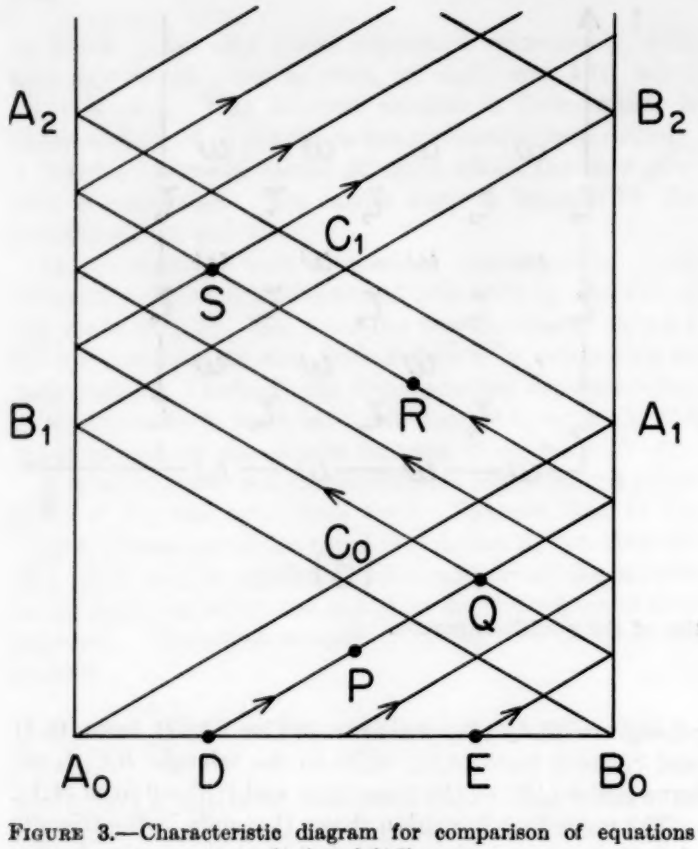

FIGURE 3.—Characteristic diagram for comparison of equations (4.1) and (4.3).

but will not coalesce with the continuous solution of the vorticity equation, and in particular, the fields ζ and ω will not themselves coalesce. This anomalous behavior of the central-difference vorticity equation is readily understood from figure 3 and the related discussion of (4.5) given above.

One way to circumvent the difficulties encountered in the central-difference vorticity equation is to use one-sided differences. In (4.1), we may take forward differences in t and (if $U>0$) backward differences in x:

$$\zeta(x,t+\Delta t)-\zeta(x,t)=\sigma[\zeta(x,t)-\zeta(x-\Delta x,t)],$$

where $\sigma\equiv U\Delta t/\Delta x$. This makes

$$\zeta(x,t+\Delta t)=(1-\sigma)\zeta(x,t)+\sigma\zeta(x-\Delta x,t).$$

The solution of this equation is obtained most readily by induction. If $\zeta(0,t)=0$, one finds

$$\zeta(x,t)=\sum_{k=0}^{n}\binom{n}{k}\sigma^{n-k}(1-\sigma)^k\zeta(x-n\Delta x+k\Delta x,0), \quad (4.7)$$

where $n\equiv t/\Delta t$, on the understanding that in the summation, $\zeta(x,0)=0$ where $x<0$.

The use of one-sided differences can be extended quite naturally to the two-dimensional vorticity equation, and in this context has been reported by Bolin [2] as having been tested by the Stockholm group. For computational stability one must make $\sigma\leq 1$; hence, if variations of U are considered, one normally will have $\sigma<<1$ over most of the field, in which case by inspection of (4.7) it is clear that the solution is highly damped.*

5. THE STABILITY OF BOUNDARY CONDITIONS

In the earlier study the writer [6] proved that instabilities are introduced by boundary conditions in which the vorticity at an outflow point is determined by "zero- or first-order extrapolation" from the concurrent vorticities at neighboring interior points. The boundary conditions of "zero-order extrapolation" (case II in the previous work) may be expressed

$$\begin{aligned}\zeta(L,t)&=\bar{\omega}(L-\tfrac{1}{2}\Delta x,t)\\ \bar{\zeta}(L,t)&=\omega(L-\tfrac{1}{2}\Delta x,t),\end{aligned} \quad (5.1)$$

where the bar signifies elements of the lattice of figure 2b. Since the two lattices were not considered separately, these conditions evidently introduce a coupling between the lattices; the result is a weak but exponential instability in the fundamental modes.

We will show now that if the outflow conditions just described are applied in such a way that the lattices are not coupled, then the instability is removed.† The appropriate revision is

$$\zeta(L,\,t)=\zeta(L-\Delta x,\,t). \quad (5.2)$$

Our proof (of stability) will consist of a construction of the fundamental modes. We begin with the expansions

$$\zeta(x,\,t)=\sum_{l=1}^{p-1}\zeta_l(t)\,\sin\,\kappa_l x \quad (5.3a)$$

$$\omega(x,\,t)=\sum_{l=1}^{p-1}\omega_l(t)\,\cos\,\kappa_l x+\Omega, \quad (5.3b)$$

which are similar to (4.6). Irrespective of the values assigned to κ_l, these satisfy the basic equations (4.3) provided $\zeta_l(t)$ and $\omega_l(t)$ are suitable linear combinations of $\cos\,\nu_l t$ and $\sin\,\nu_l t$, where ν_l is the frequency determined by (2.4). Further, (5.3a) satisfies the inflow condition $\zeta(0,t)=0$. In (5.3b), Ω is an absolute constant.

We now effect the determination of κ_l by forcing (5.3a) to comply with the outflow condition (5.2); this makes

$$\sin\,\kappa_l L=\sin\,\kappa_l(L-\Delta x),$$

the roots of which are given by

$$\begin{aligned}\kappa_l&=(l-\tfrac{1}{2})\pi/(L-\tfrac{1}{2}\Delta x)\\ &(l=1,\,2,\,3,\,\ldots,\,p-1).\end{aligned} \quad (5.4)$$

There remains only the demonstration that, with κ_l as in (5.4), the representations in (5.3) are complete. This

* In a thorough study of the finite-difference primitive and wave equations, Mihaljan [4] has pointed out that when $\sigma=1$ in (4.7), there are no truncation errors.

† For the conditions of "first-order extrapolation" (case III in the previous work), uncoupling the lattices does not completely remove the instability, but eliminates its exponential character.

hinges upon the following identities:

$$\left\{\begin{matrix}\sum_{x(\zeta)} \sin \kappa_l x(\zeta) \sin \kappa_{l'} x(\zeta) \\ \sum_{x(\omega)} \cos \kappa_l x(\omega) \cos \kappa_{l'} x(\omega)\end{matrix}\right\} = \left\{\begin{matrix}0 & \text{if } l \neq l' \\ \frac{1}{2}(p-\frac{1}{2}) & \text{if } l = l'\end{matrix}\right\}$$

$$\left\{\begin{matrix}\sum_{l=1}^{p-1} \sin \kappa_l x(\zeta) \sin \kappa_l x'(\zeta) \\ \sum_{l=1}^{p-1} \cos \kappa_l x(\omega) \cos \kappa_l x'(\omega)\end{matrix}\right\} = \left\{\begin{matrix}0 & \text{if } x \neq x' \\ \frac{1}{2}(p-\frac{1}{2}) & \text{if } x = x'\end{matrix}\right\}$$

where $x(\zeta)$ and $x(\omega)$ signify values of x at ζ-points and at ω-points, respectively, the x-sums being taken over internal points only. The first set of identities leads to the inversion

$$\zeta_l(t) = 2(p-\tfrac{1}{2})^{-1} \sum_{x(\zeta)} \zeta(x,t) \sin \kappa_l x(\zeta)$$

$$\omega_l(t) = 2(p-\tfrac{1}{2})^{-1} \sum_{x(\omega)} [\omega(x,t) - \Omega] \cos \kappa_l x(\omega),$$

and the second set insures that when returned to (5.3), the latter expressions of $\zeta_l(t)$ and $\omega_l(t)$ do, in fact, reproduce $\zeta(x,t)$ and $\omega(x,t)$.

For the determination of Ω in (5.3b), we note that, in view of (5.4), $\cos \kappa_l(L-\frac{1}{2}\Delta x)=0$; hence, from (5.3b),

$$\Omega = \omega(L-\tfrac{1}{2}\Delta x, t),$$

which means that at the point adjacent to the outflow end, ω is constant in this scheme. This completes the construction of the fundamental modes associated with the "uncoupled" outflow condition (5.2); evidently, these modes are neutral.

An alternative proof of stability can be given in terms of the "semi-discrete" equation

$$\frac{\partial^2 \zeta}{\partial t^2} = \left(\frac{U}{\Delta x}\right)^2 \delta_x^2 \zeta, \tag{5.5}$$

obtained from (4.4) by replacing the space derivative, but not the time derivative, by a difference quotient (see Platzman [6]). Let $\vec{\zeta}(t)$ denote the column vector formed from the $p-1$ values of $\zeta(x,t)$ at internal points, and define the matrix

$$\mathsf{A} \equiv \begin{pmatrix} 2 & -1 & 0 & \cdots & 0 \\ -1 & 2 & -1 & & \cdot \\ 0 & -1 & & & \cdot \\ \cdot & & & & \cdot \\ \cdot & & & & 0 \\ \cdot & & & & \\ & & -1 & 2 & -1 \\ 0 & \cdots & 0 & -1 & 1 \end{pmatrix}.$$

Then, with the boundary condition (5.2) at $x=L$ and $\zeta(0,t)=0$ at $x=0$, the equation satisfied by $\vec{\zeta}(t)$ is

$$\frac{\partial^2 \vec{\zeta}}{\partial t^2} = -\left(\frac{U}{\Delta x}\right)^2 \mathsf{A} \vec{\zeta}. \tag{5.6}$$

This has fundamental modes $\exp(\pm i\mathsf{C}t)$, where

$$\mathsf{C}^2 = (U/\Delta x)^2 \mathsf{A}.$$

Clearly, the semi-discrete system is neutral if and only if the latent roots of A are real and non-negative.

Now consider the fully-discrete system formed from (5.6):

$$\delta_t^2 \vec{\zeta} = -\sigma^2 \mathsf{A} \vec{\zeta}.$$

This has fundamental modes $\exp(\pm i\mathsf{D}t)$, where

$$4 (\sin \tfrac{1}{2}\mathsf{D}\Delta t)^2 = \sigma^2 \mathsf{A} = (\Delta t)^2 \mathsf{C}^2. \tag{5.7}$$

Evidently, the fully-discrete system is neutral only if the semi-discrete system is neutral. We now make the observation that the semi-discrete system (5.5) or (5.6) is precisely that which describes the transverse vibrations of a discretely-loaded, stretched string with one end fixed and one end perfectly free (with respect to transverse displacements). The mass of the string is assumed negligible, and the loading consists of $p-1$ equal loads each of which is concentrated at an interior ζ-point $x/\Delta x = 1, 2, 3, \ldots, p-1$. The end at $x=0$ is fixed, while at $x=L$ we have a free end which is not loaded; the condition (5.2) then expresses the requirement that the lateral component of tension must vanish at $x=L$. Since the modes for the loaded string are neutral (as is well known), it follows that the latent roots of C are real; hence, from (5.7) we see that (for sufficiently small Δt) the latent roots of D also are real.

The preceding analogue permits some insight into the nature of the instability associated with the "coupled" outflow condition. In the semi-discrete system, we have in general

$$\frac{\partial}{\partial t} \omega\left(L-\frac{1}{2}\Delta x, t\right) = -\left(\frac{U}{\Delta x}\right)[\zeta(L,t) - \zeta(L-\Delta x, t)];$$

but the "coupled" condition is

$$\zeta(L,t) = \omega(L-\tfrac{1}{2}\Delta x, t),$$

so we get the following end condition for ζ:

$$\frac{\partial}{\partial t} \zeta(L,t) = -\left(\frac{U}{\Delta x}\right)[\zeta(L,t) - \zeta(L-\Delta x, t)].$$

For the stretched string, loaded in the manner previously described, with a free end at $x=L$, this condition may be interpreted as expressing the balance (at $x=L$) between the lateral component of tension and a frictional resistance proportional to the displacement velocity of the end of the string along its support. Such a system clearly is

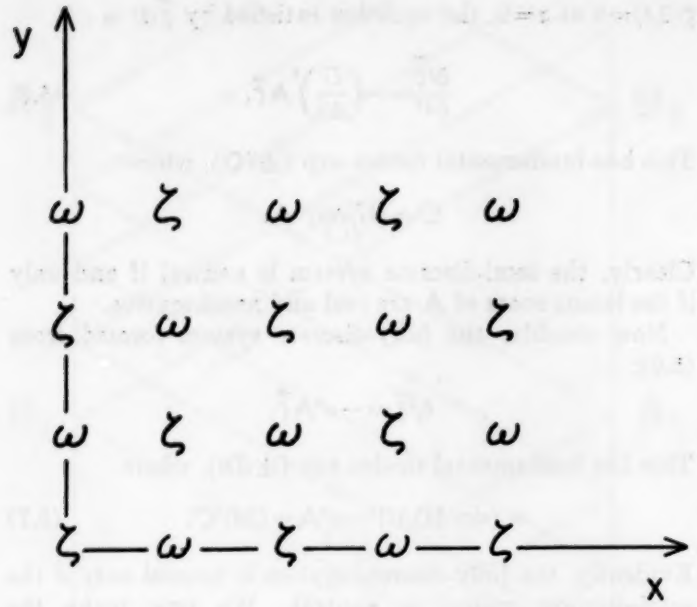

FIGURE 4.—The distribution of ζ- and ω-vorticities in the x, y-plane.

damped. The modes of the corresponding fully-discrete system therefore are amplified.

6. THE 2-DIMENSIONAL VORTICITY EQUATION

In figure 4 is shown the appropriate spatial distribution of ζ- and ω-vorticities for the two-dimensional vorticity equation

$$\frac{\partial \zeta}{\partial t}=-u\frac{\partial \zeta}{\partial x}-v\frac{\partial \zeta}{\partial y}. \tag{6.1}$$

The ω-vorticities are, as before, out of phase with the ζ-vorticities, by an interval $\frac{1}{2}\Delta t$ in time and $\frac{1}{2}\Delta s$ in space (note that figure 4 gives the distribution of these variables with respect to x and y, but not t). One may therefore identify two distinct lattices: one in which the ζ- and ω-fields are defined respectively at $t/\frac{1}{2}\Delta t=0, 2, 4, \ldots$ and $1, 3, 5, \ldots$; and the other in which the ζ- and ω-fields are defined respectively at $t/\frac{1}{2}\Delta t=1, 3, 5, \ldots$ and $0, 2, 4, \ldots$. In spite of the nonlinearity of (6.1), it is possible to formulate the difference equations in such a way that the two lattices remain permanently uncoupled, as will now be explained.

Assuming the velocity components to be derivable from a stream function, equation (6.1) may be written as a pair of equations

$$\frac{\partial \zeta}{\partial t}=\frac{\partial(\omega,\chi)}{\partial(x,y)} \tag{6.2a}$$

$$\frac{\partial \omega}{\partial t}=\frac{\partial(\zeta,\psi)}{\partial(x,y)}, \tag{6.2b}$$

where χ is the stream function for the ω-vorticities, and ψ is the stream function for the ζ-vorticities:

$$\omega=\nabla^2\chi;\ \zeta=\nabla^2\psi. \tag{6.3}$$

The procedure for replacement of (6.2) by appropriate difference equations is rather apparent and need not be elaborated here. In connection with (6.3) however, two procedures may be mentioned. If the x,y-axes and the interval $\frac{1}{2}\Delta s$ are used in the finite-difference Laplacian (to obtain the usual five-point formula), then concurrent values of ζ, ω, ψ, and χ are required, and in this way the two lattices would be coupled every time a relaxation is performed (that is, when (6.3) is solved). On the other hand, if axes inclined 45 degrees to the x,y-axes are used, together with an interval $\frac{1}{2}\Delta s\sqrt{2}$, then coupling of the lattices is avoided.

Numerical solutions of the barotropic vorticity equation have been obtained in the manner just described, in connection with an investigation of the prediction of hurricane movement, and will be reported elsewhere by Birchfield.

ACKNOWLEDGMENTS

The writer has benefited from many discussions with Mr. John M. Mihaljan and Mr. Gene E. Birchfield.

REFERENCES

1. Gene E. Birchfield, *Resonant Coupling Between Unequal Meshes in Numerical Integration of the Vorticity Equation*, The University of Chicago, Department of Meteorology, 1958.
2. Bert Bolin, "Numerical Forecasting with the Barotropic Model," *Tellus*, vol. 7, No. 1, Feb. 1955, pp. 27–49.
3. P. D. Lax and R. D. Richtmyer, "Survey of the Stability of Linear Finite-Difference Equations," *Communications on Pure and Applied Mathematics*, vol. 9, 1956, pp. 267–293.
4. John M. Mihaljan, *A Study of the Finite-Difference Solution of the Forced Wave Equation*, The University of Chicago, Department of Meteorology, 1958, 29 p.
5. George W. Platzman, *The Computational Stability of the Meteorological Prediction Equations*, The University of Chicago, Department of Meteorology, 1953, 30 pp.
6. George W. Platzman, "The Computational Stability of Boundary Conditions in Numerical Integration of the Vorticity Equation," *Archiv für Meteorologie, Geophysik und Bioklimatologie*, Ser. A, vol. 7, 1954, pp. 29–40.
7. George W. Platzman, "A Numerical Computation of the Surge of 26 June 1954 on Lake Michigan," *Geophysica*, 1958 (in press).

BAROTROPIC DIVERGENCE AND VERY LONG ATMOSPHERIC WAVES

GEORGE P. CRESSMAN, U. S. WEATHER BUREAU

Joint Numerical Weather Prediction Unit, Suitland, Md.

[Manuscript Received June 23, 1958]

ABSTRACT

The problem of spurious retrogression of very long waves by the non-divergent barotropic forecasts is shown to be the same problem discussed extensively by Rossby, Yeh, and Bolin. This difficulty is due to the failure of the non-divergent model to allow properly for the mutual adjustment of wind and pressure fields. The equation of continuity for a homogeneous incompressible fluid with an upper free surface, proposed as a remedy by Rossby nearly 20 years ago, removes much of the difficulty. Further improvements are obtained by inclusion of a tropopause in the manner adopted by Bolin. The results of a series of 10 test forecasts are shown in verification of the function of the divergence in a barotropic model.

1. INTRODUCTION

The inability of a non-divergent barotropic forecast model to describe properly the behavior of the longest atmospheric waves has resulted in large systematic height errors of the prognostic charts issued by the Joint Numerical Weather Prediction Unit. This difficulty was correctly diagnosed by Wolff [7], who also devised a method for automatic empirical correction to the forecasts. This consisted of an enforced stabilization of hemispheric wave numbers one, two, and three, such that atmospheric waves of this size were not allowed to change either position or intensity during the forecast. The remarkable success of Wolff's method was due to the fact that these very-large-scale disturbances are in fact quasi-stationary.

However, it has been our ultimate objective to include in the forecast models proper descriptions of the physical processes which actually occur in the atmosphere, wherever possible. In looking for the appropriate physical mechanism responsible for the very long waves, one may note that their positions are relatively invariant, suggesting that geographically related factors are responsible for their formation and position. Terrain-induced vertical motion and differential surface heating appear to be likely causes.

The question of the behavior of these waves, once formed, can be considered apart from the question of their formation. Abundant discussion of this problem appears in the literature. It now appears that we have paid too little attention to the work of Rossby which bears on this question.

2. THEORETICAL BACKGROUND

In his classic paper of 1939, Rossby [4] pointed out that application of the vorticity equation to a non-divergent atmosphere did not properly take into account the adjustment of pressure and wind fields. Using a homogeneous incompressible atmosphere of thickness D, he used the equation of continuity

$$\frac{\partial u}{\partial x}+\frac{\partial v}{\partial y}+\frac{1}{D}\frac{dD}{dt}=0, \tag{1}$$

where u and v are the speeds in the x and y directions. This led to the introduction of a divergence into the vorticity equation, such that

$$\frac{d\eta}{dt}-\frac{\eta}{D}\frac{\partial D}{\partial t}=0, \tag{2}$$

where η is the absolute vorticity about a vertical axis, and where the geostrophic approximation is used to set $u\frac{\partial D}{\partial x}+v\frac{\partial D}{\partial y}$ equal to zero. He then arrived at a frequency equation giving the phase velocity, C, of the divergent waves, which can be written in the form

$$C=\frac{C_{ND}}{1+\frac{2.5}{N^2}} \tag{3}$$

where C_{ND} is the phase velocity of the non-divergent waves and N is the hemispheric wave number measured at about 45° N. The coefficient 2.5 applies to a homogeneous atmosphere. The above equation and the corresponding one for the group velocity of this type of wave have been thoroughly discussed by Rossby [5] and by Yeh [8]. In a footnote to his 1939 paper, Rossby [4] mentioned that an analysis of a two-layer model having an active lower layer and an inert upper layer indicated that the divergence introduced by these considerations might reach values as high as $\frac{4}{D}\frac{dD}{dt}$.

In his 1945 paper Rossby [5] again emphasized, very explicity, the necessity for allowing for the mutual adjustment of wind and pressure by means of the above type

of divergence term. Phillips' [3] two-layer model can be specialized to describe Rossby's two-layer atmosphere. In the case where the motion in the lower fluid is parallel to the contours of the interface ($\mathbf{V}\cdot\nabla h=0$), and the horizontal motion in the upper fluid is negligible, Phillips' equations reduce to

$$\nabla^2\frac{\partial z}{\partial t}+\frac{f}{g}\mathbf{V}\cdot\nabla\eta-\frac{f\eta}{gh}\frac{\partial h}{\partial t}=0 \tag{4}$$

and

$$(1-\epsilon)\nabla^2\frac{\partial h}{\partial t}+\frac{f}{g}\mathbf{V}\cdot\nabla\eta-\frac{f\eta}{gh}\frac{\partial h}{\partial t}=0 \tag{5}$$

In the above equations, h is the height of the interface, z can be thought of as the height of an isobaric surface in the lower fluid, $\mathbf{V}$ and η are the velocity and absolute vorticity of the lower fluid respectively, and f and g are the Coriolis parameter and acceleration of gravity. The factor ϵ is given by the ratio of the density of the upper fluid to that of the lower fluid. From equations (4) and (5) and from the lateral boundary conditions where $\partial z/\partial t=\partial h/\partial t=0$ it is evident that

$$\nabla^2\frac{\partial z}{\partial t}+\frac{f}{g}\mathbf{V}\cdot\nabla\eta-\frac{f\eta}{(1-\epsilon)gh}\frac{\partial z}{\partial t}=0 \tag{6}$$

Equation (6) is consistent with a continuity equation for the lower fluid, equivalent to

$$\nabla\cdot\mathbf{V}+\frac{1}{K(1-\epsilon)z}\frac{\partial z}{\partial t}=0 \tag{7}$$

where $K=h/z$. In using equation (6) as a barotropic forecasting equation, it would be sufficient to use a mean value of h.

Bolin [1] made some computations with a barotropic model having a tropopause. This model was the same as those described above. He used a factor of $\frac{1}{5}$ for $K(1-\epsilon)$, without giving a description of how he arrived at such a number. His results were widely misinterpreted at the time (and in particular at the JNWP Unit), since this feature was presented as a cure for excessive anticyclogenesis. That problem has been shown by Shuman [6] to be related to the geostrophic approximation. Nevertheless, Bolin's results, while showing no improvement over the non-divergent forecasts in some respects, clearly resulted in greatly diminished height errors. It is evident now that Bolin was really controlling the very long waves, and that the reduced spread of excessive anticyclogenesis was merely a consequence of the smaller values of the group velocity obtained from his prognostic equation. At the JNWP Unit, we were aware of the problem of retrograde, very long waves only after we began to compute on a hemispheric grid and after Wolff's analysis was completed. This was partly due to the fact that the centers of height error from this source were very near the boundaries of our previously used grid and were confused with boundary errors. A suggestion by Dr. Norman Phillips led to the re-examination of the barotropic divergence.

3. THE PROGNOSTIC EQUATION

Equation (6) was reformulated in a finite-difference form as follows:

$$\left(\nabla^2-\frac{\mu d^2\eta}{m^2\bar{\psi}}\right)\frac{\partial\psi}{\partial t}+\frac{1}{4}\mathsf{J}(\psi,\eta)-\frac{a\eta}{4}\mathsf{J}\left(\psi,\frac{p_s}{p_0}\right)=0 \tag{8}$$

In this equation, ψ is the stream function obtained from the 500-mb. height through the balance equation [6] ∇^2 and J are the finite-difference Laplacian and Jacobian operators, d/m is the distance on the earth between grid points, and μ is the same as $1/K(1-\epsilon)$. The evaluation of ϵ seems to be a doubtful matter, since the atmosphere is not composed of two homogeneous incompressible fluids. It was finally decided to use the atmosphere as an integrating machine in order to obtain a realistic value of μ. Since we interpret h as the height of the tropopause, z as the height of the 500-mb. surface and consider that

$$\frac{\mu}{z}\frac{\partial z}{\partial t}=\frac{1}{h}\frac{\partial h}{\partial t} \tag{9}$$

we can observe the relative variation of h and z in the atmosphere. An inspection of tropopause and associated 500-mb. charts reveals μ to have an approximate value of 4.*

The second Jacobian in equation (8) is the standard large-scale mountain effect, where a, the ratio of surface to 500-mb. wind speeds, is set at 0.2, p_s is the pressure at the surface of the ground, and p_0 is 1000 mb.

4. RESULTS OF COMPUTATIONS

Equation (8) was programmed for the IBM 704 computer for the 1977-point hemispheric grid used by the JNWP Unit. Computation time averages about 35 seconds per time step.

A series of 48-hour forecasts was made for varying values of μ on one initial situation, that of 0000 GMT, February 15, 1958. This case was chosen because of the very large amplitude of wave number one.

The first forecast was made with a value of $\mu=1$, corresponding to a homogeneous atmosphere having a free upper surface. The results of this are presented in figure 1. It is evident from this figure that the upper free surface model varies greatly from the non-divergent model in its treatment of wave number one. The difference is in the direction required to reduce error. Figure 2 shows the corresponding difference map for $\mu=4$. This particular 48-hour period was characterized by several of the most severe cyclogeneses observed all winter, and

*If one follows the derivation of the equivalent barotropic model as given by Charney and Eliassen [2] but retains the term $\eta\frac{\partial\omega}{\partial p}$ at the lower boundary (ω being the vertical velocity in a pressure-time coordinate system), the resulting equation is the same as equation (8) with the important exception that the factor μ is less than 1, being the ratio of the surface to the mean wind speed. In the light of the results presented here, this formulation of the equivalent barotropic model appears to underestimate the divergence necessary to stabilize the longest atmospheric waves.

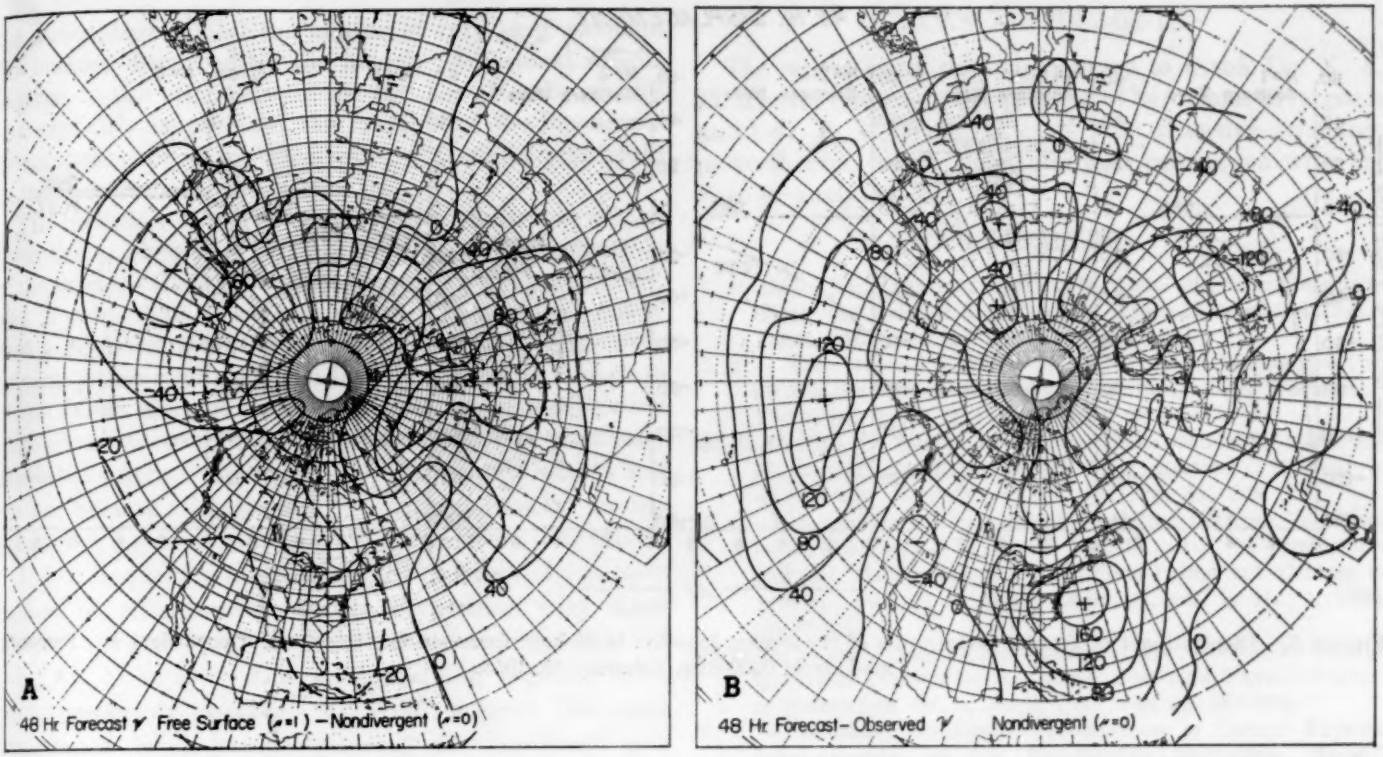

FIGURE 1.—(A) Stream function difference between 48-hour forecasts made by the barotropic model with $\mu=1$ and $\mu=0$. (B) Stream function error of the 48-hour non-divergent barotropic forecast.

it should not be expected that any barotropic forecast model could eliminate all large errors in this situation.

Fourier analyses were made by Cdr. Paul Wolff on the 48-hour stream function forecasts in order to discover the treatment of the various low-frequency components of the motion by the model. The results are presented in figure 3. The large changes of displacement with changes in μ for wave number one, compared with the minor changes for wave number five, are in good agreement with the frequency equation (3).

Figure 4 shows the errors of the 500-mb. height forecasts as a function of the coefficient μ. It is clear that the major improvement in the forecasts results from the free-surface approximation. It is also clear that little difference is made when μ is varied between values of 3 and 8.

A series of ten 48-hour forecasts was made in order to get a more representative idea of the level of accuracy of the forecasts. Comparisons were made with the JNWP Unit's operational barotropic forecast model (referred to hereafter as "O" model), which includes the very-long wave stabilization described by Wolff [7]. This was thought to be a more relevant comparison than a comparison with the unaltered non-divergent barotropic model ("N" model), since the relative levels of accuracy of the height forecasts of the O and N models were already presented by Wolff. Also, unpublished results by Wolff and Carstensen indicate a reduction of about 19 percent

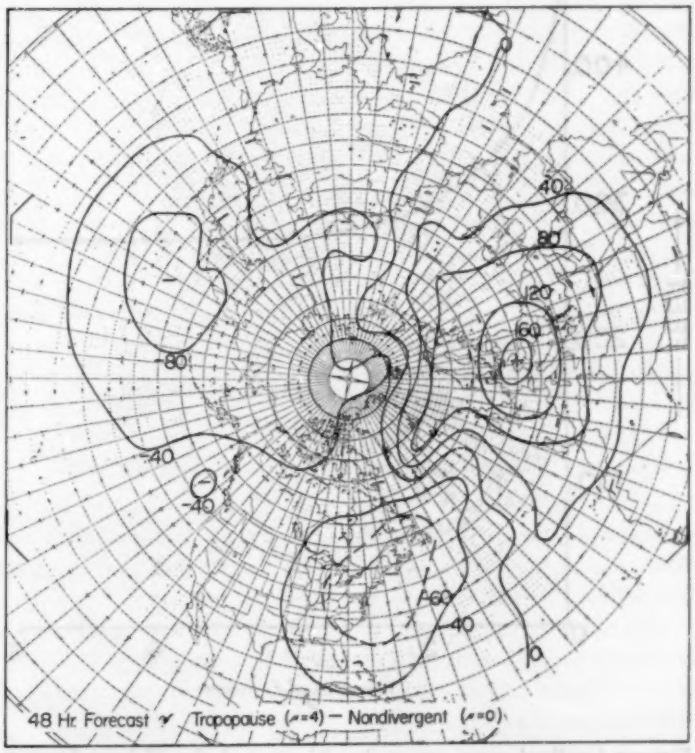

FIGURE 2.—Stream function difference between 48-hour forecasts made by the barotropic model with $\mu=4$ and $\mu=0$.

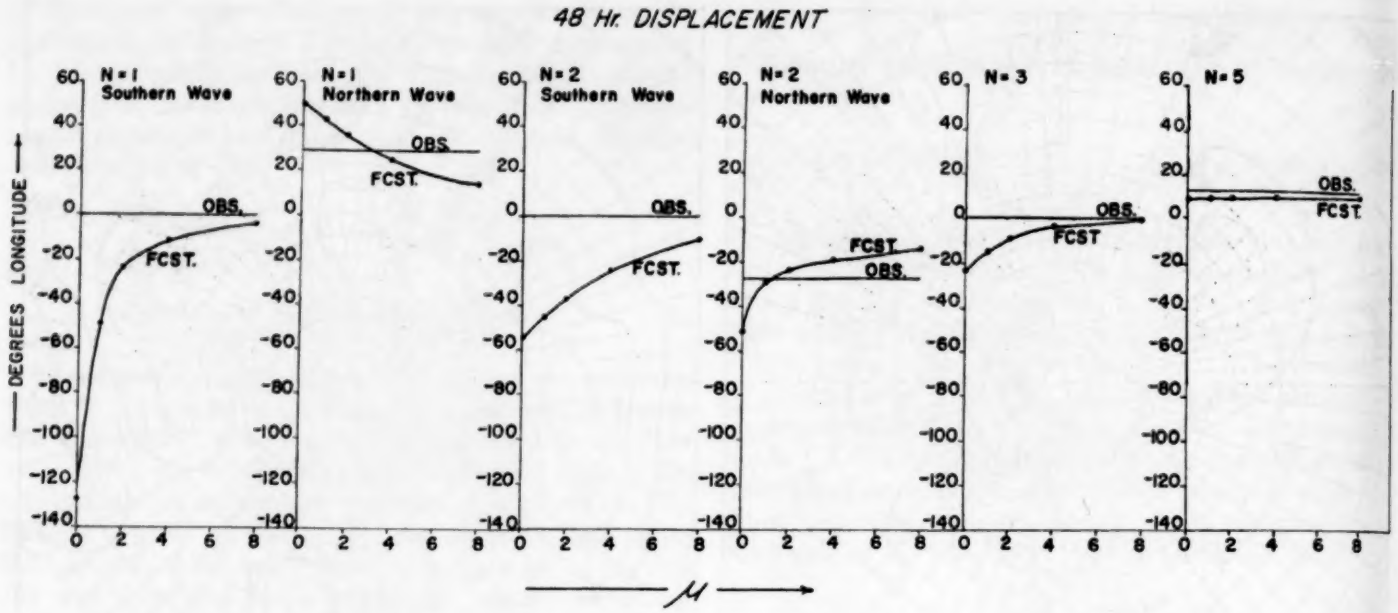

FIGURE 3.—Displacement of Fourier components of the stream function in 48-hour forecasts vs. the values of coefficient μ. Forecasts made from 0000 GMT, February 15, 1958.

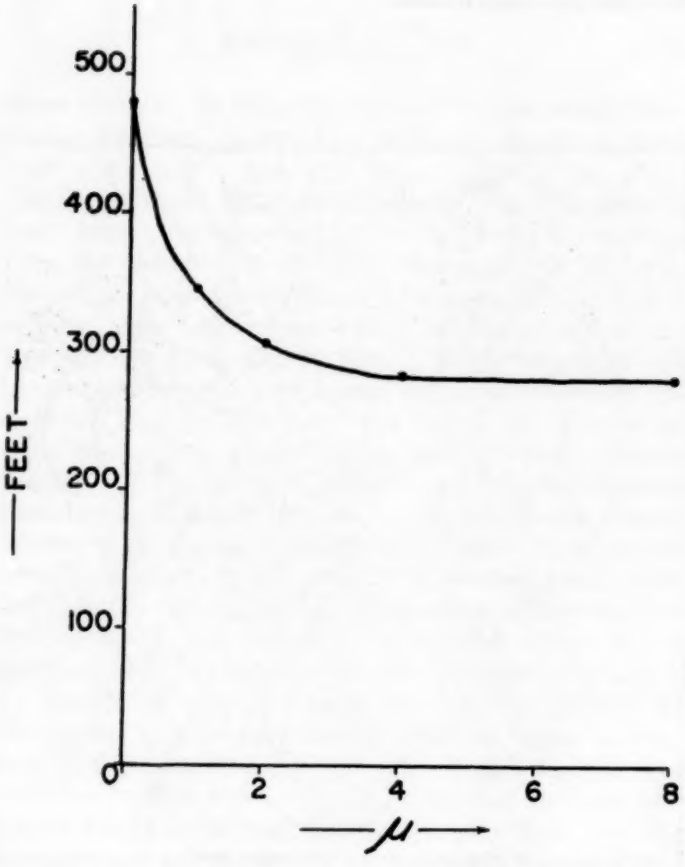

FIGURE 4.—Root-mean-square height error of the 48-hour forecast for different values of the coefficient μ. Forecast made from 0000 GMT, February 15, 1958.

in the 48-hour wind errors of a series of winter forecasts by the O model as compared with the N model. Table 1 presents the results of the ten comparative forecasts ("D" refers to the divergent barotropic model).

The average height errors for the ten forecasts show a slight but significant improvement over the O model by the D model. A correspondingly large reduction of error is obtained by the D model as compared with N model, considering the previously published results of Wolff. In comparison with the O model, the wind forecasts by the D model are not much improved. The improvement of the D model over the N model is, however, significant.

5. CONCLUSIONS

The success of forecasts made by a divergent barotropic model suggests strongly that large-scale divergences in

TABLE 1.—*Results of comparative forecasts made with the different models, D=divergent barotropic model, O=operational barotropic model, N=non-divergent barotropic model*

Initial map		RMS height error (ft.)			RMS wind error (kt.)		
Date	GMT	D	O	N	D	O	N
2/15/58	00	283	277	479	27.1	26.6	32.2
3/31/58	12	200	218	326	20.9	23.0	23.9
4/14/58	00	241	267	-------	23.0	25.3	-------
4/18/58	00	218	253	-------	22.6	22.6	-------
4/22/58	00	187	216	-------	18.9	20.5	-------
5/20/58	00	184	189	-------	19.6	19.8	-------
5/23/58	00	141	170	-------	15.4	16.6	-------
6/1/58	00	130	127	-------	16.0	15.2	-------
6/7/58	00	149	193	-------	16.9	19.0	-------
6/11/58	00	143	142	-------	16.4	16.6	-------
Average	-------	188	205	-------	19.7	20.5	-------

the atmosphere inhibit the motion of very long waves in the manner described by the model. Additional weight is given to the argument by the fact that Rossby clearly and explicitly emphasized the function of the barotropic divergence many years before numerical predictions could be made to test his conclusions.

The inclusion of a tropopause in the barotropic model, after Bolin, gives further improvement. The estimation of the proper values of the coefficient μ is a difficult matter, and is subject to some empiricism. It does not follow that a minimization of errors of the forecast heights with respect to the coefficient can lead to a correct estimation of its value, since it is possible that an overestimation might tend to compensate for correlated but physically unrelated errors. Investigations of mountain effects and surface heating with the aid of divergent forecast models may throw light on the formation of these very long waves.

It has frequently been stated that numerical forecasts cannot be considered to be in competition with other forecast systems with respect to height values (at 500 mb., for example). The above results, together with those previously published by Wolff, suggest that such statements, being based essentially on experience with the non-divergent forecast equation, and the consequently large height errors arising from misplacement of the very long waves, can no longer be considered valid. A re-evaluation of errors of height forecasts by numerical and other forecast methods appears to be desirable.

ACKNOWLEDGMENTS

The writer takes this opportunity to thank Dr. N. A. Phillips for reopening the question of barotropic divergence and Cdr. P. M. Wolff, U. S. N., for extensive assistance in verification work, particularly in connection with the Fourier analyses.

REFERENCES

1. B. Bolin, "An Improved Barotropic Model and Some Aspects of Using the Balance Equation for Three-Dimensional Flow," *Tellus*, vol. 8, No. 1, Feb. 1956, pp. 61–75.
2. J. G. Charney and A. Eliassen, "A Numerical Method for Predicting the Perturbations of the Middle Latitude Westerlies," *Tellus*, vol. 1, No. 2, May 1949, pp. 38–54.
3. N. Phillips, "A Simple Three-Dimensional Model for the Study of Large-Scale Extratropical Flow Patterns," *Journal of Meteorology*, vol. 8, No. 6, Dec. 1951, pp. 381–394.
4. C.-G. Rossby and Collaborators, "Relation Between Variations in the Intensity of the Zonal Circulation of the Atmosphere and the Displacements of the Semi-Permanent Centers of Action," *Journal of Marine Research*, vol. 2, No. 1, 1939, pp. 38–55.
5. C.-G. Rossby, "On the Propagation of Frequencies and Energy in Certain Types of Oceanic and Atmospheric Waves," *Journal of Meteorology*, vol. 2, No. 4, Dec. 1945, pp. 187–204.
6. F. G. Shuman, "Predictive Consequences of Certain Physical Inconsistencies in the Geostrophic Barotropic Model," *Monthly Weather Review*, vol. 85, No. 7, July 1957, pp. 229–234.
7. P. M. Wolff, "The Error in Numerical Forecasts Due to Retrogression of Ultra-Long Waves," *Monthly Weather Review*, vol. 86, No. 7, July 1958, pp. 245–250.
8. T.-C. Yeh, "On Energy Dispersion in the Atmosphere," *Journal of Meteorology*, vol. 6, No. 1, Feb. 1949, pp. 1–16.

Correspondence

LOWEST TEMPERATURE IN CANADA

ANDREW THOMSON

Director, Meteorological Branch, Air Services, Toronto, Ont., Canada

September 17, 1958

Regarding the article "On the Lowest Temperature on Earth" appearing in the January 1958 issue of the *Monthly Weather Review*, I have a few remarks to make which might clarify the situation regarding the lowest temperature ever recorded in Canada.

Previous to February 1947, the record Canadian low temperature was −78.5° F., observed at Fort Good Hope, N. W. T. in December 1910, as indicated in the article. This absolute low temperature has been exceeded twice at Snag, Yukon, on February 2 and 3, 1947. The corrected minimum temperature on February 2, was −80.1° and on February 3, it was −81.4°. The value of −81° F., is taken as the absolute lowest temperature ever recorded in Canada.

Since the article states that in Canada two official sources report conflicting data, it should be pointed out that the Monthly Weather Map, which is prepared about three weeks after the close of each month, must be considered as a preliminary or provisional report. As outlined in the article, the minimum originally reported from the station was −83° and was obtained by extrapolation. When the thermometers were received at these Meteorological Headquarters, several months later, and calibration tests carried out, an official value of −81.4° F. was set. Since February 1947 there have been no official temperatures in Canada lower than −80°.

I hope that this information will clarify the alleged discrepancy in the official Canadian meteorological publications.

COMMENTS ON "THE ERROR IN NUMERICAL FORECASTS DUE TO RETROGRESSION OF ULTRA-LONG WAVES"

PHILIP F. CLAPP

Extended Forecast Section, U. S. Weather Bureau, Washington, D. C.

September 22, 1958

The paper by Paul M. Wolff (*Monthly Weather Review*, July 1958) discusses some practical results of one of a class of empirical numerical models which have been suggested in recent years. I would like to point out the interesting family resemblance between these models, because all of them contain some of the more important effects of tropospheric divergence resulting from forced flow over mountains, large-scale heat and cold sources, and other complex factors which account for the special behavior of long waves.

I would also like to take this opportunity to discuss a more general formulation of this group of models, because I feel that more rapid progress may be made if researchers in this field realize that different individuals are independently attempting to develop the same fundamental idea. This generalization is obtained by borrowing an assumption from the perturbation theory of hydrodynamics. It is assumed that the actual wind field in mid-troposphere consists of a perturbation-component superimposed on a large-scale quasi-stationary flow. As in the perturbation method, it is assumed that this quasi-stationary flow, which will be called hereafter the "basic current," is given; and we seek to predict the evolution of the perturbation. Since, as will be clarified later, we are not immediately concerned with mathematical difficulties, the basic flow need not be confined to a straight zonal current with little or no shear. It may have almost any form related to the general circulation, provided its rate of evolution is small compared to that of the perturbation. Another requirement, characteristic of the simple models to be described presently, is that it must be chosen so as to minimize the divergence of the perturbation. Various possible forms of the basic current will be discussed later.

The group of models which have been proposed up to the present may be formed through use of the simplest possible vorticity equation containing divergence:

$$\frac{\partial \zeta}{\partial t} = -\mathbf{V}\cdot\nabla\eta - f\nabla\cdot\mathbf{V} \tag{1}$$

The symbols have their usual meaning and the equation applies to the actual wind field, which by definition is the sum of the basic current and the perturbation.

Equation (1) may also be applied to the basic current, whose time rate-of-change is assumed to be small:

$$0 \approx -\mathbf{V}_B\cdot\nabla\eta_B - f\nabla\cdot\mathbf{V}_B \tag{2}$$

Here, the subscript B refers to quantities measured in the basic current.

Use is now made of the assumption that the divergence of the perturbation is small. This enables us to replace the divergence of the actual flow by that of the basic flow, so that equations (1) and (2) may be combined, giving:

$$\frac{\partial \zeta}{\partial t} = -\mathbf{V}\cdot\nabla\eta + \mathbf{V}_B\cdot\nabla\eta_B \tag{3}$$

This is the prediction model proposed by the writer [1], where the basic current was taken to be the normal seasonal circulation. In this particular adaptation, the

(*Continued on page 327*)

EFFECT OF DATA COVERAGE ON THE ACCURACY OF 500-MB. FORECASTS

CHARLES L. BRISTOR, U. S. WEATHER BUREAU

Joint Numerical Weather Prediction Unit, Suitland, Md.

[Manuscript Received May 22, 1958; Revised July 3, 1958]

ABSTRACT

Networks of data are simulated by interpolating height and wind from a hypothetically "correct" analysis at a uniform array of points. The interpolated values are added to random numbers whose statistics are typical of non-systematic errors of observation, and are then regarded as genuine data. Such artificially constructed "data" for several networks of different densities are analyzed independently. The differences between these analyses and the hypothetically "correct" analysis are taken to be representative of the initial analysis error under conditions of varying station density.

Numerical forecasts computed from the different analyses are compared with the forecast made from the "correct" initial data. Several such comparisons indicate that initial analysis errors do not grow to an important degree so long as the spacing between synoptic reports confines error fields to a scale smaller than that of the synoptic disturbances. However, with data spacing comparable with that over existing regions of poor data coverage, initial errors are amplified two-fold in a 48-hr. forecast interval.

Further experiments, in which the data are analyzed objectively to eliminate inconsistencies of analysis, are carried out.

1. INTRODUCTION

The problem of resolving the initial synoptic situation in all its pertinent detail has often been mentioned as a contributing factor where critical weather developments have challenged the forecaster and found his efforts inadequate. Although forecasters justify requests for more data (at least among themselves) on the basis of this argument, additional data are more often made available in connection with some expanded commercial program such as a new air route where there is direct operational need for current observations of weather conditions. The forecaster must then plead that good forecasts on such routes are also contingent on adequate data coverage in other areas. This plea would perhaps be weighed more heavily except for the subjectivity in the argument. No matter how elegant are the forecast parameters involved or how precisely observational data are employed in their evaluation, the final result is usually a subjective combination which leaves the contribution of the avowed critical factors somewhat in doubt.

This argument could be greatly strengthened if a measure of change in forecast accuracy could be related quantitatively to a change in data coverage.[1] The problem would then be one of economics with the increased cost being weighed against the increased value of a more accurate forecast. Newton [1] has discussed this data and analysis problem at length and has shown how differences in barotropic tendency computations can be attributed to differences in analyses. Best [2] has carried through several barotropic forecasts with similar conclusions. The purpose of the present study is to strengthen this argument in a quantitative way by isolating the numerical forecast errors arising from initial analysis errors that, in turn, are made a function of data density alone. The experiment described below is actually an adjunct to a more theoretical treatment by Thompson [3]. The results, although limited, are considered meaningful in a corroborative way. Computational roundoff and truncation errors remain as contaminants to the results. Other errors such as boundary differences and analysts' subjectivity as discussed later, are controlled insofar as is practical.

2. DESIGN OF THE EXPERIMENT

The experiment was designed to indicate differences in forecasts (hereafter called errors) arising from differences in initial analyses of the same synoptic situations. Such a definition of error seems entirely fair. The objective was to measure quantitatively the reproduction of barotropic forecasts based on plentiful data by barotropic forecasts based on limited data. The similar task involving the real atmosphere or even more sophisticated models is certain to be more difficult. The barotropic forecasts were produced using an octagonal grid of 1977 points covering most of the Northern Hemisphere (fig. 1).

Four different analyses of two separate synoptic situa-

[1] Preliminary results of an investigation by Maj. E. O. Jess, USAF, have come to the attention of the writer. His approach is much the same as in the present paper although different measures of forecast error are employed. The two studies agree in a broad sense.

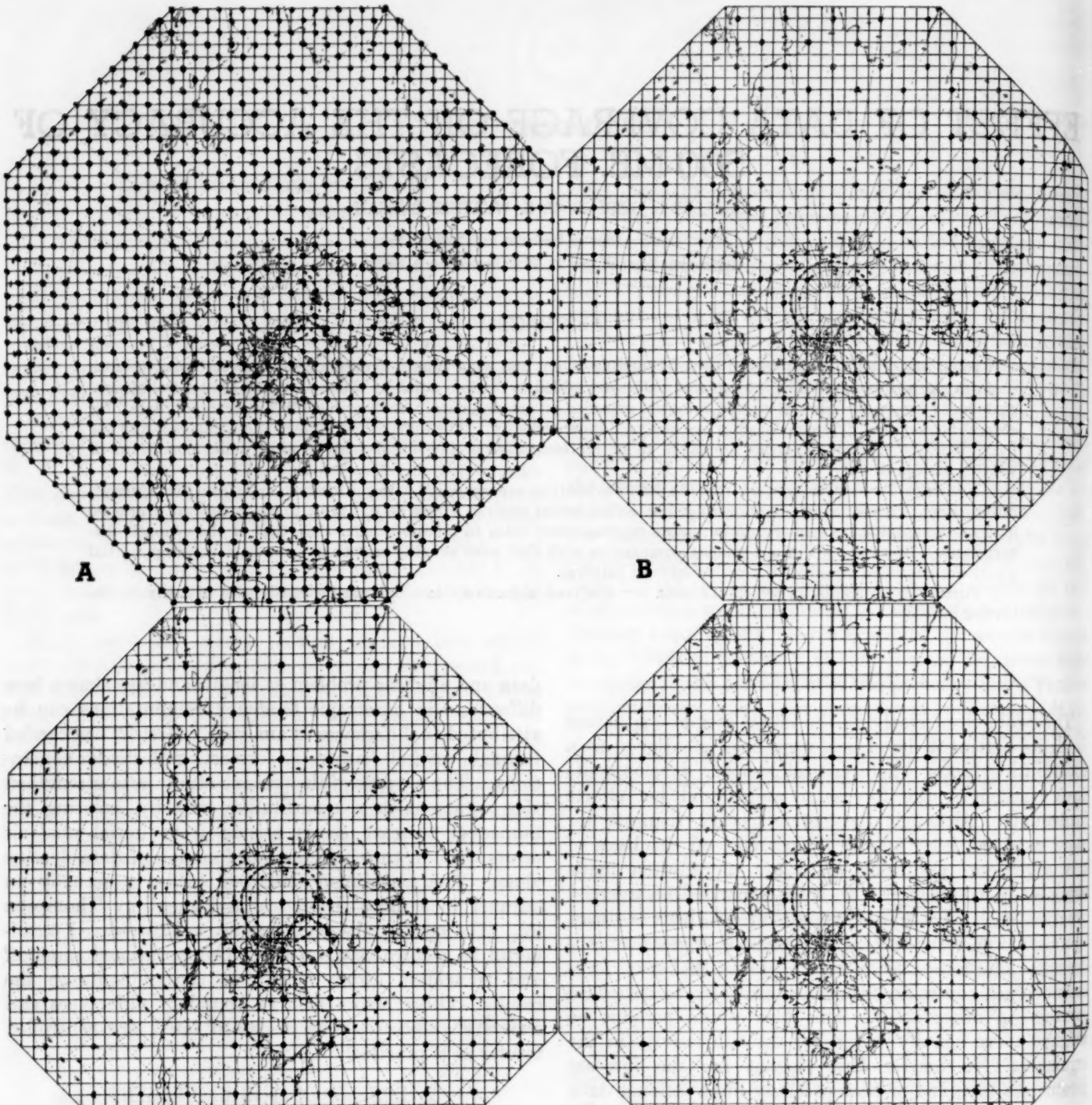

FIGURE 1.—Data coverage, shown by dots, for the octagonal grid of 1977 points currently used in the JNWP Unit (A) and successively reduced arrays (B, C, D,).

tions were provided as input data for the forecasts in the following manner. The 500-mb. data from two routine operational analyses were first interpolated at the grid points indicated by large dots in figure 1A. It was then postulated that these grid-point data were the true heights of the 500-mb. surface at the points in question. The next problem was to try to reproduce these true grid-point values with subjective analyses made under realistic operational conditions but with 500-mb. data coverage being provided in various reduced arrays. The analyst attempt-

ing the simulation had access to complete routine operational surface analyses which contained reasonably complete coverage over most geographical regions including ocean areas. The question was thus reduced to one of upper-air data coverage. Maps for 0300 GMT for April 3 and 5, 1957 were selected partly because data decks for points shown in figure 1A were readily available. Also, for a limited sampling, it is perhaps more meaningful to choose such a period having flow patterns of moderate intensity rather than either winter or summer extremes.

The grid-point 500-mb. heights (considered to be uniformly spaced perfect data) were modified by the application of random normally distributed errors having a mean value of 50 feet. Geostrophic winds measured at the grid points from the basic analysis were likewise amended by similarly applying a non-systematic 10-knot average wind speed adjustment. The realistic but uniformly distributed data thus obtained were next plotted on blank charts in three reduced arrays as shown in figures 1B, C, and D. In some of the illustrations these data arrays are referred to as maximum, intermediate, minimum, and sub-minimum for reasons which will become obvious. The same experienced analyst proceeded to analyze one series, starting with the most sparse data array first. He was provided with two preceding analyses having the same data array and was permitted use of normal differential analysis techniques. Once the coarse array had been analyzed, he was given the denser array and repeated the analysis process.

Figure 2 presents the corresponding final analyses for the data arrays shown in figure 1 for the case of 0300 GMT, April 3, 1957. As one might suspect, the patterns look strikingly similar, at least in a superficial way. Indeed one might say that the differences appear trivial if the chart is to serve as a basis for a subjective forecast. Significant differences do exist, however, and their repercussions in numerical forecasts are important.

3. COMPUTATIONS AND RESULTS

All competing forecasts were made using the operational barotropic forecast procedure being employed at the time of the experiment, except that special precautions were taken to minimize boundary error contamination. In particular an investigative code devised by 'Arnason [4] was employed to remove virtually all boundary inflow-outflow wind components from each set of input data. The technique involves replacing each boundary height by the mean of all boundary values and allows the discrepancy to be "faired" in with a weight of .4 at the first internal ring of points, a weight of .1 at the second ring, and zero correction inward. Such an adjustment may, on occasion, do harm in the already questionable boundary region but, on the basis of other tests, it appears to prevent large effects from penetrating meridionally far into the grid. In any case, rather elusive, but sometimes important, minor inflow-outflow differences have thus been removed at a slight sacrifice in realism which does not enter into the results since the error is defined as the difference between forecasts.

Berggren [5] has recently shown the importance of subjective opinion among analysts in the interpretation of identical plotted data charts. Allowing one analyst to perform all the competing simulation analyses for each case was considered to be the best practical way of alleviating this difficulty. In this way any systematic habits or model concepts held by the analyst should not cause large random elements to enter into the results. The greatest chance for such a discontinuity to enter would be between the given operational analysis and the three simulated analyses but this difference enters more or less equally into all three resulting comparisons. Actually the analyst engaged in the second case was available for only a limited period and was unable to complete the analysis for the data array of figure 1B. The analyst for the first case completed the second case. One would expect this nonhomogeneous effect to be small since the data coverage dealt with was closest to the maximum thereby offering the least opportunity for varying interpretations. The results do not appear over-sensitive to this difficulty but differences between the two cases will be discussed in this light in connection with wind error results. The distribution of geostrophic wind errors was selected as the measure of forecast skill because Thompson's conclusions involve the wind error and also because this measure is perhaps of most interest to those making direct use of 500-mb. prognostic charts. The several mean distances between observations expressed by the data arrays were selected for two reasons: (1) They approximate familiar arrays which presently exist over limited regions, and (2) error fields thus produced have different characteristic wavelengths.

The coverage expressed in figure 1B closely approximates that now in existence over most of Canada. Figure 1C corresponds rather well to the present Atlantic coverage if one excludes reconnaissance data and also excludes a vast area south of 30° N. between Africa and the West Indies. Figure 1C approximates the spacing between present subtropical Pacific islands and corresponds in general to Pacific coverage without reconnaissance. The results thus indicate error levels corresponding to uniform hemisphere-wide data distributions which exist at present over certain segments of the hemisphere. From the standpoint of scale comparisons, the mesh lengths in figure 1B and 1D permit error fields having half wavelengths of approximately 360 n. miles and 720 n. miles, respectively. The half wavelengths of many synoptic disturbances having important local weather anomalies are shorter than the mesh length of figure 1D. There are likewise very few macro-scale disturbances (beyond their embryonic stages) which are characterized by half wavelengths less than the mesh size of figure 1B. The present study thus provides some empirical evidence bearing on the first three items listed by Thompson [3]: (1) Forecast range, (2) Initial wind error, and (3) Difference in scale between disturbances and error fields.

483854—58——2

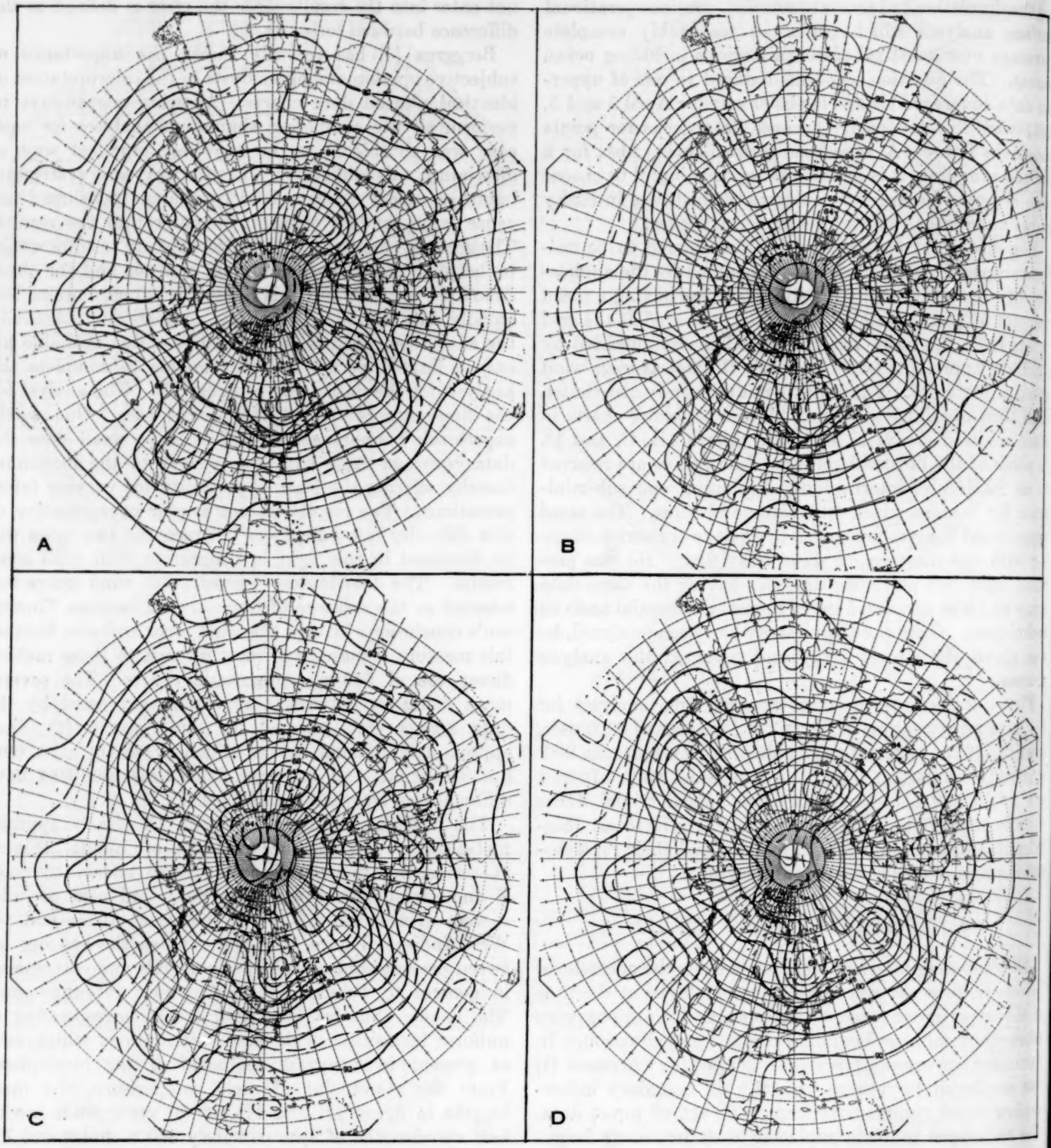

FIGURE 2.—500-mb. analyses for Case 1, 0300 GMT, April 3, 1957 based on data from the grid array with the corresponding letter in figure 1.

To summarize the procedure, the results which follow were obtained from the mentioned analysis procedure through the following computational steps:

a. Boundary heights contained in the input data decks were adjusted to a constant value as explained above.
b. Hemispheric barotropic 24-hr. and 48-hr. height forecasts from each input data deck were then produced by the current operational forecast code. This forecast procedure converts the input heights by using the balance equation (c. f. Shuman [6]) and produces the forecast internally from the resulting initial field of stream potential. The 24-hr. and

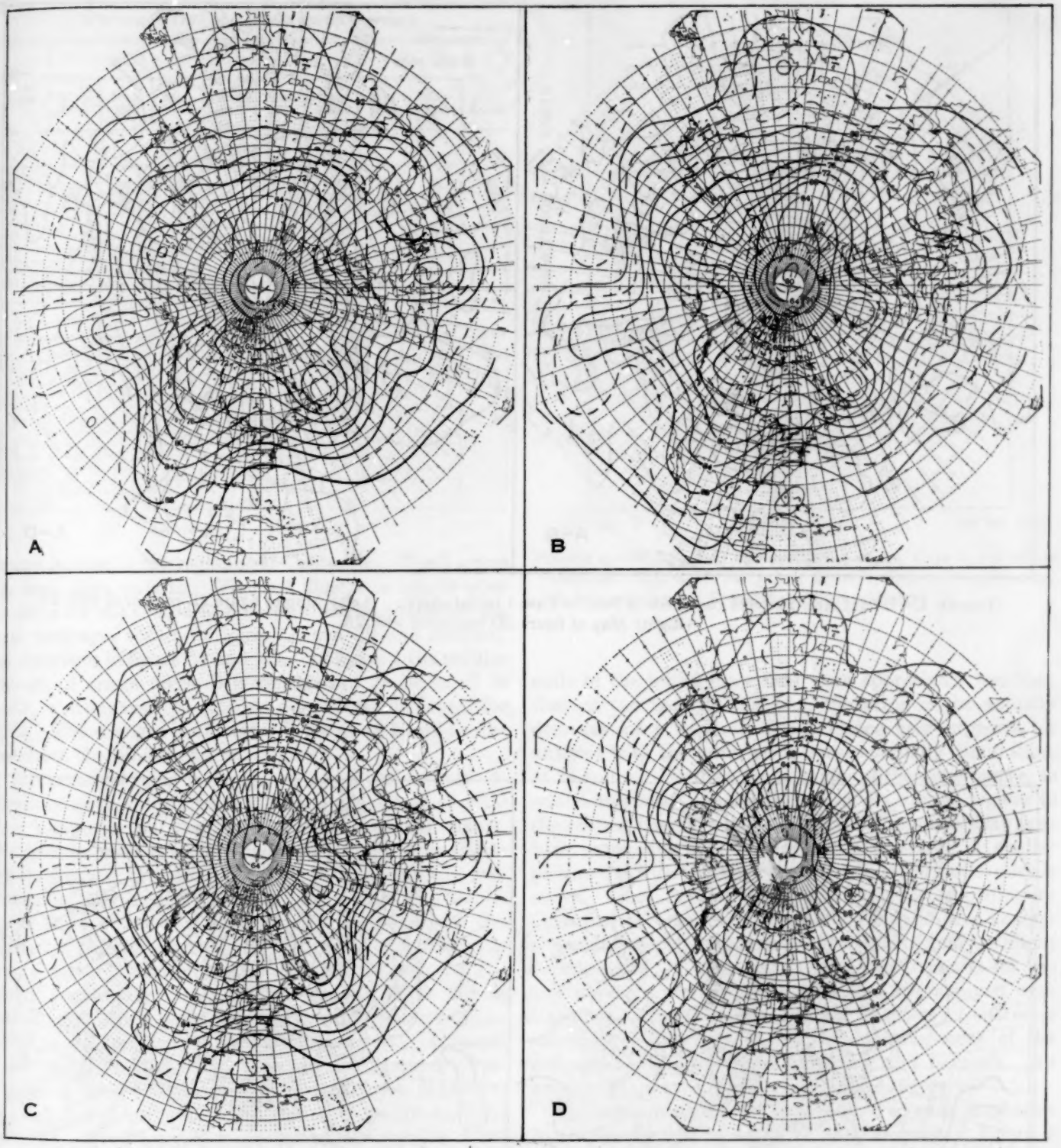

FIGURE 3.—48-hour forecasts made using the analyses of figure 2 as initial data.

48-hr. height output punch card decks are obtained by inverting back through the balance equation.

c. For each of the cases, the initial, 24-hr., and 48-hr. height field decks involving the data mesh size of figure 1A were compared with the corresponding decks involving the data mesh sizes of figure 1B, 1C, and 1D. A map showing height differences at grid points and a map of the corresponding wind errors were produced for each such comparison. Further, the wind errors were sorted by 10-knot intervals to indicate a frequency distribution.

Figure 3 displays the 48-hr. forecasts resulting from the corresponding initial charts of figure 2. Important phase differences are to be noted particularly in the

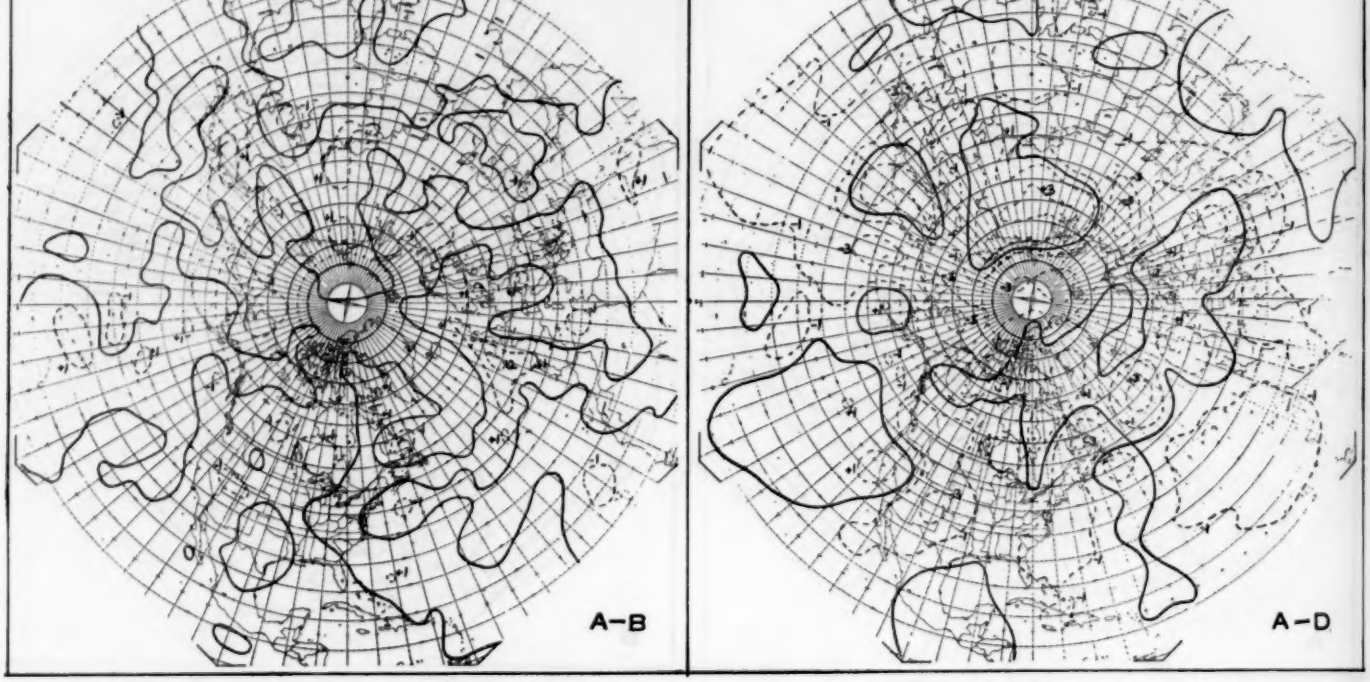

FIGURE 4.—Height error patterns (hundreds of feet) in Case 1 initial charts. (Left) Map of figure 2B compared with 2A. (Right) Map of figure 2D compared with 2A.

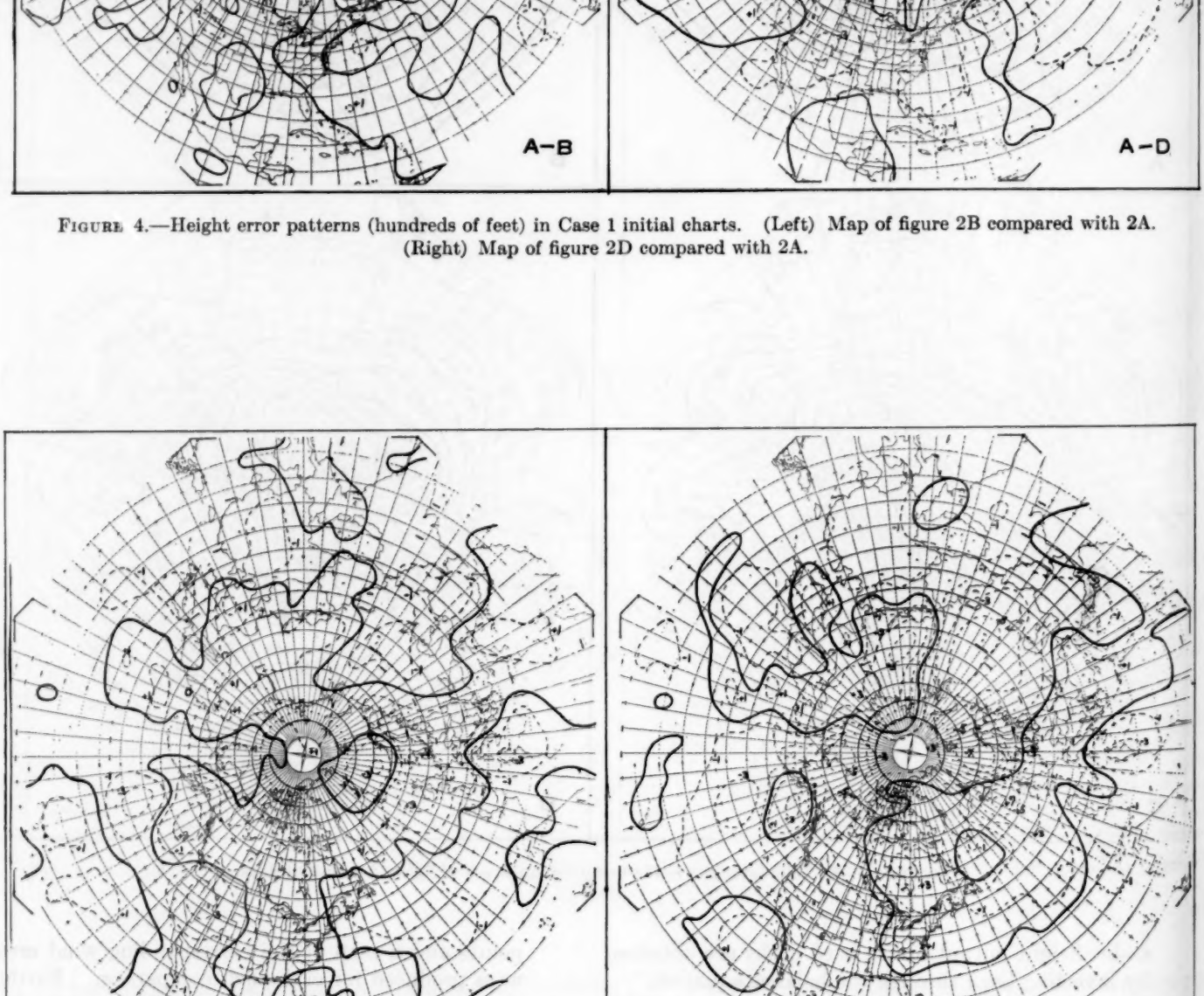

FIGURE 5.—Changes in the Case 1 height error fields at 48 hours (in hundreds of feet).

TABLE 1.—*Wind error frequency distribution: subjective analyses. (Percent of 1785 points with specified error.)*

Wind error (knots)	Initial			24-hr. forecast			48-hr. forecast		
	Max-Inter	Max-Min	Max-S-min	Max-Inter	Max-Min	Max-S-min	Max-Inter	Max-Min	Max-S-min
CASE 1									
0-10	66.2	52.5	42.0	68.6	55.2	41.5	55.4	43.4	32.7
10-20	29.2	36.5	42.9	27.7	35.6	39.4	34.5	37.0	39.3
20-30	4.1	8.5	11.3	3.4	7.8	14.8	7.5	13.4	17.6
30-40	.4	1.8	3.0	.2	1.2	3.9	2.2	4.9	7.1
40-50	.1	.3	.7		.3	.7		1.1	2.2
50-60		.1	.2			.7		.3	1.0
60-70		.1						.4	.2
70-80									.0
80-90									.1
CASE 2									
0-10	54.3	48.9	36.6	57.4	56.5	37.2	48.7	48.0	33.9
10-20	39.2	40.8	43.3	34.5	35.7	38.7	39.4	40.4	35.1
20-30	5.9	8.3	14.2	6.1	6.2	16.2	8.9	9.5	17.9
30-40	.6	1.5	4.3	1.3	1.3	5.5	1.7	1.8	7.0
40-50		.4	1.3	.4	.2	1.4	.9	.3	3.0
50-60		.2	.2	.1		.6	.3		1.6
60-70				.1		.2	.1		.8
70-80						.1			.2
80-90						.1			.1
90-100						.1			.1
100-110									.1
110-120									.1

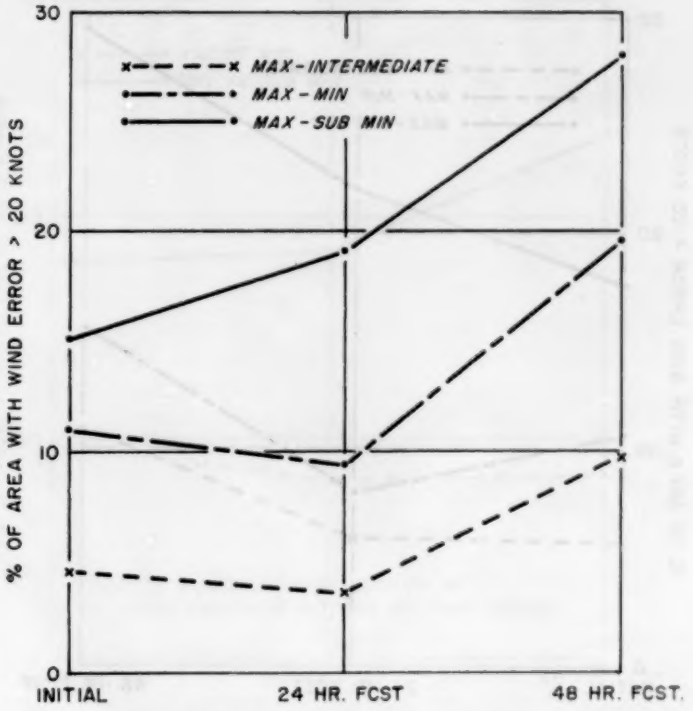

FIGURE 6.—Wind errors versus forecast range, Case 1, subjective analysis. Max=grid array A in figure 1, Intermdt=grid array B, Min=grid array C, and Sub-Min=grid array D.

trough feature in the region near California. Wind errors are even more striking. Figure 4 illustrates height error patterns for the comparison between initial charts having data coverages shown in figure 1A and 1B and similarly for coverages in figure 1A and 1D. In figure 4 the cellular pattern of errors for A–B is constrained to be small in scale as compared to similar quantities displayed for A–D. The changes in the error fields at 48 hours can be seen from the similar charts in figure 5.

The principal wind error results are given in table 1. Errors of each category are in terms of percent of total area computed on the basis of 1785 internal points. Wind errors were computed from the height error charts by considering the gradients diagonally across the grid squares of the basic 1977-point grid. This length corresponds to about 4° of latitude and approximates the portion of gradient normally used in hand measurements with a geostrophic wind scale. The results may be displayed graphically in a variety of ways. With such a limited sample it is perhaps better to suppress some of the detail in the frequency distribution of errors. A simple two-category breakdown is presented in figure 6. Percentage of area with wind errors over 20 knots is plotted as a function of forecast duration for the three comparisons involved. Even for rather intense winter regimes, a 20-knot wind error represents a large portion of the actual wind at 500 mb. From figure 6 it is first of all evident that the areas of large error increase rather uniformly as the data become more sparse with the sub-minimum (Pacific-type) coverage producing almost three times as much error as does the intermediate (Canadian-type) coverage. In addition, it is of interest to note that the minimum error is reached at 24 hours on the lower two curves whereas it occurs at the outset for the most sparse data array. According to Thompson [3], ". . . if the scale of the initial error field were appreciably less than that of the true fluctuations, the error might actually decrease for a while." The evidence here supports his analysis with the lower error curves actually diminishing at 24 hours. Further, the behavior of the upper curve, as relates to reality, implies that there are limited regions in the central Pacific, where, on occasion, predictability is at best extremely marginal. Case 2 produced a similar picture but with the lower curve much closer to the middle curve. Since the analysis with data corresponding to Canadian coverage was carried out by a different analyst one might speculate that different habits of analysis might be appearing. A comparison of the error charts for the two lower curves suggests rather that the analysis with Canadian coverage was smoothed in excess of the error tolerance in the data thereby eliminating some of the real small-scale error prescribed by the network. An average of the two cases is presented in figure 7.

The same evidence can be presented so as to emphasize more directly the question of data coverage. Figure 8 uses the same error parameter in the vertical coordinate and uses spacing between observations as horizontal coordinate. This treatment permits an estimate of error magnitude for any uniform data array. Unfortunately actual observations are not uniformly spaced except to a rough degree over limited areas. In some actual arrays one sees that isolated reports are called upon to yield detail that is clearly impossible. If one counts the number of observations in the outlined area of figure 9, excluding reconnaissance data, and weights all of them

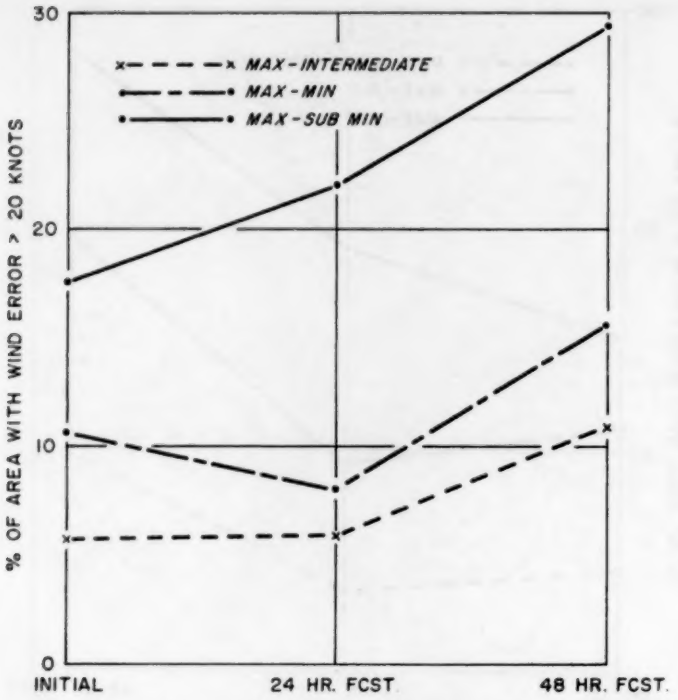

FIGURE 7.—Wind errors versus forecast range, average of Cases 1 and 2, subjective analysis.

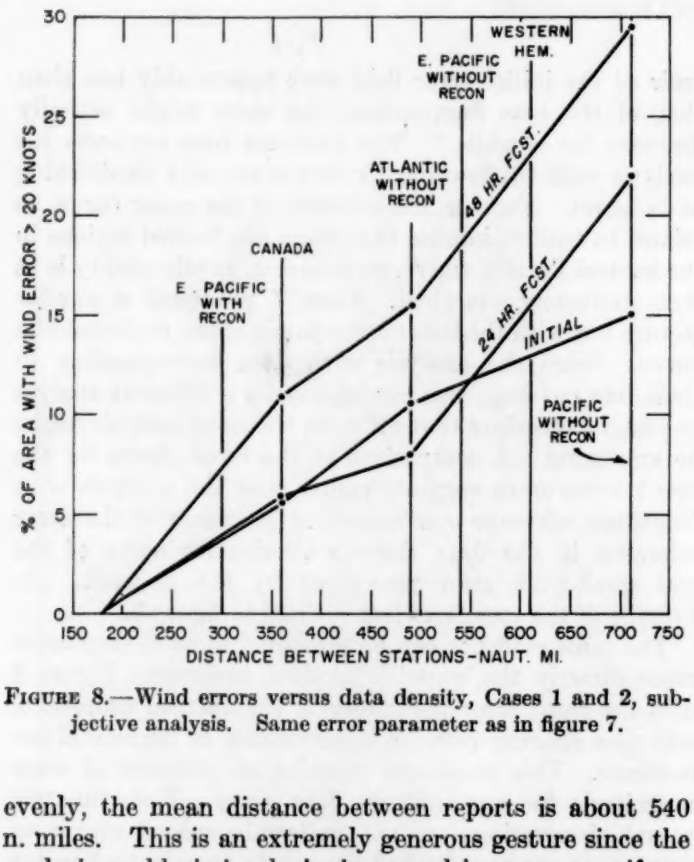

FIGURE 8.—Wind errors versus data density, Cases 1 and 2, subjective analysis. Same error parameter as in figure 7.

evenly, the mean distance between reports is about 540 n. miles. This is an extremely generous gesture since the analysis could obviously be improved by a more uniform redistribution. Even so, a uniform array of this dimension already is in a rather intolerable range of error as shown by figure 8. With the addition of the reconnaissance reports the again generous equivalent uniform array

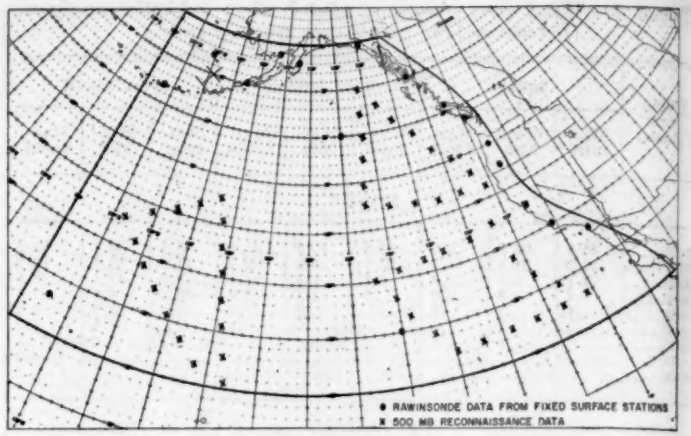

FIGURE 9.—Data coverage in eastern Pacific area.

has a data spacing of about 300 n. miles. The array, of course, still is not uniform and some of the reports are not strictly synoptic. By weighting reports by the area represented and including ". . . North America, the Caribbean Sea, the North Atlantic and most of the Pacific . . .", Thompson [3] arrived at an average distance of 610 n. miles as an equivalent mesh length for much of the Northern Hemisphere. The implication here is that if a certain data density is considered adequate for the resolution of synoptic features of a given scale, then more closely spaced data are partially redundant. Viewing from the standpoint of resolving the broad-scale features of the flow, Newton [1] cited several instances where a slight redistribution would greatly increase the value of reporting stations. The present study certainly supports such suggestions.

4. FURTHER TESTS USING OBJECTIVE ANALYSIS

The previously mentioned inhomogeneity in the subjective analyses of the second case and the large amount of chart work involved led to an attempt to enlarge the sample by using objective analysis. Accordingly a code was produced which formed an artificial input data tape to be used by the objective analysis program presently in routine use by the JNWP Unit. The data tape thus prepared contained data for the same arrays and modified them in the same manner as in the subjective analysis cases. One minor difference involved the application of random errors to the separate wind components thereby introducing variations in direction as well as speed.

The subjective analyst relies on data at other levels and a qualitative image from past data as a starting point. The technique of objective analysis used here relies more on a highly satisfactory quantitative image from past data—namely a 12-hour prognostic chart. In the present study, provision for a representative first approximation to the analyses posed a problem. In keeping with the spirit of the first cases, such a first approximation to the analysis should also reflect the analysis problems of the reduced data array. To avoid extensive

TABLE 2.—*Wind error frequency distribution: objective analyses. (Percent of 1221 points with specified error.)*

Wind error (knots)	Initial		24-hr. forecast		48-hr. forecast	
	Max-Min	Max-S-min	Max-Min	Max-S-min	Max-Min	Max-S-min
CASE 3						
0-10	56.6	42.8	58.4	43.2	56.8	37.8
10-20	33.7	39.1	33.4	38.2	34.8	38.3
20-30	7.4	13.7	6.9	13.2	7.0	15.6
30-40	1.6	3.2	1.2	3.4	1.2	5.5
40-50	.6	.8	.1	1.5	.2	2.0
50-60	.1	.4		.3		.7
60-70				.1		.1
CASE 4						
0-10	60.0	46.8	65.2	44.4	58.8	41.4
10-20	31.0	35.6	28.8	37.0	33.3	38.7
20-30	6.9	12.0	5.0	12.4	6.3	13.7
30-40	1.5	3.8	.9	4.9	1.6	4.5
40-50	.5	1.7	.1	1.3		1.4

iteration by machine to accomplish this goal, an alternate simulation scheme was employed. The operationally available 24-hour forecast from the preceding day was substituted as a first approximation. This somewhat less perfect image of the current upper flow pattern is considered to be comparable to an indirect derivation from concurrent lower-level information insofar as placement of major features is concerned. Such a forecast chart still would be expected to contain details of shear and curvature not resolvable with the most sparse data array of the experimental coverage network. Accordingly considerable smoothing was applied before substituting the forecast chart as the simulated first approximation for the analysis.

The resulting wind error information analogous to that in table 1 is presented in table 2. Case 3 employed somewhat less smoothing than did case 4. In general the main results of the subjective analysis experiments are duplicated. The comparisons involving the simulated intermediate data array (Canadian-type coverage) were not carried out. Figures 10 and 11 are to be compared with figure 6. Here one sees the same pattern. Initial analysis errors from the sub-minimum array (Pacific) are roughly twice as large as are the errors involving the minimum (Atlantic) array. Also the errors are reduced in both cases at 24 hours for the lower curve whereas they are not reduced in the upper curves. One important difference seems to be that the error growth rate is not as large for the upper curves in the objective analysis cases. Finally it should be pointed out the degree of smoothing was deliberately fixed in a separate trial case so that the scale of the error pattern initially was predominantly controlled by the mesh size of the reduced data arrays. To this extent the objective analyses were guided by the subjective tests. However this does not alter the result that, once the first approximation procedure is fixed, we see the same pattern of behavior as in the subjective cases when the data array is changed.

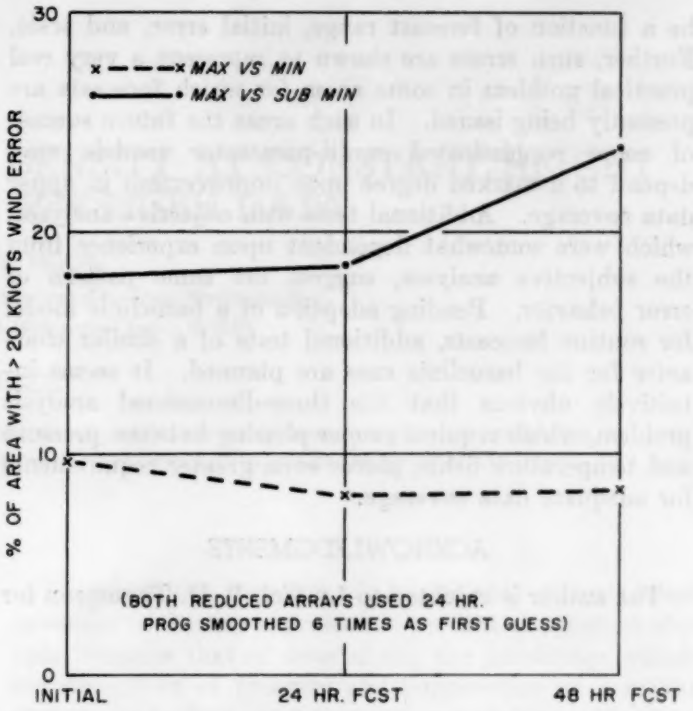

FIGURE 10.—Wind error versus forecast range, Case 3, objective analysis. Compare with figure 5.

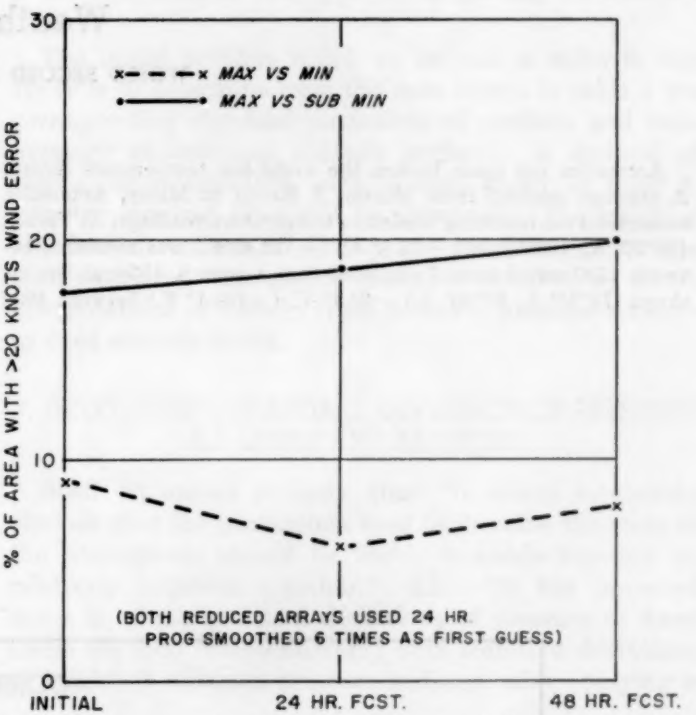

FIGURE 11.—Wind error versus forecast range, Case 4, objective analysis. Compare with figure 6.

5. SUMMARY AND CONCLUDING REMARKS

Two series of subjective analyses and the resulting barotropic forecasts indicate error behavior in accordance with that specified in Thompson's investigation. Specifically a measure of the forecast wind error is shown to

be a function of forecast range, initial error, and scale. Further, such errors are shown to represent a very real practical problem in some areas for which forecasts are presently being issued. In such areas the future success of more sophisticated multi-parameter models may depend to a marked degree upon improvement in upper data coverage. Additional tests with objective analyses, which were somewhat dependent upon experience from the subjective analyses, suggest the same pattern of error behavior. Pending adoption of a baroclinic model for routine forecasts, additional tests of a similar character for the baroclinic case are planned. It seems intuitively obvious that the three-dimensional analysis problem, which requires proper phasing between pressure and temperature fields, places even greater requirements for adequate data coverage.

ACKNOWLEDGMENTS

The author is indebted to Lt. Col. P. D. Thompson for valuable consultations and to Mr. J. Murray Mitchell, Jr. for his assistance in chart analysis

REFERENCES

1. C. W. Newton, "Analysis and Data Problems in Relation to Numerical Prediction," *Bulletin of the American Meteorological Society*, vol. 35, No. 7, Sept. 1954, pp. 287–294.
2. W. H. Best, "Differences in Numerical Prognoses Resulting from Differences in Analyses," *Tellus*, vol. 8, No. 3, Aug. 1956, pp. 351–356.
3. P. D. Thompson, "Uncertainty of Initial State as a Factor in the Predictability of Large Scale Atmospheric Flow Patterns," *Tellus*, vol. 9, No. 3, Aug. 1957, pp. 275–295.
4. G. 'Arnason, Personal Communication, 1958.
5. R. Berggren, "On the Accuracy of 500 mb. Analysis with Special Reference to Numerical Forecasting," *Tellus*, vol. 9, No. 3, Aug. 1957, pp. 323–340.
6. F. G. Shuman, "Numerical Methods in Weather Prediction: I. The Balance Equation," *Monthly Weather Review*, vol. 85, No. 10, Oct. 1957, pp. 329–332.

Weather Note

WORLD RECORD LOW TEMPERATURE

Antarctica has again broken the world low temperature record. A message received from Morton J. Rubin at Mirny, Antarctica announced the following minimum temperature readings: At Vostok (78°27′ S., 106°52′ E.) −85.8° C. (−122.4° F.) was measured between 1200 GMT August 7 and 0000 GMT August 8, 1958; at Sovietskaya (78°24′ S., 87°35′ E.) −86.7° C. (−124.1° F.) between 1900 and 2000 GMT, on August 9, 1958. The Sovietskaya minimum was measured with a remote electrical resistance thermometer with a known correction, exposed in the shelter. "The temperature was lower immediately afterward but no calibration for thermometer," the message stated.

CORRECTION

MONTHLY WEATHER REVIEW, vol. 86, July 1958, p. 253: In the second equation in column one b_1 should read $\sqrt{b_1}$.

ESTIMATING THE VARIANCE OF DENSITY AT CONSTANT HEIGHT FROM CONSTANT PRESSURE DATA

CONRAD P. MOOK

Diamond Ordnance Fuze Laboratories, Department of the Army, Washington, D. C.

[Manuscript received February 4, 1958; revised August 11, 1958]

ABSTRACT

A method is presented for utilizing atmospheric statistics developed for constant pressure surfaces in estimating the variance of density at constant height. The method depends upon recent advances in the study of the interrelation of atmospheric statistics.

1. INTRODUCTION

The determination of the variation with altitude of the standard deviation of density is of interest in many problems in aeronautics and ballistics. Dines [1] was perhaps the first to present observational upper-air data showing the magnitude of the variability of density about the mean at certain fixed altitudes. His data extended upward to 13 km.

However, in recent years, the practice of compiling upper-air statistics in terms of constant pressure surfaces rather than at intervals of constant altitude has become almost universal among the meteorological services of the world. This, though admirable from the point of view of synoptic meteorology, presents certain difficulties to those interested in obtaining summarized data for constant heights. The purpose of this report is to outline a procedure for approximating the vertical distribution of the standard deviation of density at constant height levels from constant pressure level statistics.

2. THE VARIABILITY OF DENSITY AT FIXED ALTITUDES

In 1919 Dines [1] showed how the standard deviation of the density at a given altitude could be estimated from the standard deviations of pressure and temperature. In Dines' derivation, the equation of state is differentiated logarithmically to obtain:

$$\frac{d\rho}{\rho}=\frac{dP}{P}-\frac{dT}{T} \tag{1}$$

Writing d, p, and t for the percentage variations of the quantities and squaring the result, he obtained:

$$\Sigma(d^2)=\Sigma(p^2)+\Sigma(t^2)-2\Sigma(pt) \tag{2}$$

which for small values of each term in equation (1), becomes

$$\left(\frac{\sigma_\rho}{\rho}\right)^2=\left(\frac{\sigma_P}{P}\right)^2+\left(\frac{\sigma_T}{T}\right)^2-2r_{PT}\left(\frac{\sigma_P}{P}\right)\left(\frac{\sigma_T}{T}\right) \tag{3}$$

Therefore the problem of determining the standard deviation of density expressed in percent at constant altitude becomes that of determining the percentage standard deviations of pressure and temperature at constant altitude and their coefficient of correlation. However as stated previously, data are now being made available only in terms of constant pressure surfaces. Table 1 contains data of this type for Goose Bay for January 1952.

The initial problem which we set out to solve in this study is to determine from the data shown in table 1 the corresponding standard deviations of pressure and temperature at constant altitude surfaces. A method of converting information, such as that shown in table 1, into the required form will be presented. The resulting standard deviations of density expressed in percent are then compared with similar statistics obtained by direct interpolations of density from constant pressure surfaces to fixed altitude levels.

3. DETERMINING STANDARD DEVIATION OF PRESSURE AT CONSTANT ALTITUDE

Buell [2] stated recently that "it seems intuitively obvious that the parameters used to describe the state of the atmosphere should be highly variable together or relatively constant together." Klein [3] has prepared maps in which standard deviations of pressure at fixed levels are used interchangeably with standard deviations of height of constant pressure surfaces, after applying a

TABLE 1.—*Average temperature and height for constant pressure surfaces and their standard deviations, Goose Bay, Labrador, January 1952.*

P (mb.)	$\overline{T}$ (° A.)	σ_{T_i}	$\overline{h}$ (m.)	σ_h
850	256.35	7.33	1319.27	65.37
600	248.60	6.05	3903.53	105.58
350	226.70	4.61	7648.24	169.50
200	218.82	5.99	11256.57	164.65
100	215.59	4.45	15654.14	154.78

constant conversion factor based on the hydrostatic assumption. The factor to be used can be conveniently obtained from the Smithsonian Meteorological Tables (Table 60) [4].

Thus the height change statistics in table 1 may be converted to pressure change statistics using the factor appropriate to the mean temperature at the given pressure surface. For example, for an assumed mean temperature of −20° C. at 600 mb., the ratio is 8.1 mb. per 100 m., and therefore the standard deviation of pressure at constant level in the vicinity of 600 mb. becomes:

$$\sigma_P=\frac{105.58\ (8.1)}{100}=8.44\text{ mb.} \tag{4}$$

4. DETERMINING STANDARD DEVIATION OF TEMPERATURE AT CONSTANT ALTITUDE

Stidd [5] has shown that the well known correlations between pressure and temperature at constant height (first presented by Dines [1]), also exist as a relationship between height and temperature at constant pressure. Therefore if a given temperature change in a constant pressure surface is associated with a change in height of that surface, the relationship can be used to determine approximately the temperature change which would occur at constant elevation.*

The coefficient of correlation r_{hT} may be computed directly or may be inferred from σ_h and σ_T statistics using the method of Stidd [5]. Both are shown in figure 1 which describes Goose Bay data for January 1952.

The average departure from mean temperature associated with a departure of one meter in the height of the constant pressure surface is, at 600 mb.:

$$b=r_{hT}\frac{\sigma_{T_i}}{\sigma_h}=.76\,\frac{6.05}{105.58}=.043 \tag{5}$$

where σ_{T_i} is the standard deviation of temperature at constant pressure.

Therefore at constant pressure, a 100-meter departure of height from the mean is associated with a 4.3° departure in temperature (of the same sign). Interpreted in terms of an increase in height of 100 meters, the increase in temperature which would occur at constant height would be approximately .65° C. greater than that at constant pressure, assuming a normal rate of decrease in temperature with altitude, as specified in the U. S. Standard Atmosphere in the troposphere [7].

Therefore

$$\sigma_T=\frac{4.95}{4.3}\,\sigma_{T_i}=1.15\sigma_{T_i} \tag{6}$$

where σ_T is the standard deviation of temperature at constant altitude.

At 600 mb. (from table 1)

$$\sigma_T=1.15\ (6.05)=6.96 \tag{7}$$

*Since the submission of this paper, the author has seen a paper by Crossley [6] discussing the inverse problem.

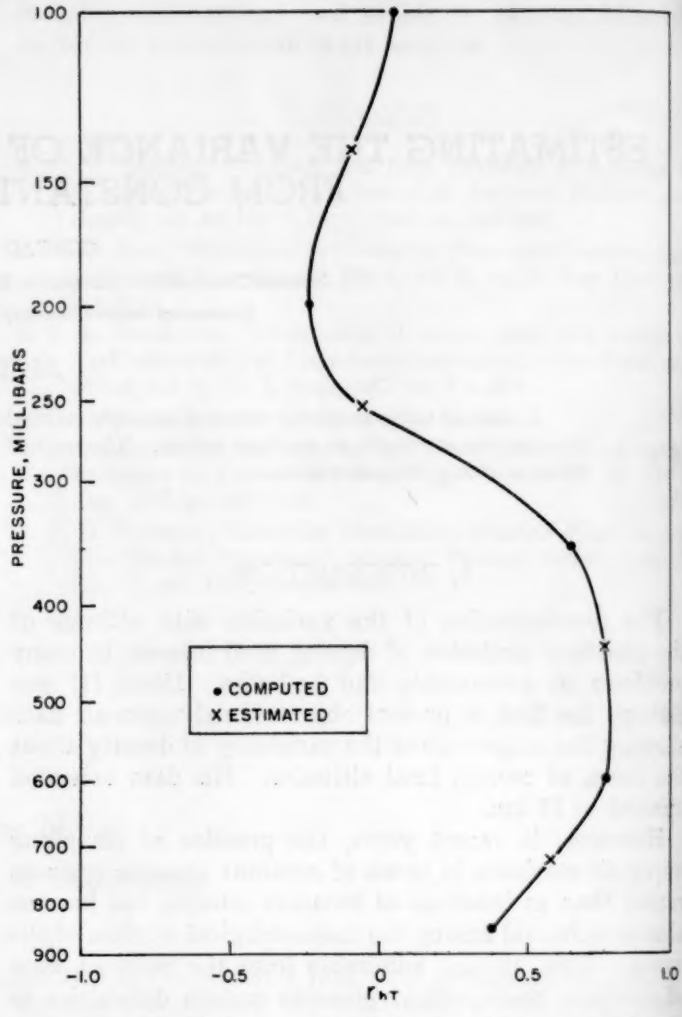

FIGURE 1.—Correlation coefficient between temperature change and height change of a constant pressure surface as computed and interpolated from σ_h and σ_T statistics.

5. INTERPRETATION OF CORRELATION BETWEEN TEMPERATURE AND HEIGHT

The remaining factor needed to evaluate the right side of equation (3) is r_{PT}. A formula for computing the coefficient of correlation where x and y are departures from their respective mean values is

$$r=(\sum xy)/\sigma_x\sigma_y \tag{8}$$

In the case wherein x and y are departures of height and temperature from their respective mean values, their standard deviations as well as their departures from the mean may be converted to constant level variations of pressure and temperature as shown in sections 3 and 4. Since the same multipliers are applied to both numerator and denominator of the right hand side of the formula for computing r, the two coefficients of correlation are equivalent, and thus may be used interchangeably.

6. APPLICATION OF THE DINES EQUATION

Having given the necessary variables in the Dines

equation we may proceed to the computation of the standard deviation of percentage density at Goose Bay at a level in the vicinity of 600 mb. as follows

$$\left(\frac{\sigma_\rho}{\rho}\right)^2=\left(\frac{8.44}{600}\right)^2+\left(\frac{6.96}{248.6}\right)^2-2(.76)\left(\frac{8.44}{600}\right)\left(\frac{6.96}{248.6}\right)$$

$$\frac{\sigma_\rho}{\rho}=1.95 \text{ percent}$$

This result may be compared with a computation of the standard deviation expressed as a percentage of mean density by actually interpolating to a fixed level between 600 and 550 mb. Such a procedure yielded 1.8 percent.

The procedure illustrated for the 600-mb. surface may be applied similarly at other elevations by using the following formula which combines the several steps expressed in general notation:

$$\frac{\sigma_\rho}{\rho}=\left[\left(\frac{a\sigma_h}{P}\right)^2+\left(\frac{(b+\Gamma_s)\sigma_{T_i}}{bT}\right)^2-2r_{hT}\left(\frac{a\sigma_h}{P}\right)\left(\frac{(b+\Gamma_s)\sigma_{T_i}}{bT}\right)\right]^{1/2}$$

Here a is the factor obtained from the Smithsonian Meteorological Tables for converting σ_h to σ_P, Γ_s is the assumed lapse rate (of NACA Standard Atmosphere, as used here), and other symbols are as previously defined.

The results of computations for Goose Bay at other pressure surfaces for January 1952 are shown in table 2.

As in the 600-mb. computation, a, the pressure change at constant level corresponding to a 10-meter height change of a constant pressure surface, was again obtained from the Smithsonian Meteorological Tables as shown in table 3. The temperatures assumed in table 3 are not precisely the mean values given in table 1, but they are within the limits defined by the standard deviation of temperature. This small departure from mean temperature has little effect on the final result. For example, if at 200 mb. the assumed temperature is varied ± 6° C., the resulting change in density variability is less than 0.1 percent.

TABLE 2.—*Standard deviation of percentage density for various pressure surfaces at Goose Bay, Labrador, January 1952 data*

Pressure (mb.)	Estimated $\frac{\sigma_\rho}{\rho}\times 100$	Interpolated $\frac{\sigma_\rho}{\rho}\times 100$
	(%)	(%)
850	3.1	2.7
600	1.95	1.8
350	2.3	1.9
200	4.1	4.3
100	3.1	3.0

TABLE 3.—*Values of "a" for various pressure and temperature combinations. From [4]*

Pressure (mb.)	Assumed temperature (° C.)	a (mb./10 m.)
850	−17	1.12
600	−20	.81
350	−46	.52
200	−50	.306
100	−57	.16

In the computations, the results of which are shown in table 2, an isothermal lapse rate was assumed to exist in the vicinity of 200 mb. and 100 mb., assuming that these surfaces were in the stratosphere [7]. Under this assumption the standard deviations of temperature at constant level were further assumed to be equivalent to those at constant pressure.

7. CONCLUSION

A procedure has been developed for estimating the vertical distribution of the standard deviation of percentage atmospheric density at constant height using data summarized with reference to constant pressure levels without specifying in advance the altitudes for which the estimates are to be made. However from these data, curves of percentage density variability vs. altitude may be constructed from which the percentage variability may be interpolated at any desired altitude.

REFERENCES

1. W. H. Dines, "The Characteristics of the Free Atmosphere," Great Britain Meteorological Office, *Geophysical Memoirs*, No. 13, 1919.
2. C. E. Buell, "An Approximate Relation between the Variability of Wind and the Variability of Pressure or Height in the Atmosphere," *Bulletin of the American Meteorological Society*, vol. 38, No. 2, Feb. 1957, pp. 47–51.
3. William H. Klein, "A Hemispheric Study of Daily Pressure Variability at Sea Level and Aloft," *Journal of Meteorology*, vol. 8, No. 5, Oct. 1951, pp. 332–346.
4. *Smithsonian Meteorological Tables*, 6th Rev. Ed., prepared by R. J. List, Smithsonian Institution, Washington, D. C., 1951.
5. C. K. Stidd, "A Note on the Application of the Hydrostatic Equation to Atmospheric Statistics," *Journal of Meteorology*, vol. 11, No. 2, Apr. 1954, pp. 165–166.
6. A. F. Crossley, "Relation between the Standard Deviations of Temperatures at Constant Pressure and at Constant Height," *Quarterly Journal of the Royal Meteorological Society*, vol. 76, No. 329, July 1950, pp. 337–340.
7. National Advisory Committee for Aeronautics, "Standard Atmosphere—Tables and Data for Altitudes to 65,800 feet," NACA TR 1235, 1955.

THE WEATHER AND CIRCULATION OF AUGUST 1958[1]

A Month with an Unusual Temperature Reversal

CHARLES M. WOFFINDEN

Extended Forecast Section, U. S. Weather Bureau, Washington, D. C.

1. INTRODUCTION

Over North America the mean flow pattern during August 1958 (fig. 1) was characterized by pronounced blocking in the extreme north and by a planetary wave in relatively fast westerlies at middle latitudes consisting of a ridge in the western United States and a trough in the East. In contrast to July 1958 [3], these features of the westerly circulations were near their climatologically preferred locations for the month and hence closely resembled the normal map but with slightly greater amplitude. They were responsible for an unusually warm regime in the West, which completely reversed the pattern of the previous month. A July-August reversal of this magnitude has occurred only once before in the past 17 years.

2. GENERAL CIRCULATION

The blocking High over northern Canada and its deep companion depression across the pole accounted for the two largest departures from normal (+410 ft. and −500 ft., respectively) which appear on the mean chart for the month (fig. 1). These two features became established early in the month, moved but little throughout the period, and completely dominated the weather of the polar basin and adjacent land areas. The polar Low was particularly persistent and vigorous, with a departure from normal at one stage in excess of 700 ft. (5-day mean map for Aug. 16–20, fig. 5). However, although a pronounced depression existed at high latitudes, the circulation over the remainder of Europe and Asia was weak and flat.

The trough normally found in the western Pacific was weak and ill-defined, with the principal Pacific trough lying well to the east between 150° and 160° W. This corresponded roughly to its position during July [3] and illustrates the tendency of this regime to persist, even though the long-period climatological statistics indicate that troughs are not at all favored in this longitudinal band in midsummer [7]. Though the amplitude of this feature remained small, its center averaged 240 ft. below normal, and it maintained sufficient vigor to sustain the downstream ridge in western North America and effectively fill the northern portion of the west coast trough, leaving the latter effective only at lower latitudes and well offshore. This constitutes a significant change from July [3] when this depression, though similarly confined to southerly latitudes, was deeper and lay inshore along the California coast. As a result of this filling and retrogression, the cyclonically curved flow, which characterized the July pattern in the West, was replaced by anticyclonic streamlines in August which resulted in profound changes in temperature and precipitation anomalies.

As mentioned, eastern North America and the Atlantic were strongly influenced by blocking. Twin warm Highs appear on the monthly mean pattern (fig. 1), one over northern Canada and the other over southern Greenland. These are associated with depressed polar vortices in eastern Canada and Iceland and the maintenance of a broad band of strong westerlies across the Atlantic at temperate latitudes. The jet stream, as illustrated by figure 2, reached a maximum speed of 14 m. p. s. at 45° N., 50° W., or 4 m. p. s. higher than the normal at that point. This broad westerly wind stream and the deeper than normal trough along the east coast, combined to favor recurvature of tropical storms at sea followed by rapid motion across the Atlantic.

3. HARMONIC ANALYSIS OF THE MEAN MONTHLY CHART

In recent years increasing study has been given to the spectrum of amplitudes and energy of meridional motions on the scale of the general circulation. Graham [5], for example, studied the latitudinal variation of the 17,800-ft. contour of the 500-mb. surface and found that the sum of the first three harmonics adequately describes the normal map for January. He also found that the total of these components remained nearly stationary on daily 500-mb. charts during the month of January 1952. More recently, others [4, 6, 11] have dealt with energy spectra of the meridional component of the circulation. In general it has been found that two distinct wave number bands exist in the atmosphere, one incorporating waves one through four, and the other wave number five and above. The first class of waves is semi-permanent and may be associated with the fixed topographic features of the earth's surface, while the second is connected with the smaller migratory systems.

In order to study the amplitude spectrum of meridional flow for August 1958, a harmonic analysis of the 700-mb. flow pattern was prepared, following the procedure described in [10]. The results are shown in figure 3 in which amplitudes are plotted against wave number for the latitudes 75° N., 60° N., 45° N., and 30° N. The pre-

[1] See Charts I-XVII following p. 328 for analyzed climatological data for the month.

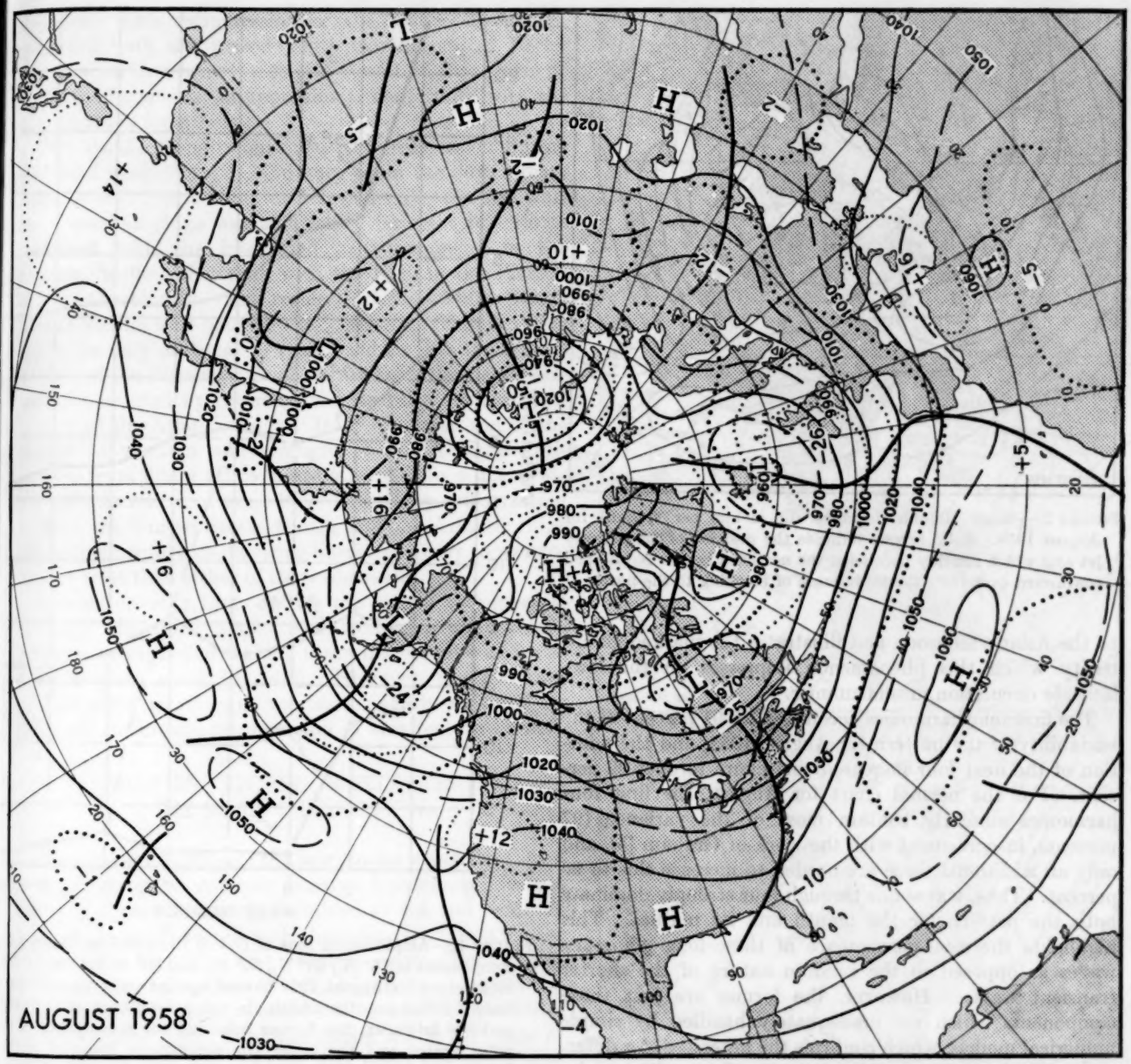

FIGURE 1.—Mean 700-mb. height contours (solid) and departures from normal (dotted) both in tens of feet with troughs indicated by heavy lines, for August 1958. The circulation pattern over North America included a ridge in the West and trough in the East. The trough along the west coast was weak and effective only at low latitudes.

eminence of the first harmonic at high latitudes is strikingly illustrated by the curve at 75° N. (and to a lesser extent by that for 60° N.). This reflects the existence of the two large anomaly centers on either side of the pole already described and indicates the degree of eccentricity introduced by such a circulation. The normal circulation for August similarly shows a maximum amplitude in wave one at 75° N. but only of about one-third the magnitude.

At 60° N. the maximum amplitude was still associated with the first harmonic, with a weak secondary peak beginning to appear in the fourth harmonic. This second maximum was also in evidence at 45° N. and 30° N. but displaced toward the higher wave numbers (dashed line). This characteristic dual maximum at temperate latitudes agrees roughly with the data of Eliassen [4] who found maximum amplitude at wave number one and again at wave number five, although his data were for a different level (500 mb.) and period (October 21 to November 30, 1950). Conspicuous in the graph for 30° N. was the very large amplitude accompanying the low wave numbers. However, interestingly enough, the normal also exhibits a similar distribution, except that the amplitude of the first harmonic is even larger, a surprising 167 ft. The phase angle is such in each instance that it is largely attributable

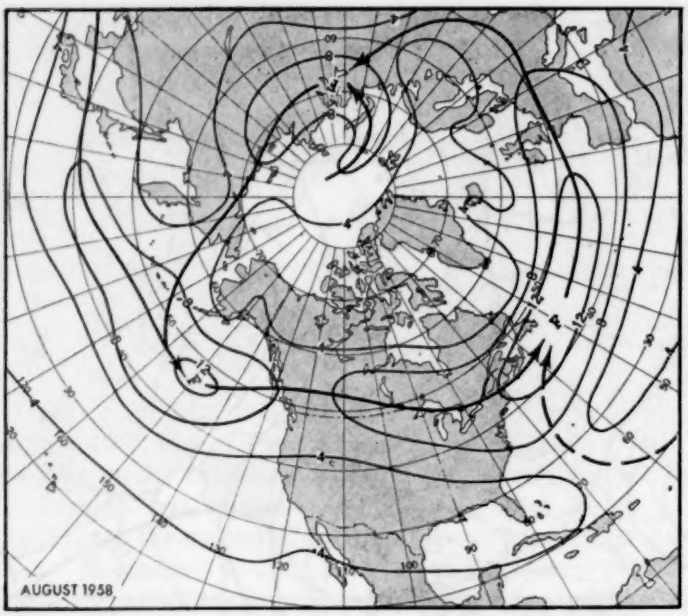

FIGURE 2.—Mean 700-mb. isotachs (in meters per second) for August 1958. Solid arrows indicate the position of the primary jet axis which roughly paralleled the northern border but dipped southward over the Atlantic because of blocking to the north.

to the Asiatic monsoon and illustrates the marked eccentricity which this phenomenon impresses on the low-latitude circulation in midsummer.

The first four harmonics accounted for 91 percent of the variability of the pattern for August 1958, and the addition of the next four increased this figure to over 99 percent. For the normal chart for August, the first four harmonics similarly contain most of the variance (97 percent), in agreement with the work of Graham [5], and only an additional three are needed to increase this to 99 percent. Thus, waves one through four strongly dominate both the pattern for the month and its normal. This highlights the semi-permanence of these long planetary waves as opposed to the random nature of the shorter transient waves. However, the former are just those components which are inadequately handled by simple numerical models, which confirms the necessity of a different approach to this problem, as recently emphasized by Burger [1]. A step in this direction was taken by the Joint Numerical Weather Prediction Unit at Suitland in an attempt to take into consideration the special behavior of these ultra-long waves [2, 12]. Also it was this consideration which led Namias [9] to incorporate the extraction of "latitudinal anomalies" as an integral part of his "basic current" model.

4. RETROGRESSION OF 5-DAY MEAN FEATURES

As is often the case, considerable variation about the monthly mean occurred, and one of the more interesting trends discernible on 5-day mean charts was a long-period retrogression. To illustrate this tendency, three 5-day mean maps centered one week apart were selected (fig. 4).

In the initial state, represented by the chart for August

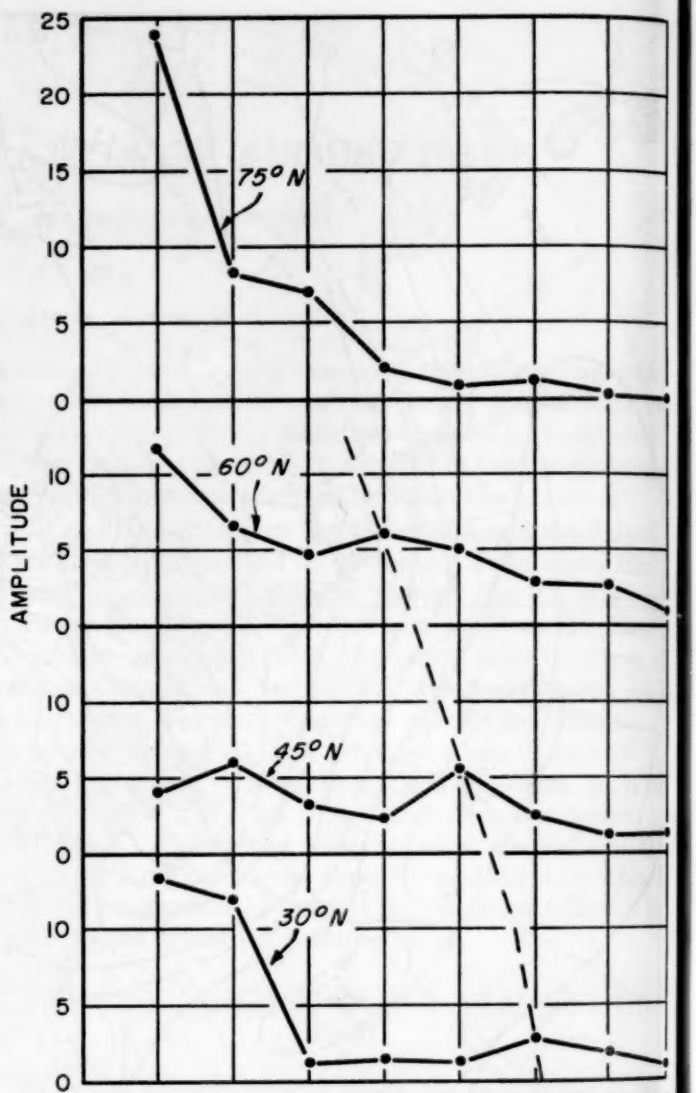

FIGURE 3.—Amplitude in tens of feet of the zonal harmonic wave components at 75° N., 60° N., 45° N., and 30° N. for the 700-mb. mean chart for August 1958 plotted against wave number. For wave number one the amplitude was a maximum at both high and low latitudes, the former reflecting the eccentricity of the polar vortex and the latter the eccentricity imposed by the Indian monsoon. A secondary peak appeared at 60° N. in the fourth harmonic which was displaced toward higher wave numbers.

7 to 11 (fig. 4A), a fast westerly flow characterized the circulation with two pronounced troughs in the Pacific and a third off the United States east coast. One week later (fig. 4B) the pattern in the Pacific underwent a major transformation. The deep trough off Japan filled abruptly, resulting in an extended wavelength between the eastern Pacific trough and its new upstream counterpart over eastern Asia. It adjusted to the new situation by retrograding to the position shown in figure 4B, leaving in its wake a cut-off and greatly weakened trough near the California coast. This was associated with a westward displacement of the ridge-trough structure over North

America. This retrogression of the east coast trough coincided with the period when tropical storm Becky was approaching recurvature and permitted that storm to recurve off the coast in approximate conformity with the normal track for August.

The Pacific trough continued its retrogression during the third week (fig. 4C), and once again the downstream features over North America followed suit. By this time the Canadian ridge was sufficiently far west to become realigned with the intensified maritime ridge in the eastern Pacific rather than with the High in the Plateau States as previously. As a result, the United States trough shifted all the way back to the Mississippi Valley, which led to the only outbreak of really cold air into the central portion of the country. At this time, the Atlantic circulation also reacted by reversing the tendency for eastward motion of the Atlantic ridge. In fact, comparison of the change in position and strength of the Atlantic anticyclone from figure 4B to figure 4C indicates a net westward displacement of some 10°. This sharp retrogression of both the United States trough and the Atlantic ridge was instrumental in influencing hurricane Daisy to recurve farther west than either of its predecessors.

It is noteworthy that, despite the overall retrogressive tendency described above, the trough in the eastern Atlantic succeeded in making eastward progress as far as the European coast (fig. 4C). However, the resultant overextended wavelength was subsequently adjusted by rapid discontinuous retrogression of this feature as well.

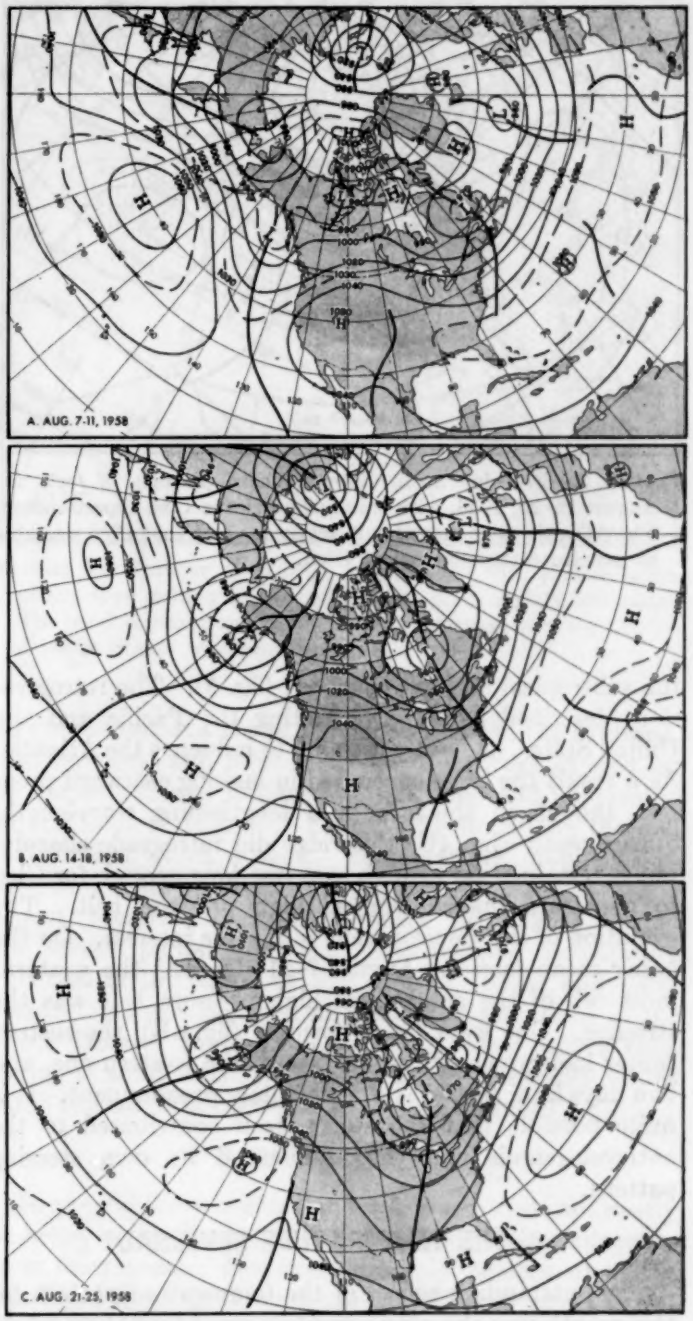

FIGURE 4.—Five-day mean 700-mb. charts (in tens of feet) for (A) August 7–11, (B) August 14–18, and (C) August 21–25, 1958. The filling of the deep mean trough in the western Pacific resulted in retrogression of the west coast trough the following week (B) and of the United States trough and Atlantic ridge the third week (C). After the first period the west coast trough was weak and confined mainly to low latitudes.

5. TROPICAL STORMS IN RELATION TO THE MEAN CIRCULATION

During August, three of the four storms which developed over the tropical Atlantic became hurricanes. Except for Ella, these fortunately remained at sea and recurved offshore, in rough accord with the mean circulation for the month (fig. 1). The first tropical storm, Becky, was detected near the Cape Verde Islands on August 10, though its exact position could not be established until a reconnaissance flight fixed the center about 20° east of San Juan on the 12th. From that point the storm continued moving westward at a rapid rate, averaging over 20 knots over its entire course prior to recurvature and at one time reaching a forward motion of 25 knots. As it came under the influence of the mean trough along the east coast it turned northward and recurved well offshore (Chart X). Becky never attained full maturity as a hurricane but remained fairly weak over most of its long trajectory.

On the other hand, Cleo, the second storm, which followed Becky by only two days, was already a severe hurricane when first explored by reconnaissance on August 14 when about 750 miles east of the Lesser Antilles. Although reports were insufficient to establish a definite track, it is probable that this storm had its origin in a tropical depression to the southeast of the Cape Verde Islands on the 11th. If this is the case, it progressed rather rapidly (about 21 m. p. h.) over the first portion of its journey, but deceleration must have begun near 45° W. prior to the reconnaissance penetration of the storm since thereafter it moved more slowly and shifted to a more north-northwesterly course (fig. 5).

The key transformation, accompanying this shift in trajectory from that of Becky appears to have been the eastward motion of the Atlantic ridge and the splitting of

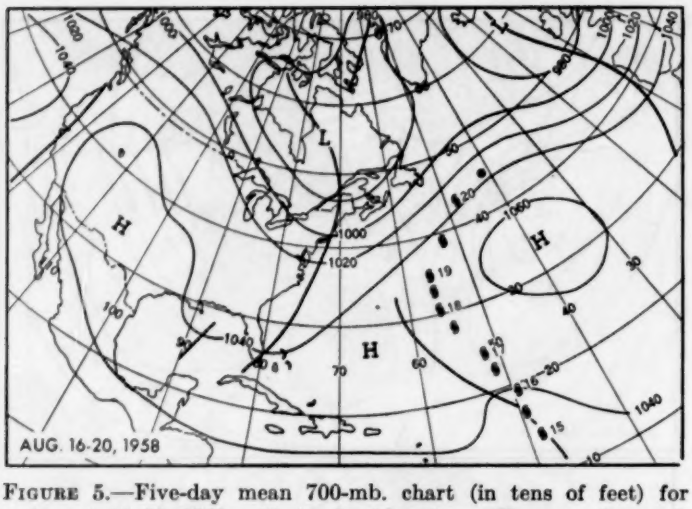

FIGURE 5.—Five-day mean 700-mb. chart (in tens of feet) for August 16–20, 1958, with track of hurricane Cleo superimposed. The Atlantic ridge moved sufficiently far east that Cleo was able to penetrate the subtropical High.

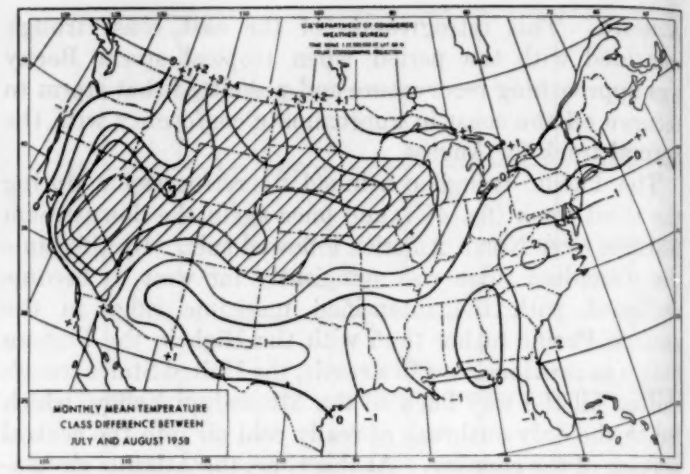

FIGURE 6.—The number of classes the anomaly of temperature changed from July to August 1958. A marked reversal in temperature took place over a broad area in the West and North Central Plains.

the subtropical high pressure cell (fig. 5). The retrogression, described earlier as affecting the Pacific and the United States, had not yet begun to influence the Atlantic. As a result the ridge succeeded in making eastward progress, though in the face of a lengthening wavelength. Subsequently (fig. 4C) this ridge did retrograde sharply, but it remained far enough east just long enough for Cleo to penetrate the subtropical high pressure belt. The evolution of this development is of some interest. On the 5-day mean map for August 7–11 (fig. 4A) the westernmost cell of the subtropical high pressure belt was the stronger. One week later, however (fig. 4B), the eastern center had grown at the expense of the western one, and two days later (fig. 5) it was definitely predominant. It is quite possible that the storm itself contributed to the anticyclogenesis and thus influenced its own steering pattern.

6. THE TEMPERATURE REVERSAL

The outstanding aspect of the temperature pattern for this month was the pronounced reversal from July which took place over most of the western portion of the country. Ordinarily, the reverse is true and the transition from July to August has usually been characterized by marked stability of the temperature pattern. In fact, in a study based on the period 1942 through 1950 and later extended to 1957, Namias [8] found persistence to be higher between this pair of months than for any other pair during the year. In his paper, persistence was expressed in terms of the percentage of stations at which the temperature did not vary by more than one class (out of five). For the change from July to August this statistic turned out to be 80 percent, the maximum for the year. This August, however, only 59 percent of the stations fell within this interval. Since the chance expectance of this event is also 59 percent, no significant persistence occurred. During the past 17 years, only August 1947 had a lower persistence tendency, with 51 percent.

In August 1958, warming of two classes or more (cross hatched in fig. 6) encompassed an extensive area from the interior of California to Illinois, with maximum change (four classes) over Nevada and western Montana. The departure from normal of the monthly mean temperature rose 9.5° and 9.2° at Billings and Havre, Mont., respectively, and 9.1° at Winnemucca, Nev., to cite the three highest. These are unusually high figures and highlight the unusual nature of the change which occurred this month.

The key changes in circulation accompanying this reversal in pattern have already been described in section 2, namely, the strong ridging in the West which changed the flow from cyclonic in July to anticyclonic in August and relegated the west coast trough to a minor role offshore.

Temperatures along the Pacific coast continued well above normal for the fourth successive month. Record warmth for August was reported from several locations in Oregon and from Seattle, Wash. Tatoosh Island experienced the warmest August in at least 56 years, and record or near record temperatures were the rule at most California coastal locations. This prolonged period of warmth along the Pacific coast has constituted one of the most distinctive characteristics of the temperature regime so far this year and has been linked to abnormally warm ocean temperatures in previous articles of this series [3]. While a similar effect in all likelihood continued this month, the heat wave in the West can be adequately explained in terms of the large-scale ridging in the West, above normal sunshine, and southerly components of flow.

In general, temperatures in the rest of the country remained nearer normal, ranging slightly above normal over the Appalachians and eastward and slightly below normal over the States bordering the western Lakes and in

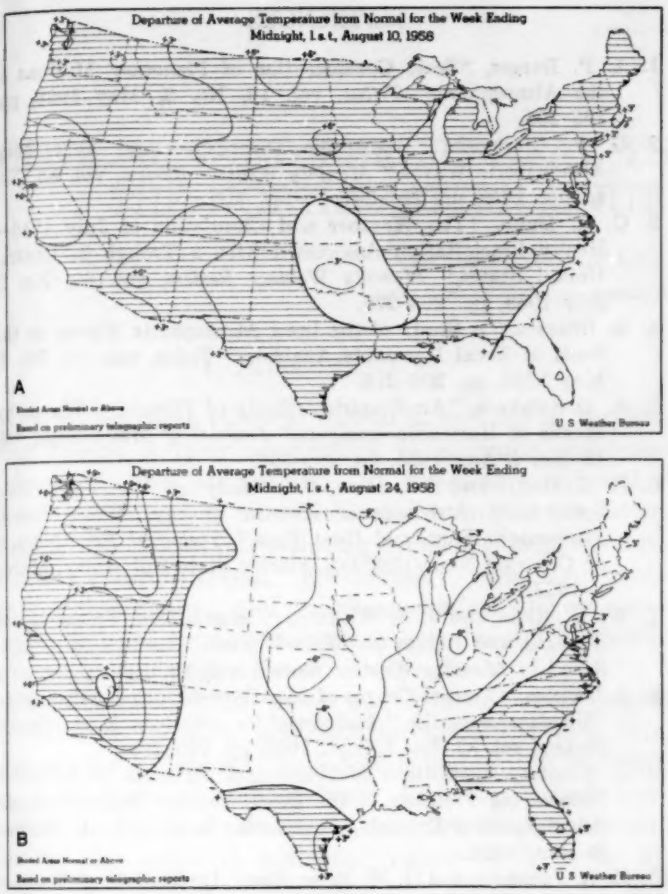

FIGURE 7.—Departure of average surface temperature from normal (° F.) for the weeks ending at midnight (A) August 10 and (B) August 24. The abnormal warmth which prevailed during the first period, especially over the Northern Plains, was followed two weeks later by an intense cold snap affecting central portions of the country.

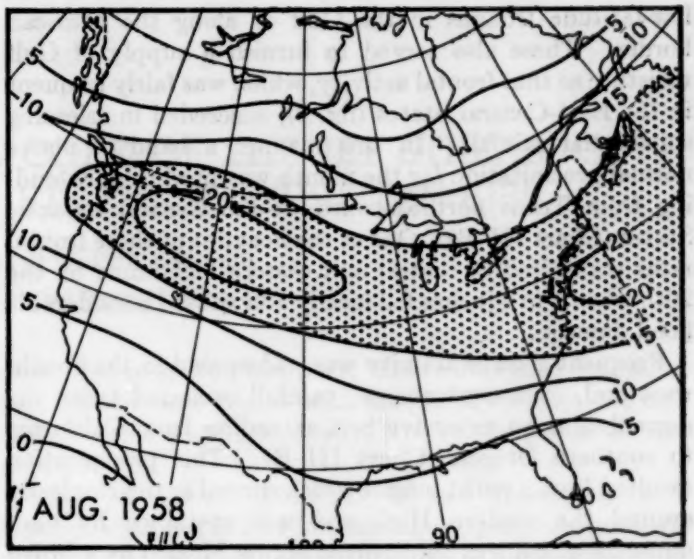

FIGURE 8.—Number of days in August 1958 with surface fronts of any type (within squares with sides approximately 500 miles). The band of maximum frontal activity extended from the Central Atlantic States west-northwestward.

the Ohio and Lower Mississippi Valleys. Departures from normal were small because a warm regime early in the month was largely cancelled in the mean by a marked outbreak of polar air in the eastern two-thirds of the country toward month end. Figure 7A was selected to represent the warm regime. During this week temperatures were unseasonably high nearly everywhere but, relative to normal, were warmest in the northern Great Plains and Southwest where temperatures ranged up to 6° above normal. Maximum temperatures in the northern Great Plains rose into the 100's on the 8th and 9th, and Bismarck, N. Dak. recorded 107° F., the highest there since 1949. For these States and for those bordering the Lakes, where June and July had been unusually cool, this was the first real taste of summer weather. The circulation for this period (fig. 4A) was characterized by broad westerly flow along the northern border with mainly anticyclonic curvature. However, it will be recalled from section 4 that the stage was about to be set for a large-scale retrogression of planetary waves on 5-day mean maps. This was accomplished by the week of August 18–24, and during this period (fig. 4C) the principal mean trough became entrenched over the Mississippi Valley, bringing an abrupt termination to the hot weather in the Midwest. The strongest and most widespread outbreak of cold air of the month was initiated at this time and penetrated to the Gulf of Mexico. Figure 7B depicts the thermal distribution which ensued. Temperatures dropped rapidly, and Madison, Wis. recorded 37° F. on the 25th, the lowest temperature reached there in August during the 80-year period of record. Near-freezing temperature occurred in the region of the western Lakes, and early season frost was reported in the higher elevations in the Black Hills of South Dakota. Thus, after only a brief period of summerlike weather in the Midwest, conditions more typical of fall were suddenly reintroduced.

7. PRECIPITATION

In general the precipitation for August, while not nearly as heavy as for June and July, was nevertheless adequate over most areas. However, the July pattern of heavy rains and flooding through the Ohio Valley and Central Plains continued to dominate early August. Flood stages maintained in a number of streams in Illinois and Indiana; some of these streams had been in flood since about mid-June. A record 30.0-ft. stage was reached at New London, Mo. as a result of rains in excess of 6 in. in the upper reaches of the Salt River. This exceeded the previous high reached in June 1928 by 1.2 ft. Thereafter, however, these excessive rains terminated as the ridge moved into the Midwest and brought warm drying winds to the area.

During this period, when the subtropical ridge was at its strongest across the Atlantic and the Southern States (fig. 4A), onshore winds and easterly wave activity brought tropical rains to the Gulf States. In fact, this type of activity was quite prominent during August, and a number of 5-day mean maps (figs. 4, 5) exhibit pieces of weak

483854—58——3

low-latitude troughs in the Gulf or along the Mexican border. These also served to furnish a supply of Gulf moisture so that frontal activity, which was fairly frequent in the East-Central States (fig. 8), succeeded in releasing substantial rainfall. In this manner a band of above normal precipitation for the month was produced, extending from Texas northeastward to the Central Atlantic States (Chart III–B). One of the heaviest of these frontal rains transpired in central and eastern Oklahoma on the 20th when 5 to 9 inches fell locally and caused considerable flood damage.

Frequent shower activity was widespread in the Southwest and, as a consequence, rainfall exceeded twice the normal over an extensive belt extending from California to southern Oregon (Chart III–B). This precipitation resulted from a moist tongue which curved anticyclonically around the western High and was sustained by Gulf moisture which was transported across Mexico by a broad current from the east-southeast.

During this period Blue Canyon, Calif. reported the greatest number of thunderstorms ever to occur in August; Winnemucca, Nev. experienced the wettest August of record; and heavy showers and even a few flash floods occurred over the southern Sierras and desert regions of California. On the other hand, Grand Junction, Colo., which lay in the dry tongue on the opposite side of the mean ridge, (fig. 1), experienced the driest August in the station record which dates back to 1892

In the Northwest, which remained hot and tinder-dry for the entire month, a serious range and forest fire hazard developed. Scores of fires were reported in the mountains of Oregon with several reaching significant proportions before being brought under control. Also, lightning started many fires in the Sequoia National Forest and other brush and forest covered regions of California.

REFERENCES

1. A. P. Burger, "Scale Consideration of Planetary Motions of the Atmosphere," *Tellus*, vol. 10, No. 2, May 1958, pp. 195–205.
2. G. P. Cressman, "Barotropic Divergence and Very Long Atmospheric Waves," *Monthly Weather Review*, vol. 86, No. 8, Aug. 1958, pp. 293–297.
3. C. R. Dunn, "The Weather and Circulation of July 1958—Heavy Precipitation Associated with a Trough in Central United States," *Monthly Weather Review*, vol. 86, No. 7, July 1958, pp. 268–276.
4. E. Eliassen, "A Study of the Long Atmospheric Waves on the Basis of Zonal Harmonic Analysis," *Tellus*, vol. 10, No. 2, May 1958, pp. 206–215.
5. R. D. Graham, "An Empirical Study of Planetary Waves by Means of Harmonic Analysis," *Journal of Meteorology*, vol. 12, No. 4, Aug. 1955, pp. 298–307.
6. R. M. Henry and S. L. Hess, "A Study of the Large-Scale Spectra of Atmospheric Kinetic Energy, Wave Speed, Momentum Flux, and Heat Flux," *Technical Report* No. 9 on Contract Nonr–1600(00), Florida State University, March 1, 1957.
7. W. H. Klein and J. S. Winston, "Geographical Frequency of Troughs and Ridges on Mean 700-mb. Charts," to be published in *Monthly Weather Review*, vol. 86, 1958.
8. J. Namias, "Annual Course of Month-to-Month Persistence in Climatic Anomalies," *Bulletin of the American Meteorological Society*, vol. 33, No. 7, Sept. 1952, pp. 279–285.
9. J. Namias, Application of Numerical Methods to Extended Forecasting Practices in the U. S. Weather Bureau, unpublished report of Extended Forecasting Section, U. S. Weather Bureau, 1958.
10. H. A. Panofsky and G. W. Brier, *Some Applications of Statistics to Meteorology*, The Pennsylvania State University, 1958, 224 pp. (See Chap. VI.)
11. R. M. White and D. S. Cooley, "Kinetic-Energy Spectrum of Meridional Motion in the Mid-Troposphere," *Journal of Meteorology*, vol. 13, No. 1, Feb. 1956, pp. 67–69.
12. P. M. Wolff, "The Error in Numerical Forecasts Due to Retrogression of Ultra-Long Waves," *Monthly Weather Review*, vol. 86, No. 7, July 1958, pp. 245–250.

VERTICAL WIND SHEARS NEAR THE CORE OF THE JET STREAM OVER THE NORTHEASTERN UNITED STATES, AUGUST 1–2, 1958

ROBERT O. COLE AND LLOYD W. CHAMBERLAIN

National Weather Analysis Center, U. S. Weather Bureau, Washington, D. C.

1. INTRODUCTION

One of the most valuable uses of knowledge of vertical wind shears is their application to planning optimum flight paths for jet aircraft. In forecasting winds for aircraft, their use as an incremental term has tended to simplify the task of interpolating winds between standard constant pressure levels. Furthermore, from the standpoint of flying safety and passenger comfort, the observation of extreme vertical shears has been helpful in identifying regions of possible clear air turbulence.

On August 1, 1958 there was evidence that strong vertical wind shears existed near the core of the jet stream over the northeastern United States, and within 24 hours the magnitude of these shears had diminished considerably. Wind shears computed directly from rawin reports (see table 1) indicated values as large as 21 kt./1000 ft. Shears of this magnitude greatly exceed the value of 10 kt./1000 ft. which has been regarded as critical enough to divert a jet aircraft from its optimum flight path [1]. The purpose of this article is to analyze the conditions under which these extreme vertical wind shears occurred and to demonstrate their effective usefulness by integrating them into a vertical wind shear chart.

2. RELATIONSHIP OF SYNOPTIC FEATURES AND JET STREAM MODEL

At 0000 GMT, August 1, the 250-mb. chart (fig. 1A), which usually represents the standard level nearest the core of the jet stream, indicated a Low over eastern Canada with a flat short-wave trough extending southwestward from the Gulf of St. Lawrence to southeastern Michigan. The wind flow over the northeastern United States was generally from the west or northwest and contained two jet streams which tended to approach each other over New England. One wind speed maximum was located near Maine with speeds of at least 120 kt., and the other was near Albany, N. Y. with speeds of more than 100 kt.

TABLE 1.—*Occurrence of large vertical wind shears, August 1–2, 1958*

Location	Date	Time (GMT)	Magnitude (kt./1000 ft.)	Height (Thsds. of ft.)	Depth (ft.)
Caribou, Maine	1	0000	−10	35–40	5000
Idlewild, N. Y.	1	0000	20	40–41	1000
Idlewild, N. Y.	1	0000	−12	41–43	2000
Dayton, Ohio	1	0600	−9	44–46	2000
Caribou, Maine	1	1200	−18	46–48	2000
Dayton, Ohio	1	1800	15	28–30	2000
Dayton, Ohio	1	1800	−9	30–32	2000
Pittsburgh, Pa.	2	0000	−21	40–43	3000
Idlewild, N. Y.	2	0000	9	30–35	5000
Dayton, Ohio	2	1200	9	32–40	8000

Both jet stream positions seemed reasonably well located with respect to horizontal temperature gradient and contour spacing. Associated with the northern jet was a steep tropopause slope, while the southern jet appeared to be related to the surface frontal system. The surface front at this time was quasi-stationary with weak minor waves and extended westward from the Atlantic Ocean to a position south of Idlewild, on Long Island, N. Y., and into central Ohio. In view of the upper confluent pattern superimposed on the surface front, it seemed unlikely that any strong development was possible at this time.

In conjunction with this synoptic pattern, Caribou, Maine reported a maximum vertical wind shear near the core of the jet of −10 kt./1000 ft. and Idlewild reported 20 kt./1000 ft. The strong shear at Caribou occurred over a 5000-ft. layer located above the jet stream, to the rear of the trough, and in relation to a steep tropopause slope. When compared to the jet stream models described by either Endlich [2] or Riehl et al. [3], the magnitude of Caribou's vertical wind shear seemed quite valid, especially since it was apparently associated with strong horizontal wind shears to the left of the jet.

While the northern jet stream was either over or just south of Caribou, the southern jet was at least 120 miles north of Idlewild. As would be expected, there was no evidence of strong horizontal temperature gradients south of the jet stream, yet Idlewild reported a positive shear of 20 kt./1000 ft. over a 1000-ft. layer beneath the peak wind and a shear of −12 kt./1000 ft. over a 2000-ft. layer above the peak wind. The short-wave trough at this time was about 250 miles northwest of Idlewild and the slope of the tropopause in the area was negligible.

According to the jet stream model, the largest vertical wind shears are usually found just above the core of the jet stream and on the left or cold side in conjunction with strong horizontal wind shears and temperature gradients. Strong vertical shears have also shown some tendency to be associated with strong peak winds, but the correlation was found by Dvoskin and Sissenwine [4] to be rather low. When compared to the jet stream model, the magnitude of Idlewild's extreme vertical shears seemed highly questionable.

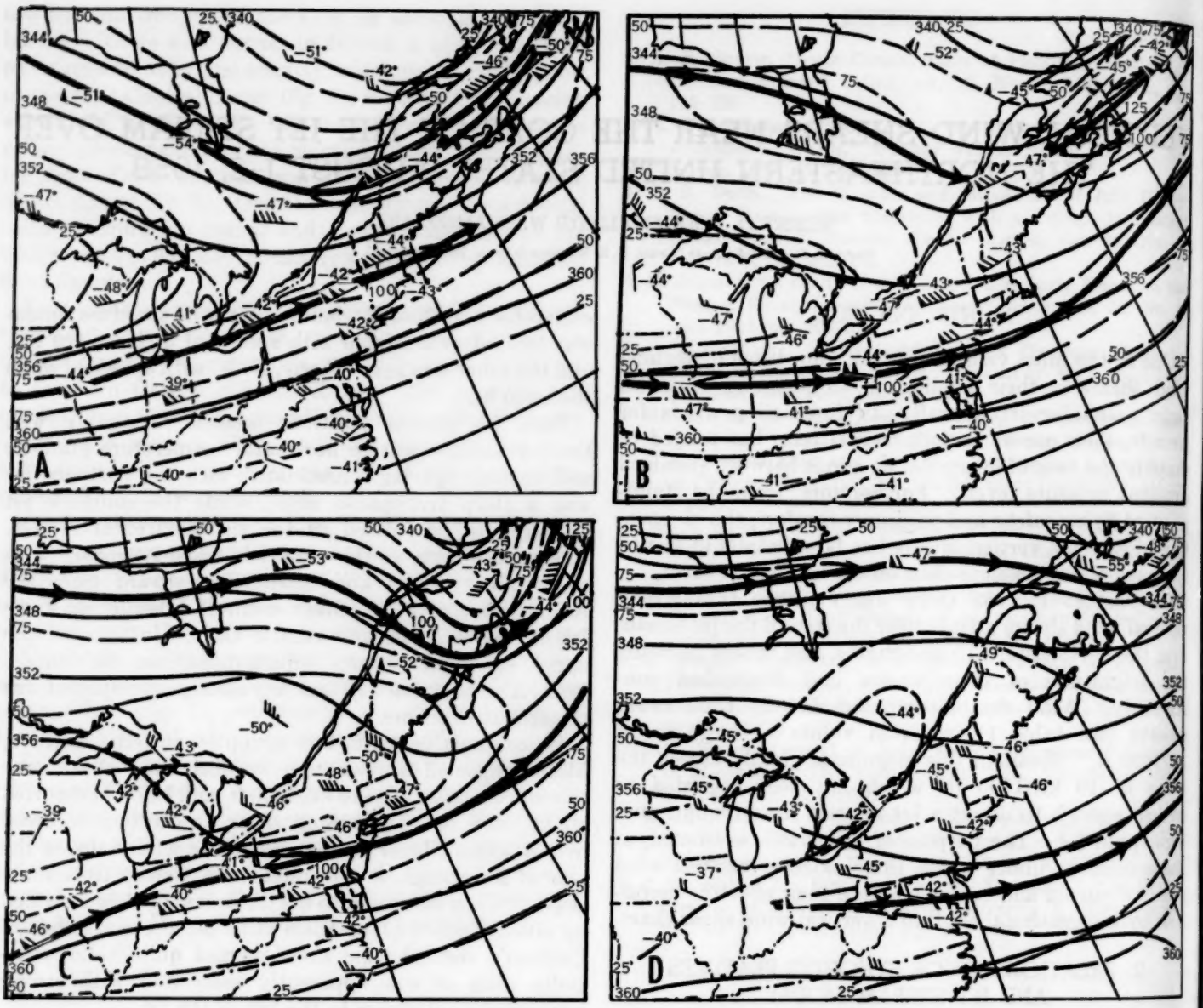

FIGURE 1.—250-mb. contour pattern including jet streams and isotach analysis (dashed). (A) 0000 GMT, August 1; (B) 1200 GMT, August 1; (C) 0000 GMT, August 2; and (D) 1200 GMT, August 2, 1958. The eastward progression of the flat short-wave trough is indicated with its influence on the southern jet stream. The strong horizontal wind shears appeared in conjunction with the largest horizontal temperature gradient.

Although the horizontal temperature gradient was rather weak, a computation was made to determine a reasonable vertical wind shear value for Idlewild, using the thermal wind equation

$$\frac{\partial V}{\partial z}=\frac{g}{fT^*}\frac{\partial T^*}{\partial s}$$

where V is the speed of the westerly wind, g is acceleration of gravity, f is Coriolis parameter, T^* is virtual temperature, z is the vertical coordinate, and s is the horizontal coordinate, positive southward. For an average temperature gradient south of the jet of 1° C. per 125 miles at the 250-mb. level, the vertical wind shear at Idlewild was computed to be a little more than 1 kt./1000 ft. Actually, the computation showed no vertical wind shears for the temperature gradient with respect to Albany since the temperatures at Idlewild and Albany were identical. For the temperature gradient with respect to Washington, the shear at Idlewild was computed to be 2.5 kt./1000 ft.

From the large difference between the theoretical and observed vertical wind shears at Idlewild, it seemed likely that the strong reported shears were related to either instrumental error, reporting procedure, or microscale phenomena. In any case, the shears were regarded as having little or no effective value for prognostic purposes.

At 1200 GMT, August 1, the short-wave trough at the 250-mb. level (fig. 1B) was still quite flat but appeared to be located along a line through Maine, west of Albany, and in the vicinity of Pittsburgh. The northern jet stream was in about the same latitudinal position with respect to Caribou, but the wind maximum had moved

on eastward to Nova Scotia. The southern jet stream had moved southward to an east-west line through southern Pennsylvania with a wind maximum near Pittsburgh exceeding 100 kt. The horizontal temperature gradient to the north of the southern jet was estimated at 3° C./180 mi.

Albany's rawin at this time presented an analysis problem in properly locating the jet since its wind at the 250-mb. level was within about 5 kt. of that at Pittsburgh. However, in view of the horizontal temperature gradient north of the jet and the apparent streamline relationship between Buffalo, Albany, and Portland (fig. 1B), Albany's wind was regarded as unrepresentative.

At the surface (fig. 2) the front was still weak with minor waves but had shifted a little southward to a position through Virginia and Kentucky. Except for Maine and portions of northern New York, there was a wide band of cloudiness over the area; and rain prevailed over much of Pennsylvania and nearby States. The position of the rainfall area had the conventional relation to the jet stream position and helped confirm the upper-air analysis.

Coincident with the synoptic features for 1200 GMT, August 1, a vertical wind shear of −18 kt./1000 ft. over a 2000-ft. layer above the peak wind was reported by Caribou. While this value seemed rather excessive in relation to a reported peak wind of only 72 kt., there was some continuity with the past 12 hours for a large shear to exist. In relation to the tropopause, this large shear occurred in a zone of steep slope which was estimated at 75 ft. per mile. With respect to the jet stream, it was difficult to determine from surrounding data whether the jet was north or south of Caribou; but in any event, the horizontal wind shear appeared rather weak on both sides of the jet and implied a smaller vertical wind shear than that reported. Computation of a vertical wind shear at Caribou by the thermal wind equation gave a value of only .86 kt./1000 ft. In view of these features, Caribou's shear of −18 kt./1000 ft. seemed much too large and had little or no useful value.

Along the southern jet stream there were no vertical wind shear values exceeding the critical 10 kt./1000 ft. The largest shears computed directly from rawin data were 8 kt./1000 ft. at both Dayton and Pittsburgh which were near the base of the short-wave trough. Idlewild and Flint, Mich. had wind shear values of 3 kt./1000 ft. and 5 kt./1000 ft., respectively.

Although these shear values did not conflict with the jet stream model to any great extent, it was rather surprising that Pittsburgh's vertical shear was not larger. The core of the jet stream appeared to be located either over or just south of Pittsburgh, the peak wind was 102 kt., and the 250-mb. temperature gradient over a 130-mi. distance north of the jet was estimated at 1° C./25 mi. Nevertheless, a computed vertical wind shear value of only 5.4 kt./1000 ft. was obtained from the thermal wind equation. The slope of the tropopause over Pittsburgh at this time was negligible.

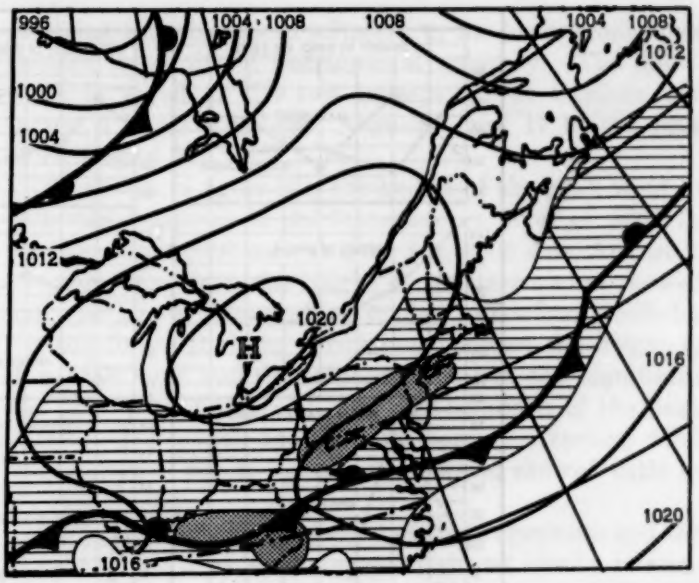

FIGURE 2.—Surface chart for 1200 GMT, August 1, 1958, which was characteristic of the entire period. The surface front and the weather pattern appeared to be related to the southern jet. Area of cloudiness is hatched; precipitation areas are stippled.

At 1800 GMT, August 1, wind reports from Dayton indicated a positive vertical wind shear of 15 kt./1000 ft. over a 2000-ft. layer below the peak wind and −9 kt./1000 ft. over a 2000-ft. layer above the peak wind. Since it was assumed that there had been little or no change in the synoptic pattern since 1200 GMT, it seemed rather unusual for Dayton to have such strong vertical wind shears, expecially in conjunction with a peak wind of only 62 kt. Another suspicious factor was that the peak wind was reported at the 30,000-ft. level when only 6 hours previous it had been at 42,000 ft. From these facts with respect to continuity and the jet stream model, it appeared that these large vertical shears were unrepresentative and had little or no effective value for forecasting.

By 0000 GMT, August 2, the short-wave trough at the 250-mb. level (fig. 1C) appeared to be near the east coast of the United States, but the contours remained cyclonically curved to the north of the southern jet stream from the Midwest to the Atlantic Ocean. The southern jet stream position was along a line north of Dayton, over Pittsburgh, and south of Idlewild, while the northern jet was about 100 mi. northeast of Caribou. The wind flow pattern was still west to northwest, but wind speeds at Albany, Caribou, Portland, and Nantucket had decreased to 50 kt. or less. Winds along the southern jet remained fairly strong with a maximum of at least 120 kt. over southern Pennsylvania.

The tropopause chart at this time showed an unusual ridge across Pennsylvania separating low tropopause heights over Ohio from those in New England. The slope of the tropopause normal to the jet was greatest between Idlewild and Albany with a value estimated at 50 ft. per mile. Parallel to the jet stream, the tropopause slope between Dayton and Pittsburgh was about 34 ft. per mile.

483854—58——4

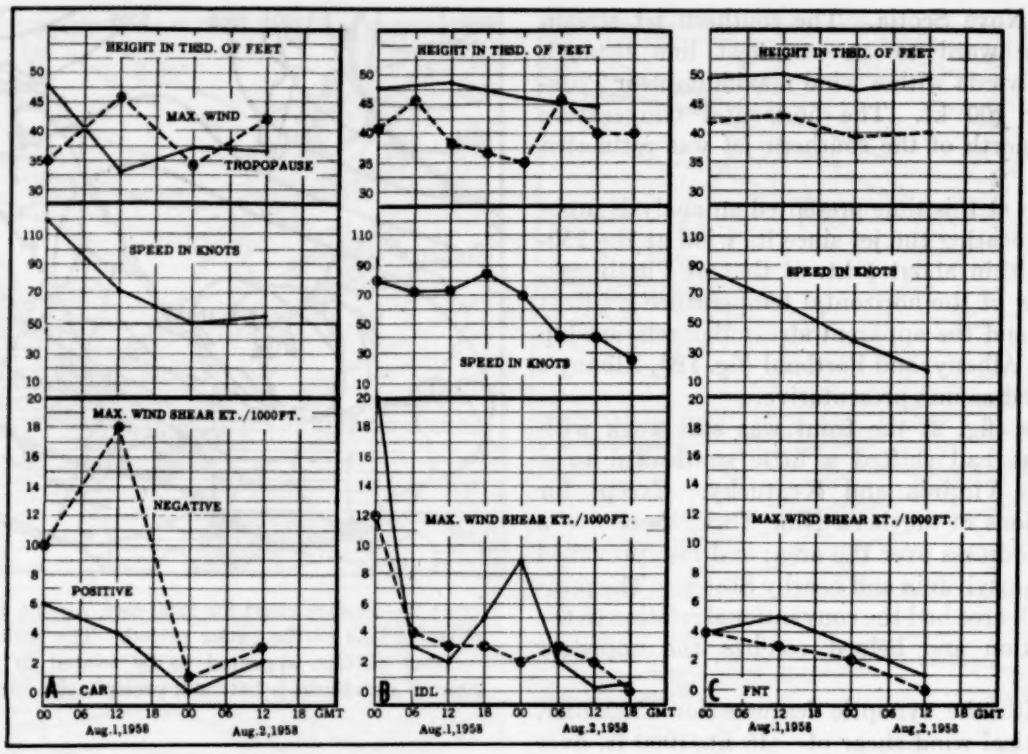

FIGURE 3.—A composite time graph which shows the random fluctuation of several wind field parameters at stations near the core of the jet stream. Upper panel compares the height of tropopause with the height of the peak wind (dashed line). The center panel shows the magnitude of the peak wind; and the bottom panel compares the maximum positive vertical wind shears with the negative (dashed line) wind shears. All wind values were taken directly from reported rawin data. (A) Caribou, (B) Idlewild, (C) Flint.

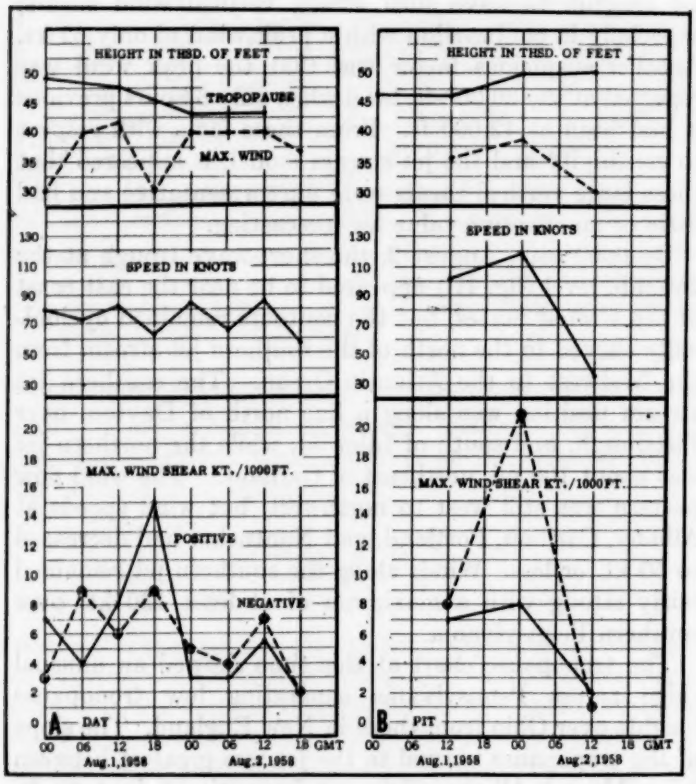

FIGURE 4.—Composite time graph of wind field parameters for (A) Dayton and (B) Pittsburgh.

Concurrent with these synoptic features, Pittsburgh reported a vertical wind shear of −21 kt./1000 ft. over a 3000-ft. layer directly above the peak wind of 119 kt. This strong shear was compatible with both the strength of the peak wind and the isotach pattern, which suggested that the horizontal wind shears were approaching a maximum value. In figure 1C, the horizontal wind shears near Pittsburgh and to the south of the jet stream were estimated to be a little less than 25 kt./deg. lat., and those to the north of the jet at about twice that value. Riehl's [5] computations for maximum horizontal shear for straight or slightly cyclonic flow have shown similar values.

Although the occurrence of this strong shear at Pittsburgh appeared quite reasonable with respect to the jet stream model, the magnitude of the shear was regarded as excessively large. Kochanski [6] has computed vertical shear of this magnitude by using horizontal temperature gradients of 10° C./deg. lat. In this case, the horizontal temperature gradient normal to the jet was only 1° C./26 mi., and the theoretical shear value computed from the thermal wind equation was only 5.4 kt./1000 ft. Although this computed value appeared too low at first, it seemed in good agreement with the value of 6 kt./1000 ft. obtained by averaging Pittsburgh's vertical wind shears over a 10,000-ft. layer above and below the level of maximum wind. Therefore, in view of this analysis, the extreme vertical wind shear at Pittsburgh at 0000 GMT, August 2, was assumed to be the result of either some microscale

phenomenon of short duration or of errors in wind measuring equipment or reporting procedure.

At the same time, Pittsburgh had also reported a positive shear of 8 kt./1000 ft. over an 8000-ft. layer beneath the peak wind. This value seemed compatible with the shear of 5 kt./1000 ft. reported at Dayton and 9 kt./1000 ft. at Idlewild. All of these vertical wind shears were in general agreement with the jet stream model and acceptable for a useful analysis. As a matter of interest, a comparison between theoretical wind shears and the above shears determined directly from rawin data showed the latter to be about 3 times larger than those computed by the thermal wind equation.

By 1200 GMT, August 2, the short-wave trough at the 250-mb. level (fig. 1D) was off the east coast of the United States. The southern jet stream was in about the same latitudinal position as 12 hours earlier, but wind speeds had diminished considerably. As might be expected, both positive and negative vertical wind shear values had also diminished. With the exception of Dayton, most wind reports along the jet stream indicated vertical shears of 3 kt./1000 ft. or less. Dayton reported a positive shear of 9 kt./1000 ft. and a negative shear of 7 kt./1000 ft. over 8000-ft. and 10,000-ft. layers, respectively. Although these shears were neither extreme nor in direct conflict with the jet stream model, it seemed curious that they should have occurred with such strength near the end of a declining jet and in an area of rather weak horizontal temperature gradient.

3. COMPATIBILITY OF DATA

Since it has been established that wind data are subject to considerable variation near the core of the jet stream, figures 3 and 4 have been prepared to summarize the fluctuations during August 1–2 and to compare some of the wind field parameters. At 1200 GMT on both August 1 and 2, Caribou (fig. 3A, upper panel) presented an analysis problem when the height of the tropopause appeared to be out of phase with the height of the peak wind. Actually, subsequent investigation disclosed the presence of two tropopause points, and both met the currently adopted definition. Since the jet axis had been analyzed within 150 miles of Caribou (fig. 1B), this out-of-phase relationship appeared to conflict with the jet model of Riehl [3] but seemed compatible with Endlich's model [2].

Endlich has found similar out-of-phase relationships between the height of the tropopause and that of the peak wind and has classified them as type "A" tropopauses that are characteristic of the anticyclonic side of the jet. Type "A" is described as a high cold tropopause in conjunction with a lower, weaker tropopause that is about 10° C. warmer than the higher one. The average height of the lower tropopause was found to be 4000 ft. below the average height of the peak wind. While Caribou's upper-air data exhibited some similarities to Endlich's type "A" tropopause, it seemed quite likely that the analysis problem could best be solved by arbitrarily increasing the wind speed adjacent to the lower tropopause within the limits of instrumental accuracy. The difference in speed at the two tropopauses at Caribou was about 5 kt. at 1200 GMT, August 1, and 17 kt. at 1200 GMT, August 2.

As shown in figure 3B, the height of the peak wind at Idlewild appeared to fluctuate over a layer of 8000 ft. or more from 0600 GMT, August 1 to 0600 GMT, August 2. At the same time, the height of the tropopause showed only minor variations which tended to confirm Endlich's [2] conclusion that the correlation between the height of the peak wind and the tropopause is not too significant for prognostic purposes. Also a comparison of the peak wind (center panel, fig. 3B) and maximum vertical wind shears (lower panel, fig. 3B) at Idlewild showed little or no relationship.

At Flint (fig. 3C), the height of the tropopause and the height of the peak wind appeared almost ideally related. By contrast to this ideal relationship, the vertical wind shears at Flint, though small, were incompatible with the model. Reiter [7] and others have found that the magnitude of negative shears is slightly larger than that of positive ones. During August 1–2, the magnitudes of Flint's vertical wind shears were the reverse of those found in the model.

The relative strength of the positive and negative shears at Dayton (fig. 4A) fluctuated in random fashion during the period and showed little conformity to the jet stream model. Another incompatible feature in Dayton's wind occurred at 1800 GMT, August 1. At this time, the height of the peak wind was reported at 30,000 ft., which was more than 10,000 ft. lower than previous continuity would suggest. As was the case at Idlewild, there appeared to be little or no correlation between the speed of the peak wind at Dayton and the magnitude of the vertical wind shears.

Of all the winds near the core of the jet stream during August 1–2, those at Pittsburgh (fig. 4B) seemed to fit the model best. The magnitude of the negative shears was larger than that of the positive shears in two out of three cases, and the largest shear tended to occur with the strongest wind. The heights of the tropopause exceeded the heights of the peak wind, but the difference between the two values averaged more than 10,000 ft. which seemed quite large when compared to Endlich's and Riehl's models.

Most of the unrepresentative wind reports found near the core of the jet stream were attributed to the inability of wind-measuring equipment to measure accurately strong winds at high altitudes because of low elevation angles. According to U. S. Signal Corps tests [4] on GMD–1 wind equipment, the root-mean-square wind error was found to be about 18 kt. at an altitude of 40,000 ft. and an elevation angle of 6 degrees. Since numerous oscillations of wind speed with height are often found in a complete rawin sounding, an error of 18 kt. at either the top or bottom of a 1000-ft. layer could have introduced a fictitious vertical wind shear of 18 kt./1000 ft. If both the top and bottom were in error, a random relationship could have yielded a

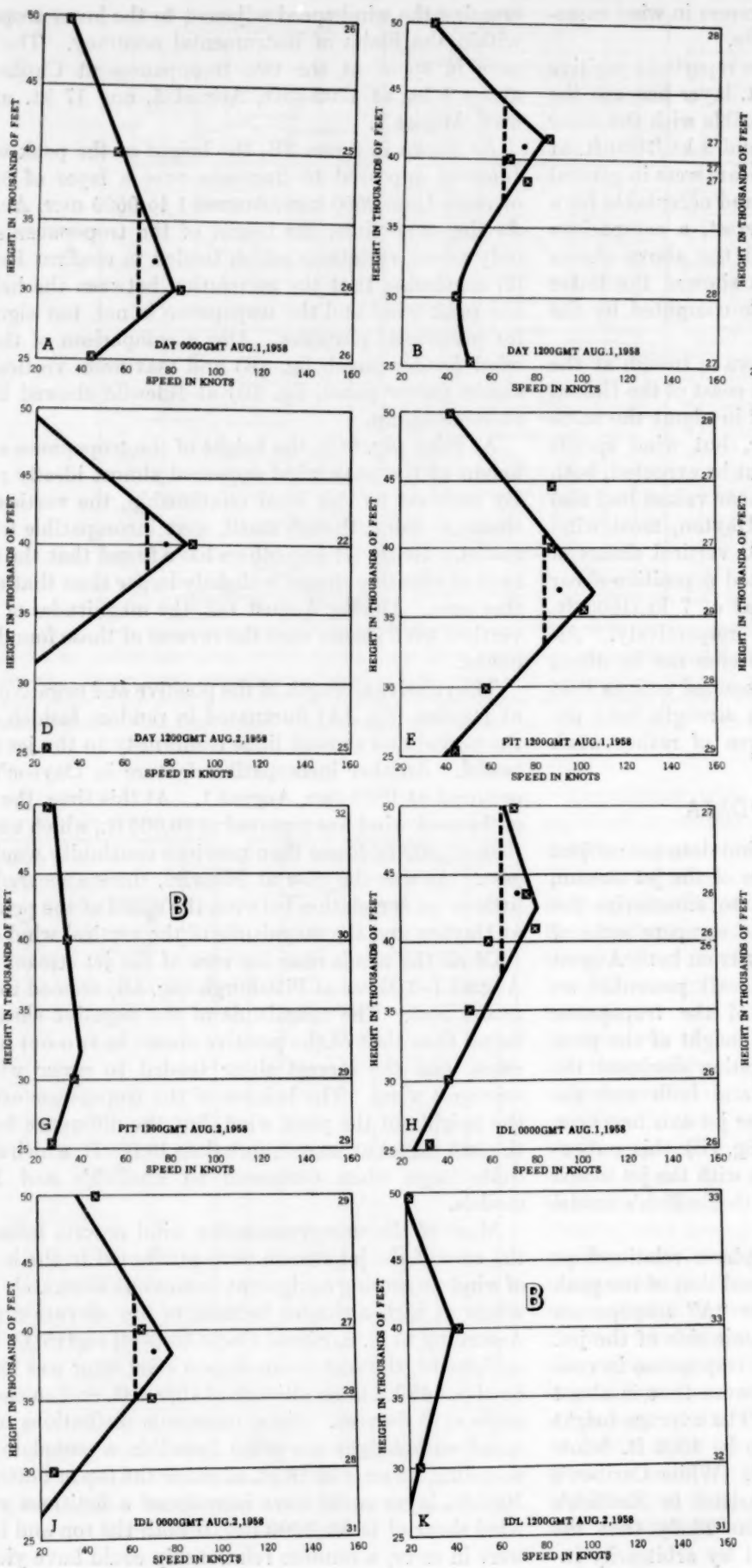

FIGURE 5.—Smoothed vertical wind profiles along jet stream. "X" reported wind speed, with direction in 10's of degrees at right edge of each section. Dot shows maximum wind (90 percent of peak) at middle of maximum wind layer defined by dashed line connecting points of 80 percent peak wind. Large B = barotropic. DAY = Dayton, Ohio; PIT = Pittsburgh, Pa.; IDL = Idlewild, N. Y.

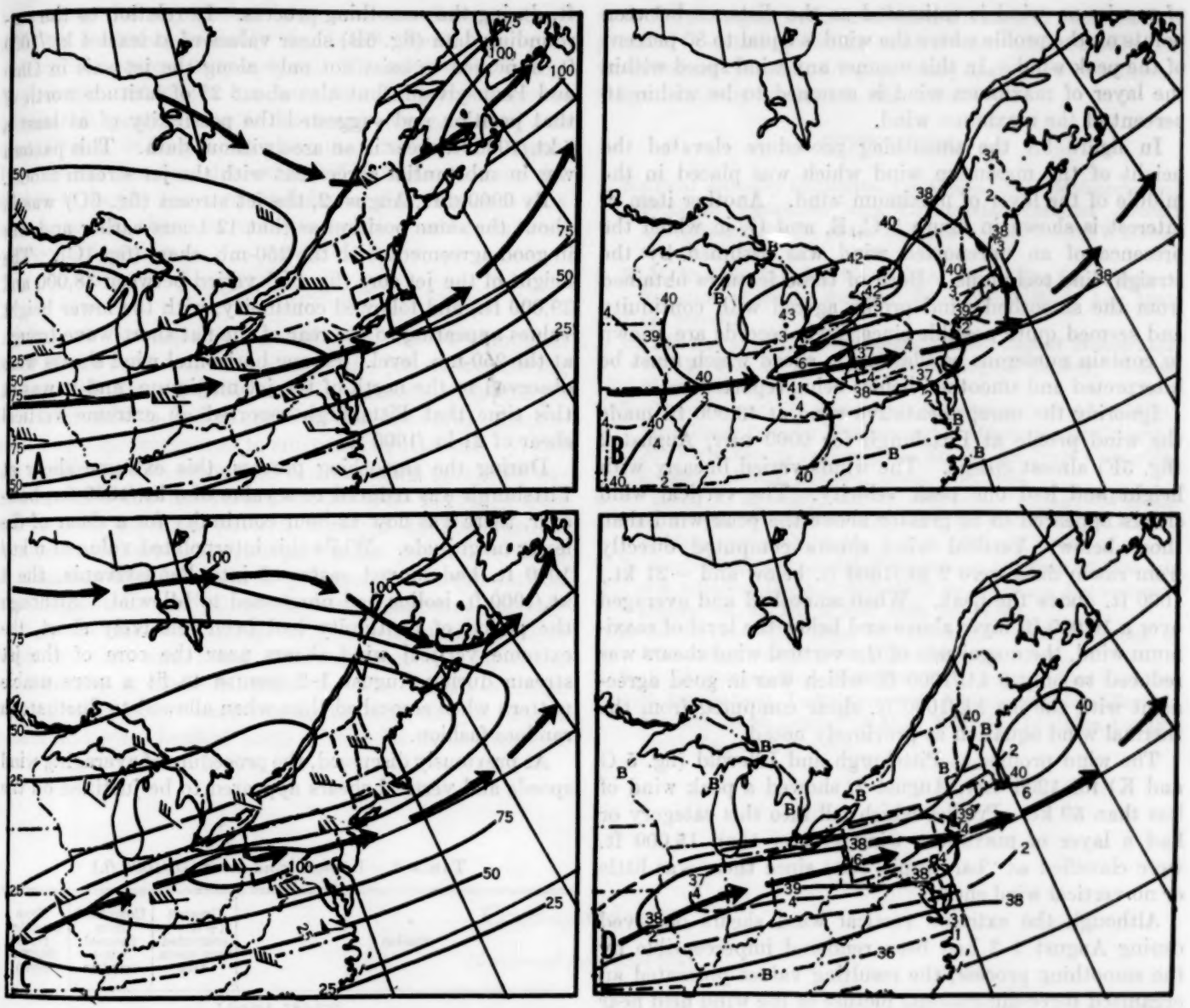

FIGURE 6.—Vertical wind shear charts which represent the 3-dimensional aspects of a smoothed wind field. Maximum winds and isotachs for (A) 1200 GMT, August 1 and (C) 0000 GMT, August 2 are within 10 percent of the reported peak winds and consistent with the 250-mb. pattern. The height of maximum winds and the averaged vertical wind shears (dashed lines) for (B) 1200 GMT, August 1 and (D) 0000 GMT, August 2 show the topography of the jet stream. Strongest vertical shear values lie north of the jet stream and their 12-hour displacement suggests continuous eastward movement.

maximum fictitious shear of 36 kt./1000 ft. Questionable vertical wind shears similar to these values occurred at both Idlewild and Pittsburgh and were observed near the 40,000-ft. level in conjunction with peak wind speeds of 90 kt. and 119 kt., respectively.

4. ANALYSIS OF VERTICAL WIND SHEAR CHARTS

In the vertical wind shear charts prepared experimentally at NAWAC, the unrepresentative wind features near the core of the jet stream during August 1–2 appeared to be smoothed into a systematic and useful analysis. The procedure of constructing these charts at NAWAC is based on a technique proposed by Reiter [7], with the main difference being that the vertical wind shears are averaged over a 10,000-ft. layer above and below the level of maximum wind. Then isolines are drawn directly for vertical shear values instead of depth of shear layer values as proposed by Reiter. In this manner, the magnitude of average vertical shear can then be used as an incremental term for rapidly estimating wind speeds for almost any altitude between the 500-mb. and 100-mb. levels by subtracting the shear term from the maximum wind value.

Smoothed vertical wind profiles for several stations along the southern jet stream for the period August 1–2 are shown in figure 5 to illustrate the procedure of analysis. In general the profiles were drawn subjectively to conform with the assumption that winds near the jet stream increase and decrease linearly and have one peak velocity. In figure 5 the maximum wind is shown as the point equal to 90 percent of the peak wind, and the depth of the layer

of maximum wind is estimated as the distance between points on the profile where the wind is equal to 80 percent of the peak wind. In this manner any wind speed within the layer of maximum wind is assumed to be within 10 percent of the maximum wind.

In figure 5A the smoothing procedure elevated the height of the maximum wind which was placed in the middle of the layer of maximum wind. Another item of interest is shown in figure 5 C, E, and G, in which the presence of an unreported wind was assumed by the straight-line technique. Both of these features obtained from the smoothed wind profile agreed with continuity and seemed quite possible since rawin records are known to contain numerous oscillations in speed which must be interpreted and smoothed before being reported.

Ignoring the unrepresentative wind at 43,000 ft. made the wind profile at Pittsburgh for 0000 GMT, August 2 (fig. 5F) almost classic. The winds varied linearly with height and had one peak velocity. The vertical wind shears appeared to be greater above the peak wind than those below. Vertical wind shears computed directly from rawin data were 9 kt./1000 ft. below and −21 kt./1000 ft. above the peak. When smoothed and averaged over a 10,000-ft. layer above and below the level of maximum wind, the magnitude of the vertical wind shears was reduced to only 6 kt./1000 ft. which was in good agreement with the 5.4 kt./1000 ft. shear computed from the thermal wind equation as previously noted.

The wind profiles at Pittsburgh and Idlewild (fig. 5 G and K) for 1200 GMT, August 2, showed a peak wind of less than 50 kt. Profiles which fell into this category or had a layer of maximum wind greater than 15,000 ft. were classified as "barotropic" (B) since there was little or no vertical wind shear.

Although the extreme vertical wind shears observed during August 1–2 had been rendered imperceptible by the smoothing process, the resulting values presented an organized three-dimensional picture of the wind field near the core of the jet stream when plotted on the vertical wind shear chart (fig. 6). The jet stream position for 1200 GMT, August 1 (fig. 6A) was in essentially the same position as that on the 250-mb. chart (fig. 1B). The isotach pattern near the core of the jet had been altered from that at the 250-mb. level, but then the winds had been computed with a 10 percent tolerance and were representative of a layer about 7000 ft. deep (fig. 5 B, E, I).

The height of the jet stream core (fig. 6B) appeared to undulate from 40,000 ft. at Dayton to 37,000 ft. at Pittsburgh and back again to 39,000 ft. at Idlewild. In relation to the synoptic situation, the lower heights of the jet stream core seemed to be associated with the position of the flat short-wave trough at the 250-mb. level (fig. 1B).

Although there were no extreme vertical shears reported along the southern jet stream at this time, both Dayton and Pittsburgh reported modest and reasonable values of 8 kt./1000 ft. These values were reduced to 4 kt./1000 ft. during the smoothing process. In relation to the surrounding data (fig. 6B) shear values of at least 4 kt./1000 ft. appeared to exist not only along the jet axis in Ohio and Pennsylvania but also about 2° of latitude north of that position and suggested the possibility of at least a 6 kt./1000 ft. shear in an area without data. This pattern was in substantial agreement with the jet stream model.

By 0000 GMT, August 2, the jet stream (fig. 6C) was in about the same position as that 12 hours earlier and was in good agreement with the 250-mb. chart (fig. 1C). The height of the jet core (fig. 6D) varied between 38,000 and 39,000 ft., and followed continuity, with the lower height values appearing to the rear of the flat short-wave trough at the 250-mb. level. Strong horizontal wind shears were observed to the north of the jet maximum, and it was at this time that Pittsburgh reported an extreme vertical shear of 21 kt./1000 ft.

During the smoothing process, this extreme shear at Pittsburgh was reduced to a value of 6 kt./1000 ft.; however, there was now 12-hour continuity for a shear of the lesser magnitude. While this interpolated value of 6 kt./1000 ft. had moved eastward into Pennsylvania, the 4 kt./1000 ft. isoline had progressed to Idlewild. Although the period of continuity had been relatively short, the extreme vertical wind shears near the core of the jet stream during August 1–2 seemed to fit a more usable pattern when smoothed than when allowed to fluctuate in random fashion.

As previously discussed, the procedure of averaging wind speeds and vertical shears appeared to be justified on the

TABLE 2.—*Vertical wind shear (kt./1000 ft.)*

Station	Greatest (+ or −) computed from rawin data	Computed from thermal wind equation	From smoothed profile (20,000-ft. layer)
0000 GMT, August 1			
Idlewild	20	2.5	2.5
Dayton	7	1.5	3.4
Pittsburgh	(1)	2.1	(1)
Flint	4	1.5	1.6
Caribou	−10	1.3	4.7
1200 GMT, August 1			
Idlewild	−3	2.3	4.0
Dayton	8	3.9	1.5
Pittsburgh	−8	5.4	4.1
Flint	5	3.7	2.3
Caribou	−18	.86	1.2
0000 GMT, August 2			
Idlewild	9	2.4	3.5
Dayton	−5	1.8	3.6
Pittsburgh	−21	5.4	6.1
Flint	3	1.5	<1
Caribou	−2	1.5	<1
1200 GMT, August 2			
Idlewild	−2	3.5	1.4
Dayton	9	.81	6
Pittsburgh	2	3.2	<1
Flint	1	.58	<1
Caribou	−3	2.3	1.5

[1] Missing.

basis that wind equipment in current use does not have sufficient accuracy reliably to detect small-scale phenomena in the upper troposphere. The microscale feature of clear air turbulence has been found [8] by numerous jet aircraft penetrations to have an average size of less than 50 mi. in length and less than 2000 ft. in depth. In view of these considerations, it is believed more desirable to locate zones of turbulence with reference to a model rather than to unrepresentative wind data of questionable value.

5. CONCLUSIONS

Most of the extreme vertical wind shears computed from rawin data near the core of the jet stream during August 1–2 showed little or no agreement with the jet stream models, lacked continuity, and appeared unrepresentative when compared to surrounding stations. When the wind data were smoothed to remove the unrepresentative features and the vertical shears were averaged over a 20,000-ft. layer, a pattern emerged on the vertical wind shear chart that indicated some prognostic value in planning wind forecasts for jet aircraft. A comparison of the greatest vertical wind shears computed directly from rawin data with those computed from the thermal wind equation and those obtained from the smoothed wind profile is made in table 2. The largest average vertical wind shears were compatible with the jet stream model and were located north of the jet in conjunction with the strongest horizontal wind shears and temperature gradient. Although some errors were undoubtedly introduced in the smoothing process, they were considered insignificant in the broadscale sense.

REFERENCES

1. National Advisory Committee for Aeronautics, "Meteorological Problems Associated with Commercial Turbojet Aircraft Operations," *NACA Research Memorandum* 54L29, Washington, D. C. 1955.
2. R. M. Endlich, S. B. Solot, and H. A. Thur, "The Mean Vertical Structure of the Jet Stream," *Tellus*, vol. 7, No. 3, Aug. 1955, pp. 308–313.
3. H. Riehl et al., "The Jet Stream," *Meteorological Monographs*, vol. 2, No. 7, American Meteorological Society, Boston, Mass., Aug. 1954.
4. N. Dvoskin and N. Sissenwine, "Evaluation of AN/GMD–2 Wind Shear Data for Development of Missile Design Criteria," *Air Force Surveys in Geophysics* No. 99, Air Force Cambridge Research Center, Bedford, Mass., Apr. 1958.
5. H. Riehl, F. A. Berry, and H. Maynard, "Exploration of the Jet Stream by Aircraft during the 1952–1953 Winter," *Journal of Meteorology*, vol. 12, No. 1, Feb. 1955, pp. 26–35.
6. A. Kochanski, "Horizontal Temperature Gradient at 200 mb. and Adjacent Levels," *Bulletin of the American Meteorological Society*, vol. 37, No. 2, Feb. 1956, pp. 47–54.
7. E. R. Reiter, "The Layer of Maximum Wind," *Journal of Meteorology*, vol. 15, No. 1, Feb. 1958, pp. 27–43.
8. R. L. McDougal, T. I. Coleman, P. L. Smith, "The Variation of Atmospheric Turbulence with Altitude and Its Effect on Airplane Gust Loads," NACA RM No. L53G15a, Langley Field, Va., Nov. 9, 1953.

Correspondence

(Continued from page 298)

divergence of the actual flow is replaced by that of the normal, which presumably is in turn a reflection of the large-scale planetary influences mentioned earlier.

Variants of this method, based on recognition that the second term on the right of equation (3) is related to the errors of the barotropic model, have been suggested by Berson [2] and Williams [3].

The relation to Wolff's model may be seen if the basic current is defined to be the sum of the first three harmonics of the actual flow pattern. The analogy becomes more exact if the fictitious changes in the three harmonics are removed at the end of each time-step. Perhaps some difference still remains due to the fact that Wolff's model permits the changes (or tendency) of the three harmonics to be influenced by non-linear interaction with the shorter waves, while this is not permitted when using equation (3).

A method very similar to that of Wolff, but dealing with one-dimensional wave motions, is that proposed by Graham [4].

Another in this family is the present operational model of the Extended Forecast Section, U. S. Weather Bureau, proposed by Namias [5]. Here a "fictitious" wind ($\mathbf{V}_F$) is defined by the equation:

$$\mathbf{V}_F=\mathbf{V}-(\mathbf{V}_B-\mathbf{V}_B^{\phi}) \tag{4}$$

where $\mathbf{V}$ is the actual wind, $\mathbf{V}_B$ is the basic current at the same point and $\mathbf{V}_B^{\phi}$ is the latitudinal average, or zonal component of the basic current for the latitude of $\mathbf{V}$. The predictive equation is then obtained by assuming that the absolute vorticity of the fictitious current is conserved:

$$\frac{\partial \zeta_F}{\partial t}=-\mathbf{V}_F\cdot\nabla\eta_F \tag{5}$$

The close correspondence between equations (5) and (3) can be seen by expanding them using the definition of the perturbation current ($\mathbf{V}^*$):

$$\mathbf{V}=\mathbf{V}^*+\mathbf{V}_B \tag{6}$$

In this manner equations (3) and (5) become (7) and (8) respectively:

$$\frac{\partial \zeta^*}{\partial t}=-\mathbf{V}_B\cdot\nabla\zeta^*-\mathbf{V}^*\cdot\nabla(\zeta_B+f)-\mathbf{V}^*\cdot\nabla\zeta^* \tag{7}$$

$$\frac{\partial \zeta^*}{\partial t}=-\mathbf{V}_B^\phi\cdot\nabla\zeta^*-\mathbf{V}^*\cdot\nabla(\zeta_B^\phi+f)-\mathbf{V}^*\cdot\nabla\zeta^* \tag{8}$$

It will be seen that these two equations are identical except that in equation (8) the zonal component of the basic current replaces its value at a point. Physically, the difference appears to be related to the fact that in the Extended Forecast Section's operational model the perturbation is initially uncoupled from the basic current. This appears to prevent any important non-linear exchange of energy between these two currents, while such an exchange is permitted using equation (3).

The normal circulation was first used as the basic current in equation (4), but later it was decided to replace this with a large-scale flow pattern more characteristic of the particular season during which the forecast is prepared. A monthly-mean chart, centered on forecast day, is now used for this purpose. Tests indicate that this results in considerable improvement (Namias, to be published). Although the monthly-mean circulation evolves more rapidly than the normal, this apparently is more than compensated by a reduction in magnitude of the perturbation divergence.

It must be clear that perturbation models such as those described above need not be derived solely by using the approximate vorticity equation (1). For example, the writer is at present working with one of several single-parameter models where a direct estimate is made of the divergence associated with large-scale planetary waves. In this case, equation (1) cannot be used in the perturbation method, and at least one more term must be added, preferably one which expresses some unknown or difficult-to-measure property of the actual flow. This unknown property is then replaced by the corresponding known property of the basic current.

It is believed that this procedure has the advantage that the models are constrained to behave in a fashion consistent with the observed behavior of the general circulation, because in essence the errors of any model are replaced by estimates based on experience. It is also felt that this procedure may lead to a better physical understanding of the circulation. In this connection it may be noted that the success of Wolff's model, which makes use of the observed stationary character of long waves, stimulated the successful search for a new operational model which contains a more satisfactory physical basis for this characteristic [6]. This new model is based on the theoretical work of Rossby [7]. Another important theoretical paper which treats the special problem of planetary waves is that of Burger [8]. Perhaps a more general formulation of the empirical approach, together with these theoretical studies, can lead to a practical solution of the preferred geographical locations and observed motions of the long waves.

REFERENCES

1. P. F. Clapp, "Application of Barotropic Tendency Equation to Medium-Range Forecasting," *Tellus*, vol. 5, No. 1, Feb. 1953, pp. 80–94.
2. F. A. Berson, "A Quantitative Analysis of Large-Scale Flow Patterns with Special Regard to the Effect of Eddy Motion," *Quarterly Journal of the Royal Meteorological Society*, vol. 79, No. 340, Apr. 1953, pp. 210–223.
3. S. Williams, "An Empirical Correction to the Barotropic Forecast," *Tellus*, vol. 10, No. 2, May 1958, pp. 216–224.
4. R. D. Graham, "An Empirical Study of Planetary Waves by Means of Harmonic Analysis," *Journal of Meteorology*, vol. 12, No. 4, Aug. 1955, pp. 298–307.
5. J. Namias, "Progress in Objectivization and Automation of Extended Forecasting," *Transactions of the New York Academy of Sciences*, Series II, vol. 19, No. 6, Apr. 1957, pp. 581–592.
6. G. P. Cressman, "Barotropic Divergence and Very Long Atmospheric Waves," *Monthly Weather Review*, vol. 86, No. 8, Aug. 1958, pp. 293–297.
7. C.-G. Rossby and collaborators, "Relation Between Variations in the Intensity of the Zonal Circulation of the Atmosphere and the Displacements of the Semi-Permanent Centers of Action," *Journal of Marine Research*, vol. 2, No. 1, 1939, pp. 38–55.
8. A. P. Burger, "Scale Consideration of Planetary Motions of the Atmosphere," *Tellus*, vol. 10, No. 2, May 1958, pp. 195–205.

U. S. GOVERNMENT PRINTING OFFICE: 1958

Chart I. A. Average Temperature (°F.) at Surface, August 1958.

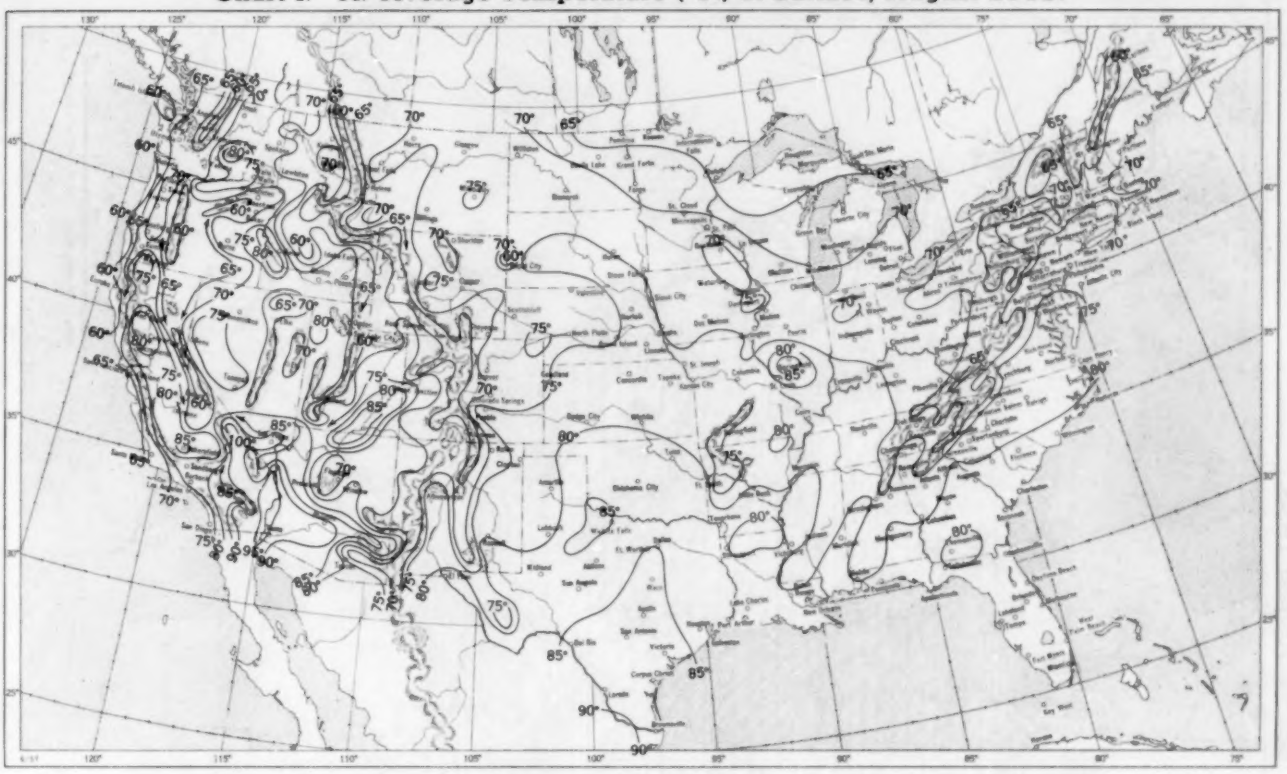

B. Departure of Average Temperature from Normal (°F.), August 1958.

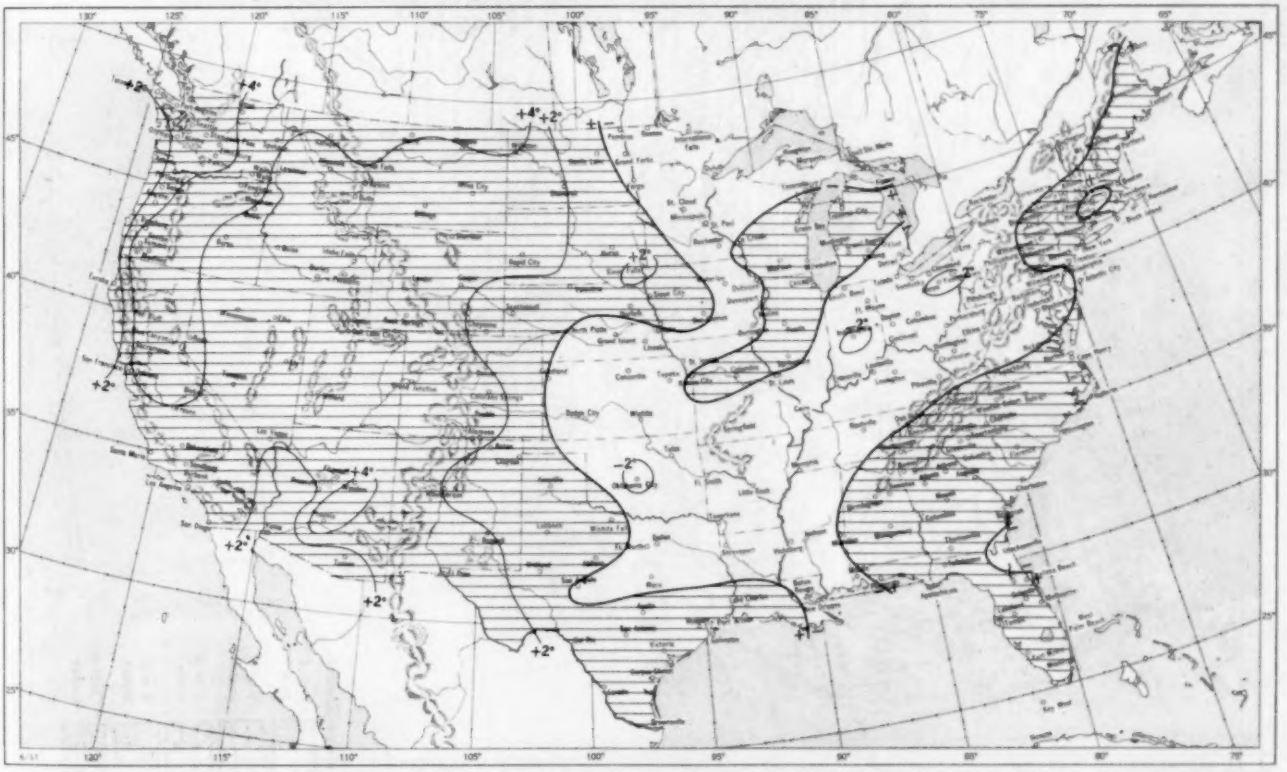

A. Based on reports from over 900 Weather Bureau and cooperative stations. The monthly average is half the sum of the monthly average maximum and monthly average minimum, which are the average of the daily maxima and daily minima, respectively.

B. Departures from normal are based on the 30-yr. normals (1921-50) for Weather Bureau stations and on means of 25 years or more (mostly 1931-55) for cooperative stations.

Chart II. Total Precipitation (Inches), August 1958.

Based on daily precipitation records at about 800 Weather Bureau and cooperative stations.

Chart III. A. Departure of Precipitation from Normal (Inches), August 1958.

B. Percentage of Normal Precipitation, August 1958.

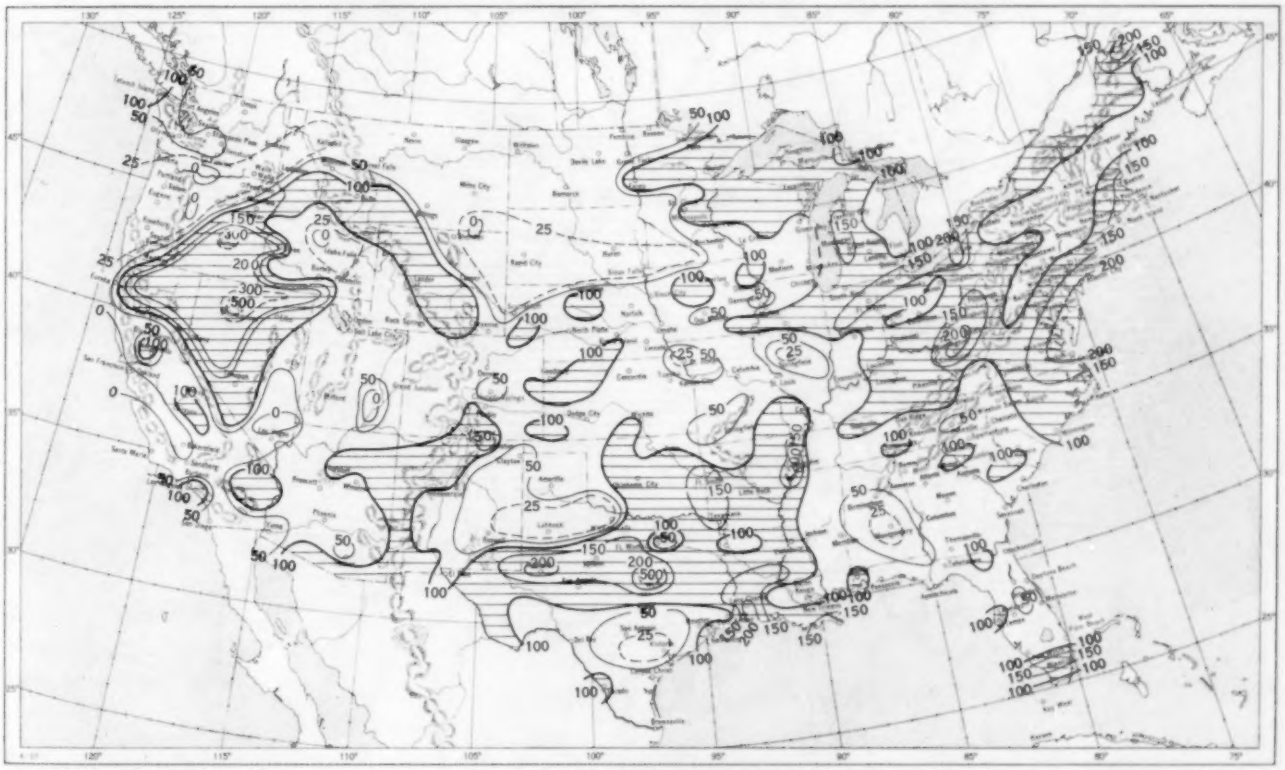

Normal monthly precipitation amounts are computed from the records for 1921-50 for Weather Bureau stations and from records of 25 years or more (mostly 1931-55) for cooperative stations.

Chart VI. A. Percentage of Sky Cover Between Sunrise and Sunset, August 1958.

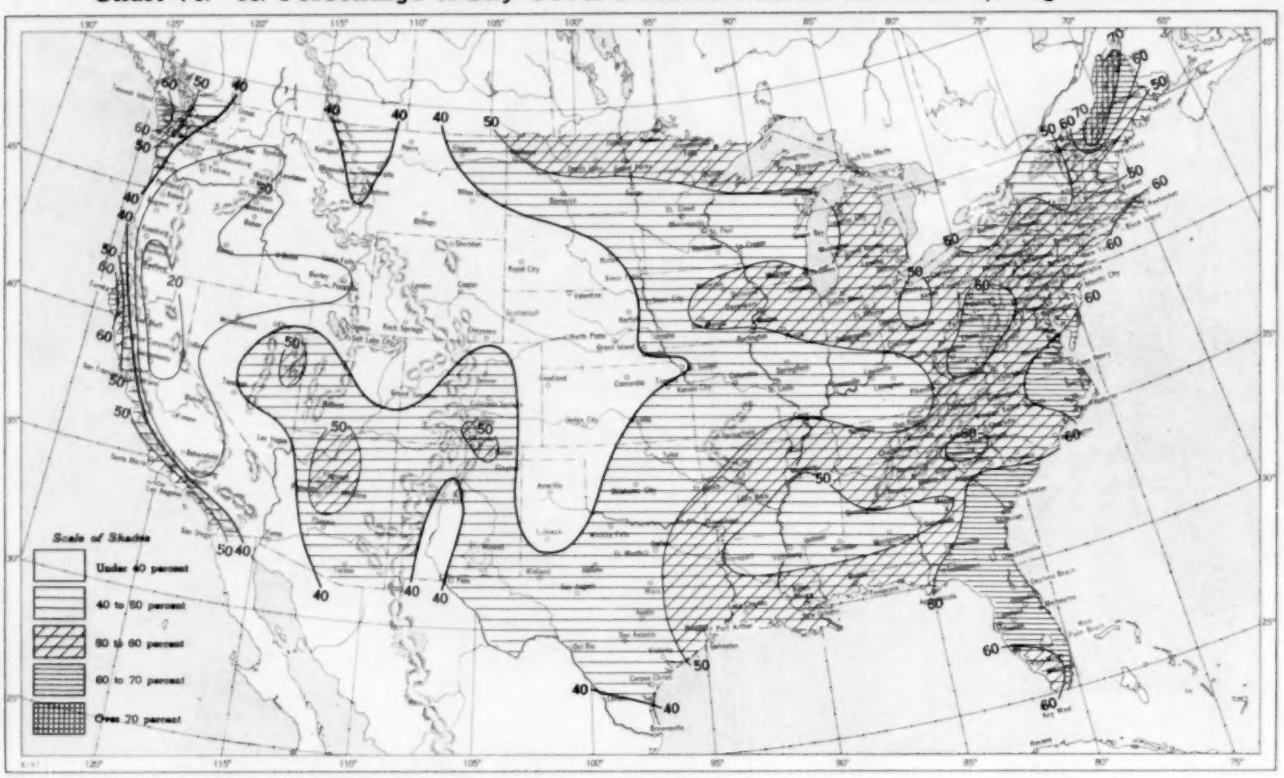

B. Percentage of Normal Sky Cover Between Sunrise and Sunset, August 1958.

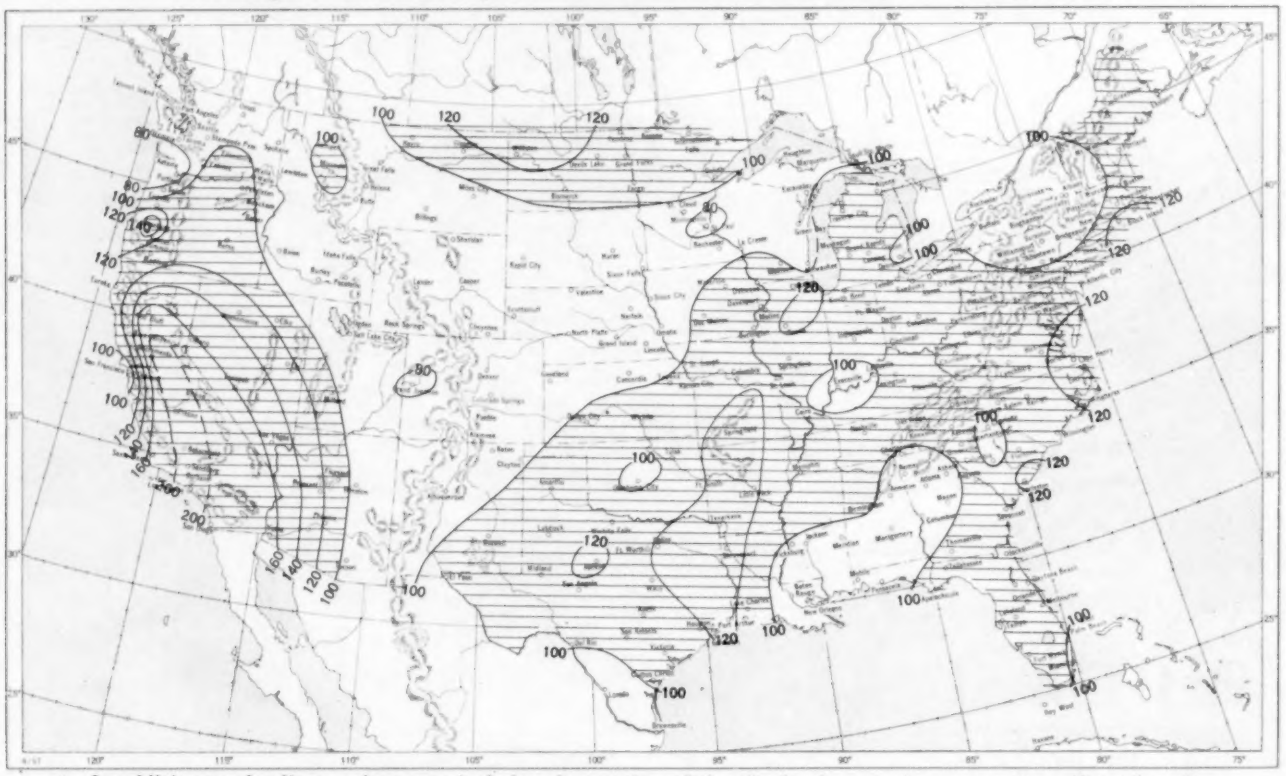

A. In addition to cloudiness, sky cover includes obscuration of the sky by fog, smoke, snow, etc. Chart based on visual observations made hourly at Weather Bureau stations and averaged over the month. B. Computations of normal amount of sky cover are made for stations having at least 10 years of record.

Chart VII. A. Percentage of Possible Sunshine, August 1958.

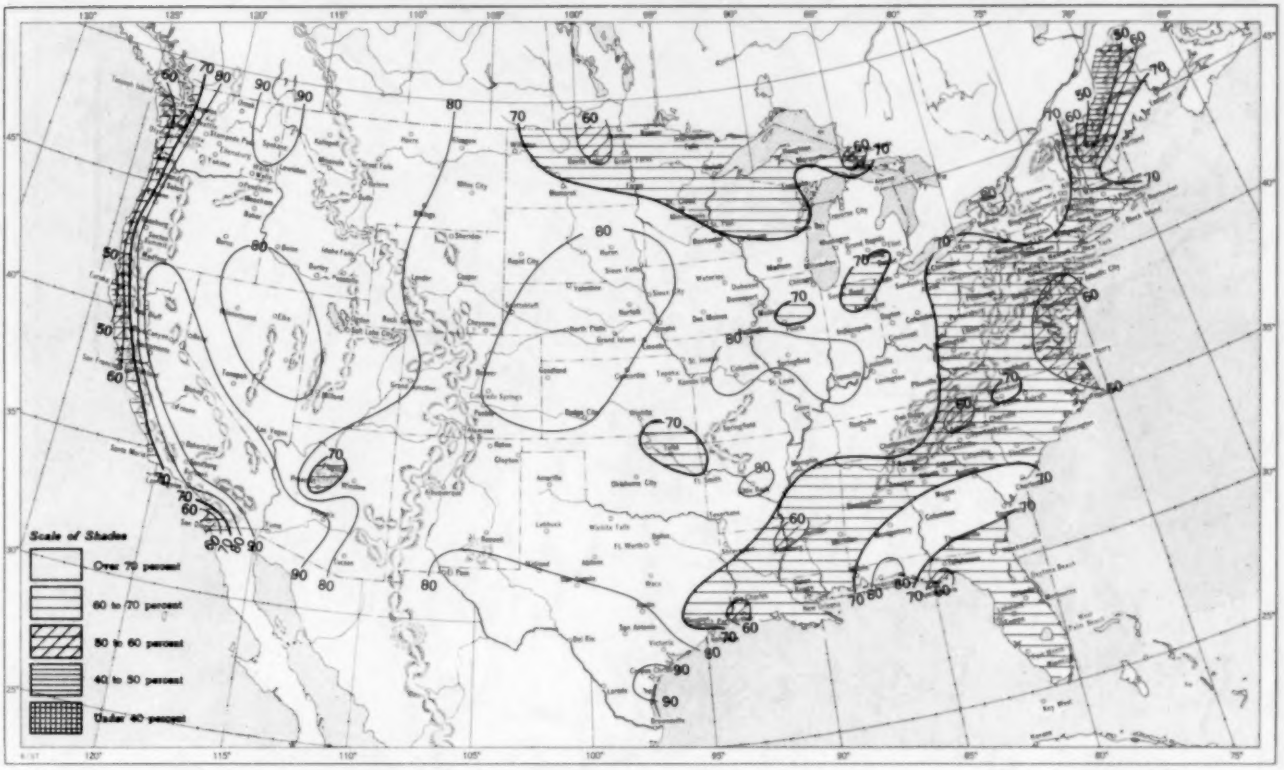

B. Percentage of Normal Sunshine, August 1958.

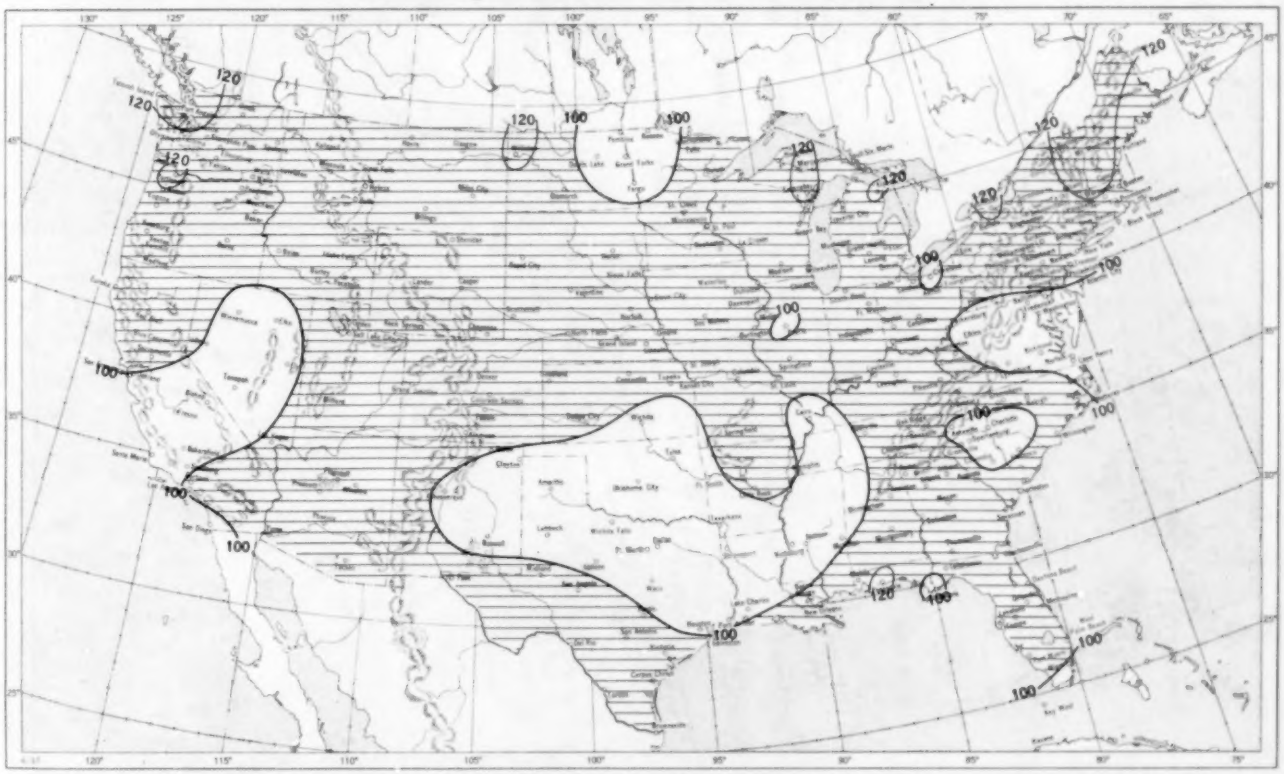

A. Computed from total number of hours of observed sunshine in relation to total number of possible hours of sunshine during month. B. Normals are computed for stations having at least 10 years of record.

Chart VIII. Average Daily Values of Solar Radiation, Direct + Diffuse, August 1958. Inset: Percentage of Mean Daily Solar Radiation, August 1958. (Mean based on period 1951-55.)

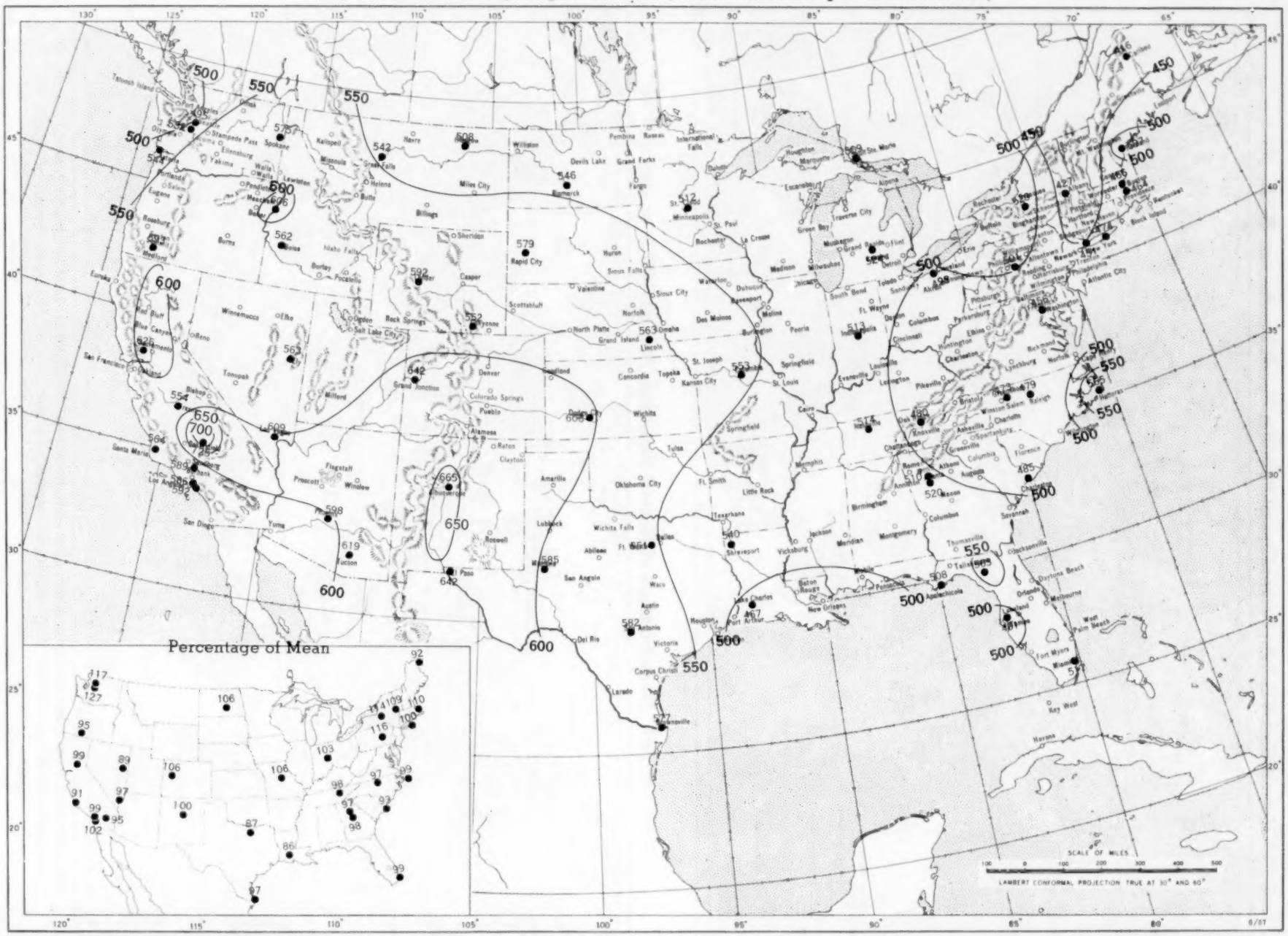

Chart shows mean daily solar radiation, direct + diffuse, received on a horizontal surface in langleys (1 langley = 1 gm. cal. cm. $^{-2}$). Basic data for isolines are shown on chart. Further estimates are obtained from supplementary data for which limits of accuracy are wider than for those data shown. The inset shows the percentage of the mean based on the period 1951-55.

Chart IX. Tracks of Centers of Anticyclones at Sea Level, August 1958.

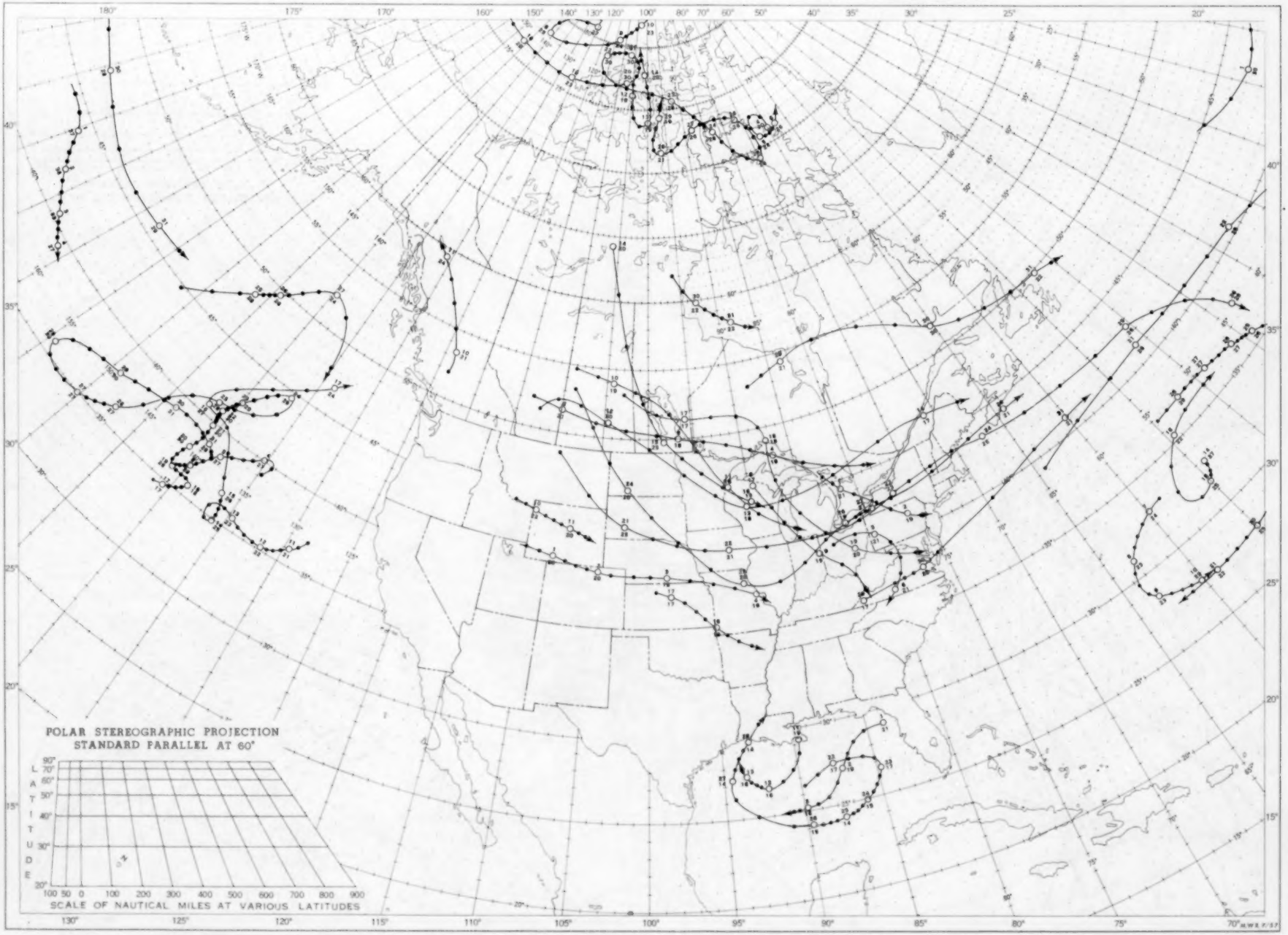

Circle indicates position of center at 7:00 a. m. E. S. T. Figure above circle indicates date, figure below, pressure to nearest millibar. Dots indicate intervening 6-hourly positions. Squares indicate position of stationary center for period shown. Dashed line in track indicates reformation at new position. Only those centers which could be identified for 24 hours or more are included.

Chart X. Tracks of Centers of Cyclones at Sea Level, August 1958.

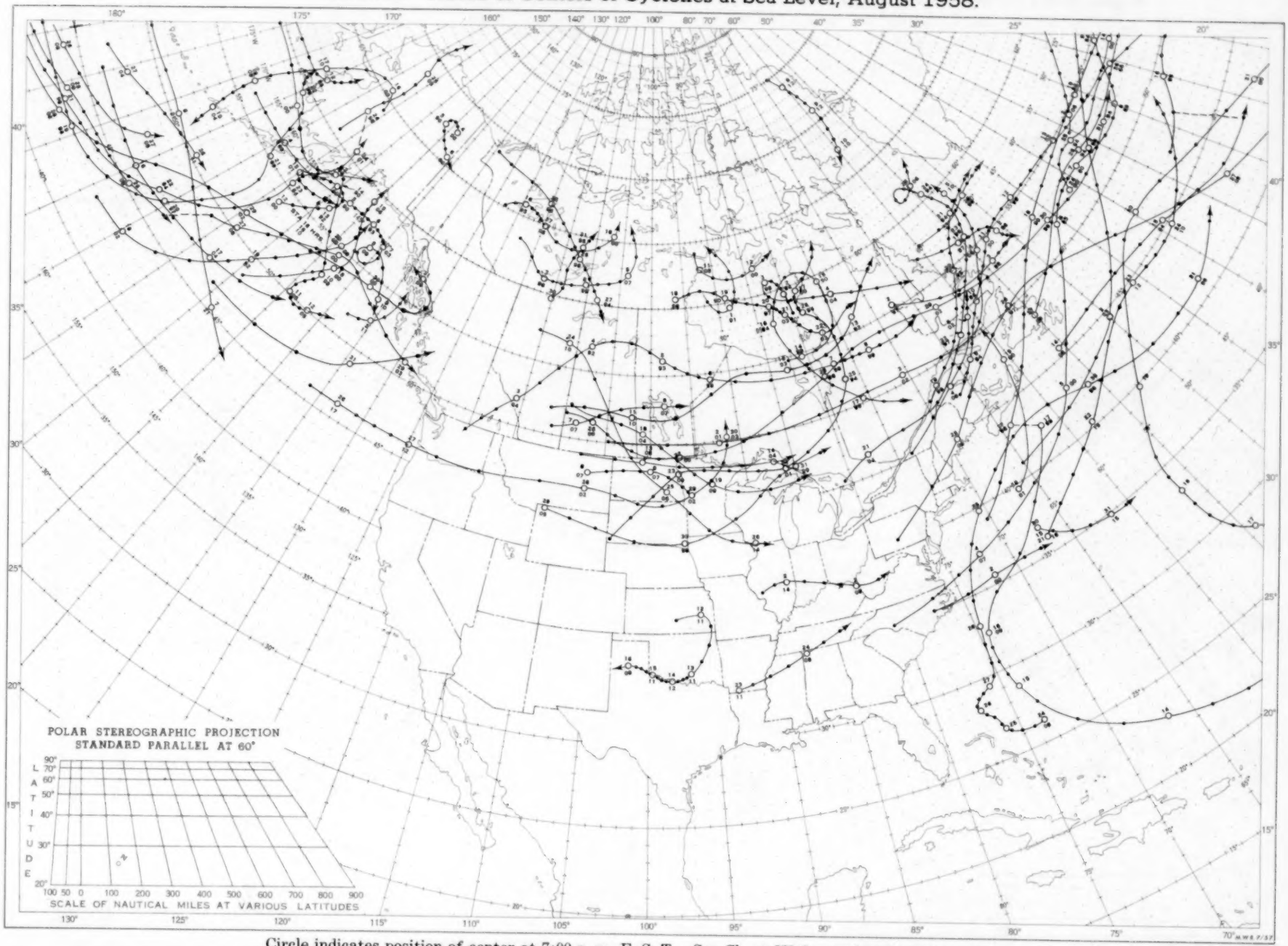

Circle indicates position of center at 7:00 a. m. E. S. T. See Chart IX for explanation of symbols.

Chart XI. Average Sea Level Pressure (mb.) and Surface Windroses, August 1958. Inset: Departure of Average Pressure (mb.) from Normal, August 1958.

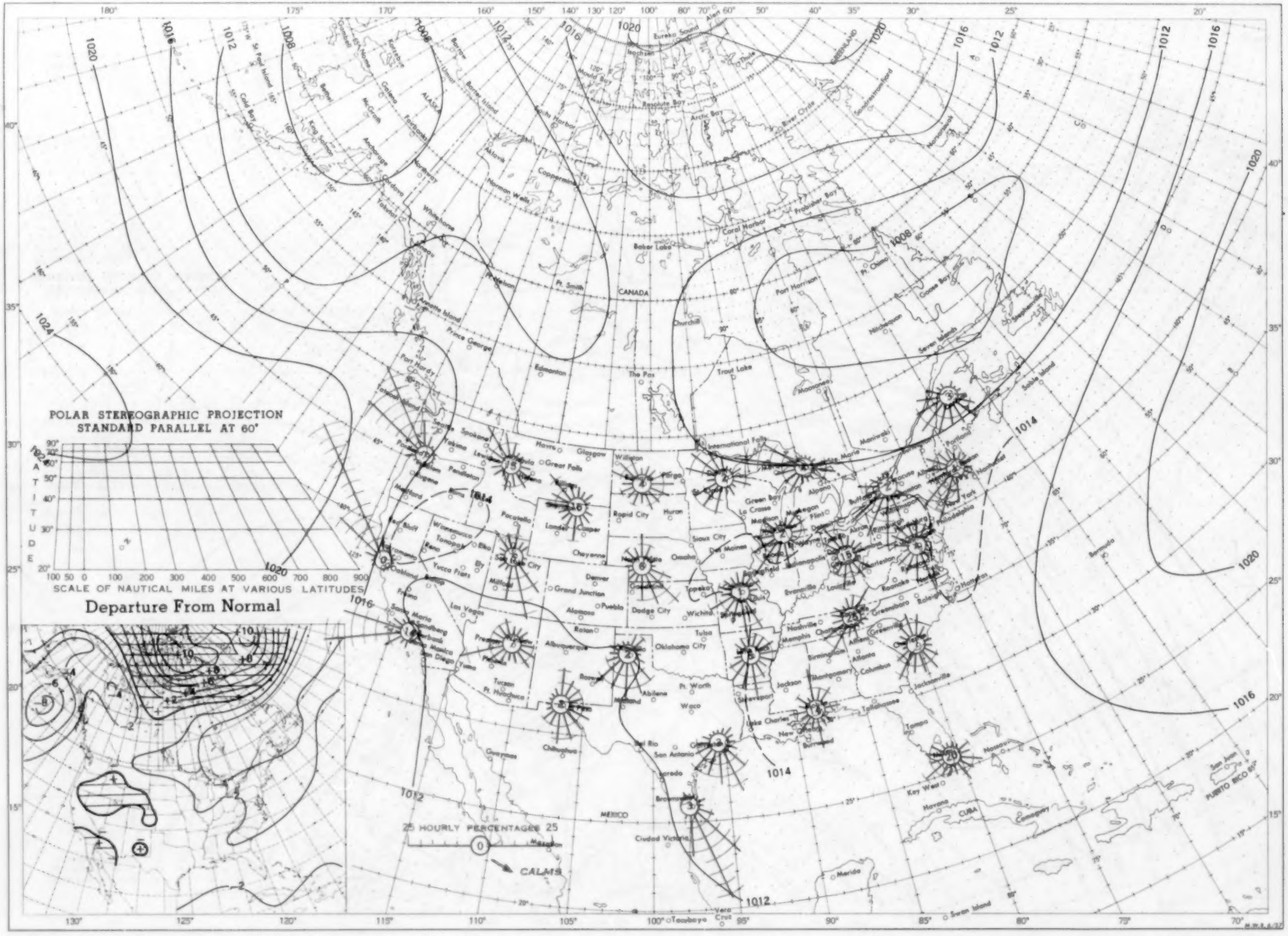

AUGUST 1958

Average sea level pressures are obtained from the averages of the 7:00 a.m. and 7:00 p.m. E.S.T. readings. Windroses show percentage of time wind blew from 16 compass points or was calm during the month. Pressure normals are computed for stations having at least 10 years of record and for 10° intersections in a diamond grid based on readings from the Historical Weather Maps (1899-1939) for the 20 years of most complete data coverage prior to 1940.

Chart XII. 850-mb. Surface, 1200 GMT, August 1958. Average Height and Temperature, and Resultant Winds.

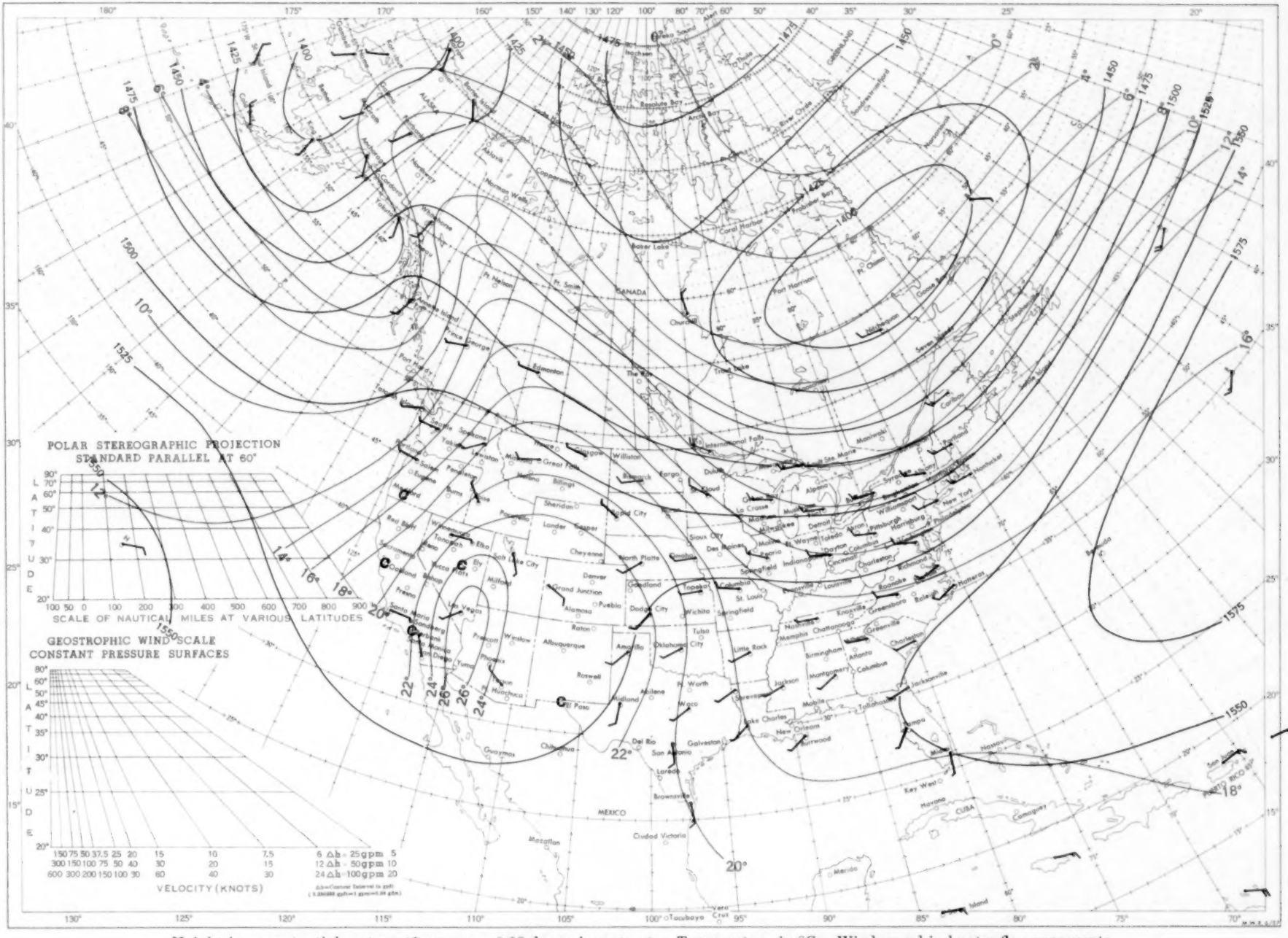

Height in geopotential meters (1 g.p.m. = 0.98 dynamic meters). Temperature in °C. Wind speed in knots; flag represents 50 knots, full feather 10 knots, and half feather 5 knots. All wind data are based on rawin observations.

Chart XIII. 700-mb. Surface, 1200 GMT, August 1958. Average Height and Temperature, and Resultant Winds.

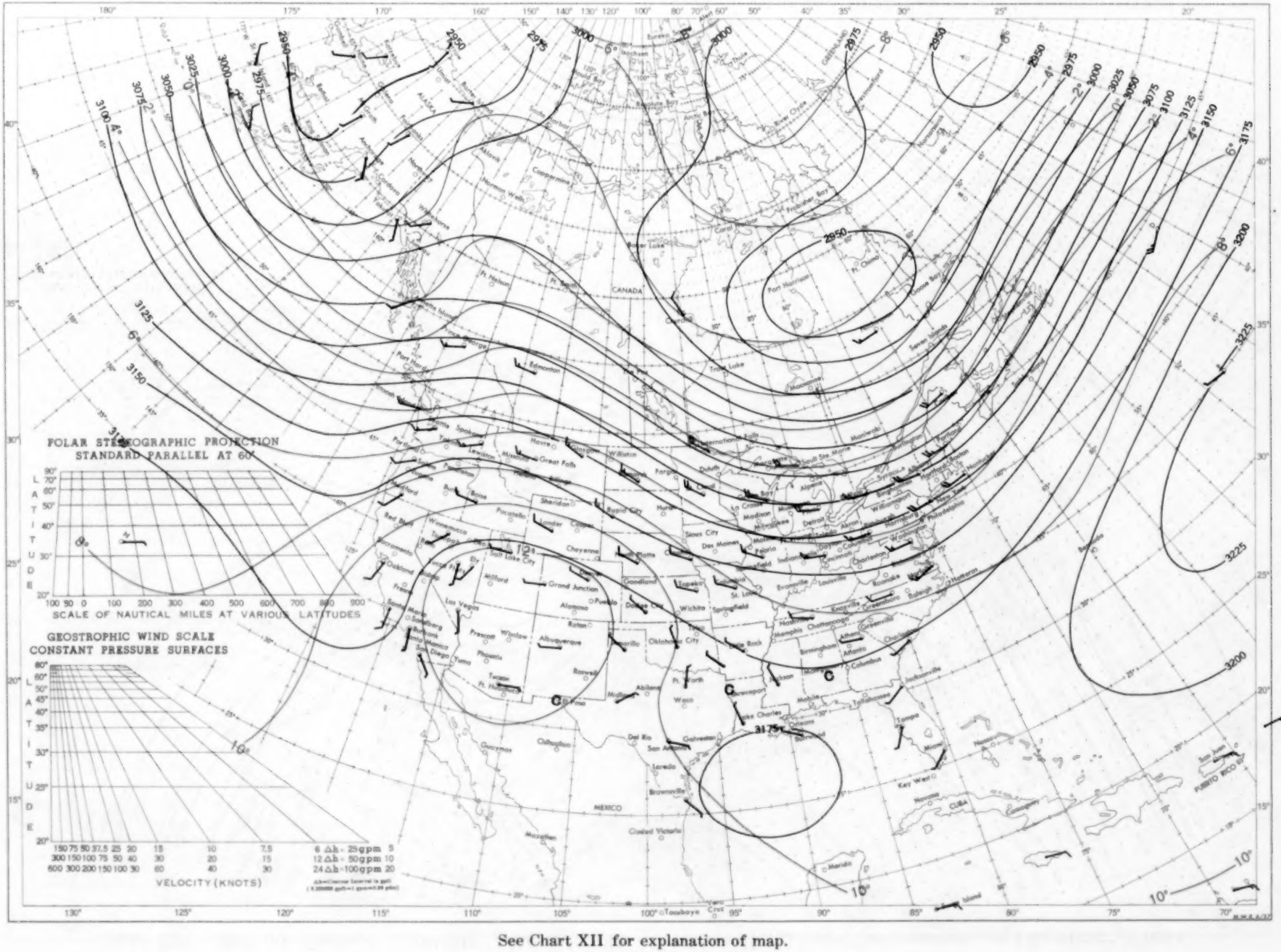

See Chart XII for explanation of map.

Chart XIV. 500-mb. Surface, 1200 GMT, August 1958. Average Height and Temperature, and Resultant Winds.

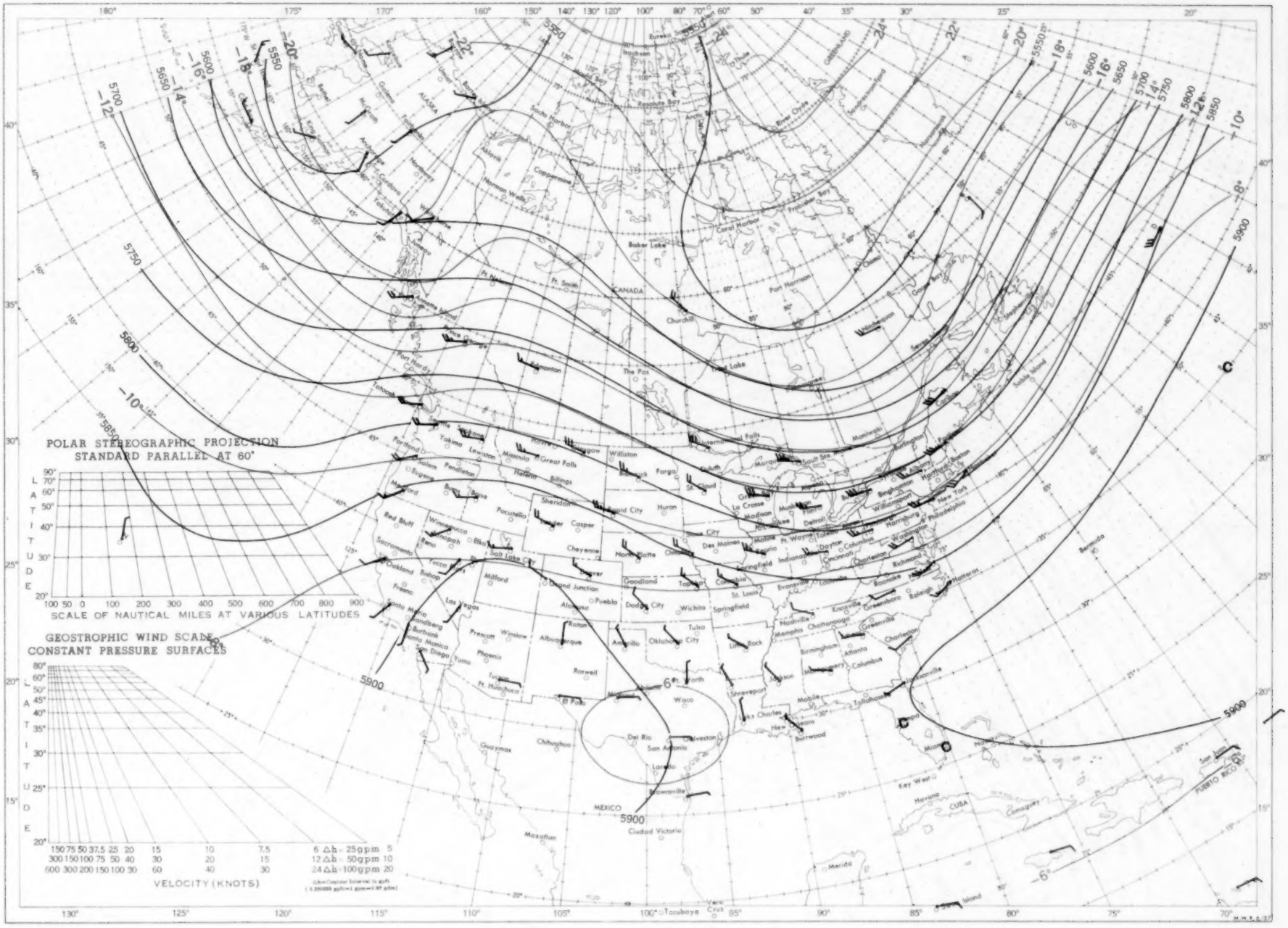

See Chart XII for explanation of map.

Chart XV. 300-mb. Surface, 1200 GMT, August 1958. Average Height and Temperature, and Resultant Winds.

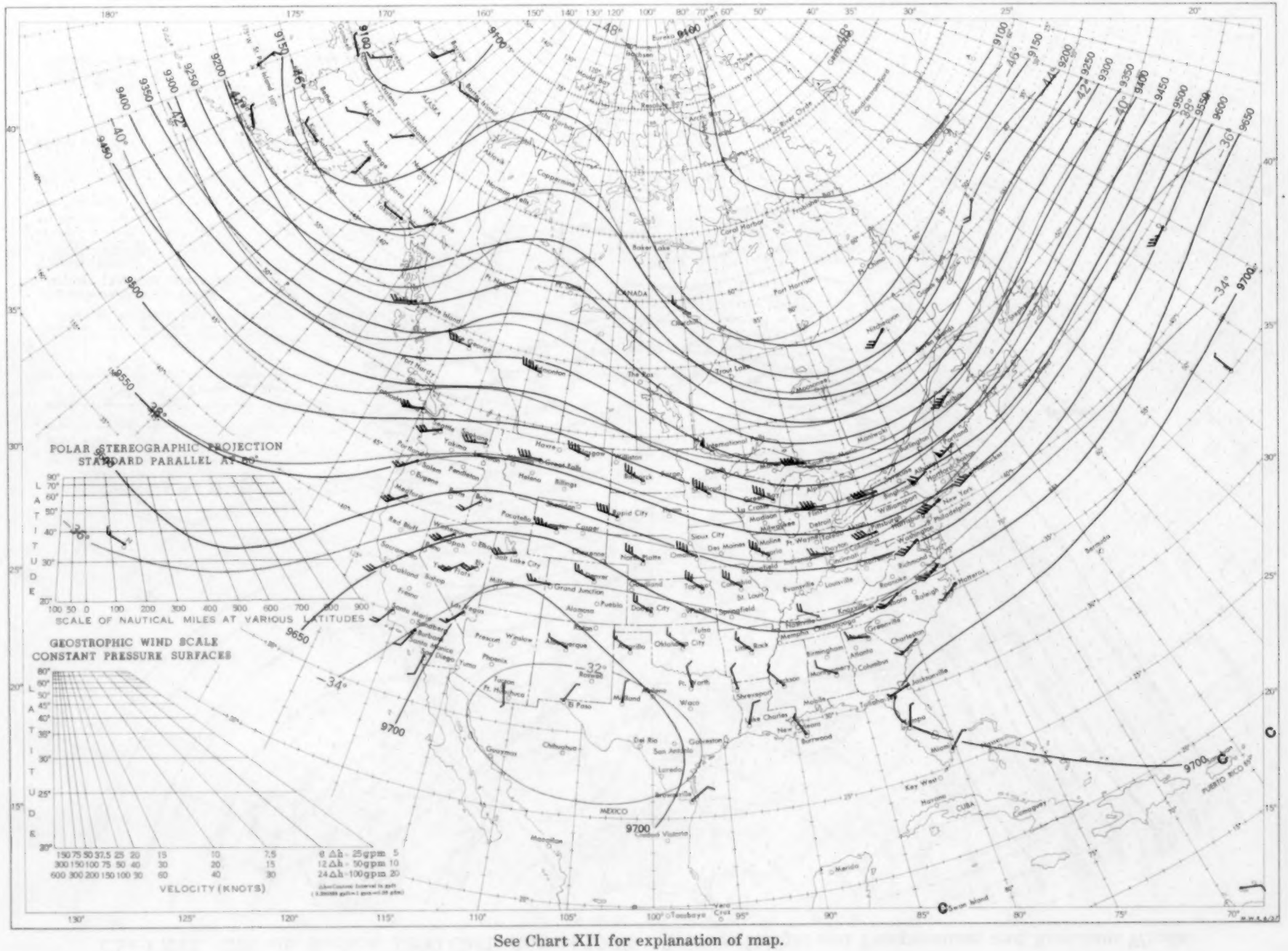

See Chart XII for explanation of map.

AUGUST 1958

Chart XVI. 200-mb. Surface, 1200 GMT, August 1958. Average Height and Temperature, and Resultant Winds.

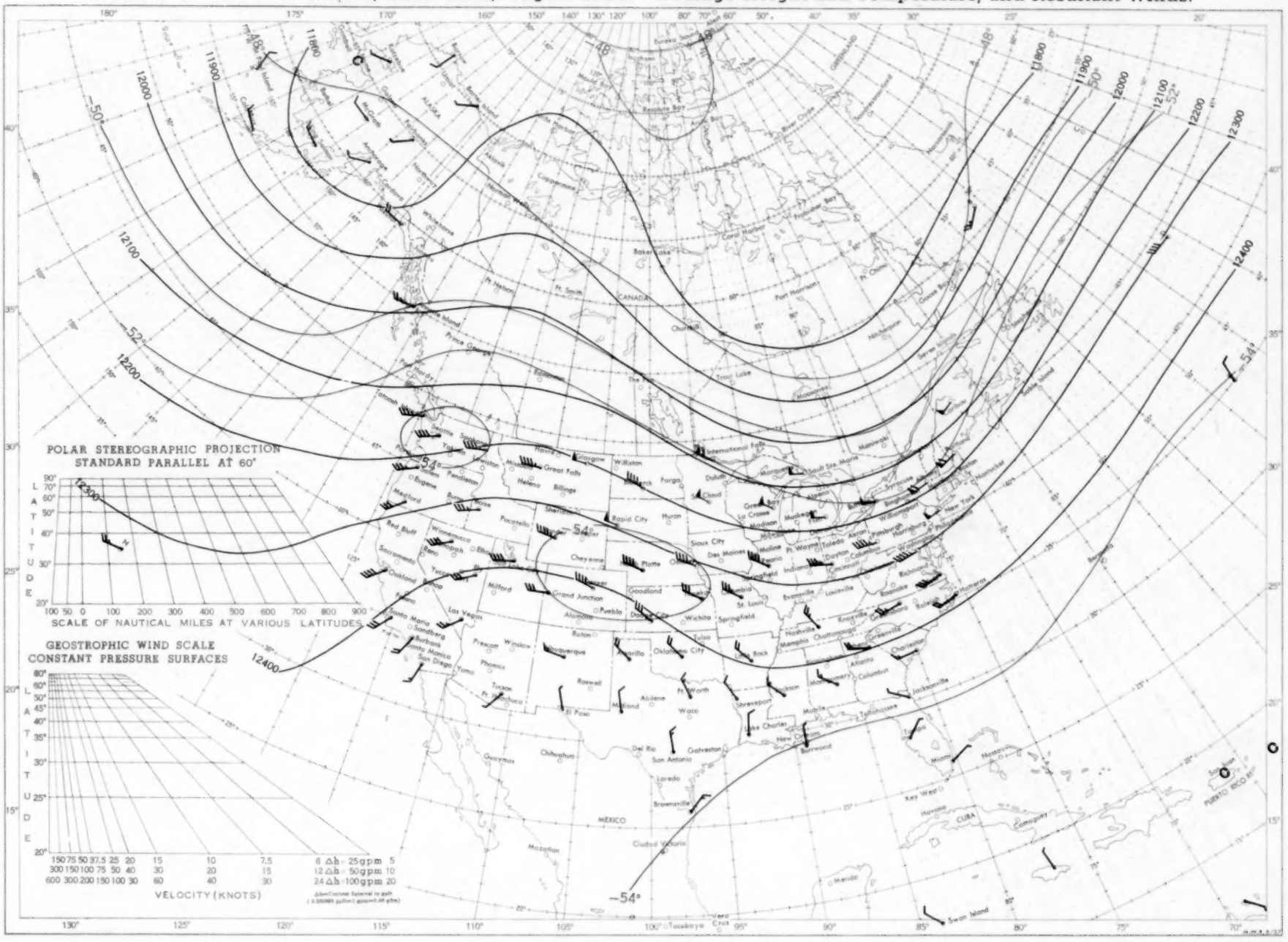

See Chart XII for explanation of map.

Chart XVII. 100-mb. Surface, 1200 GMT, August 1958. Average Height and Temperature, and Resultant Winds.

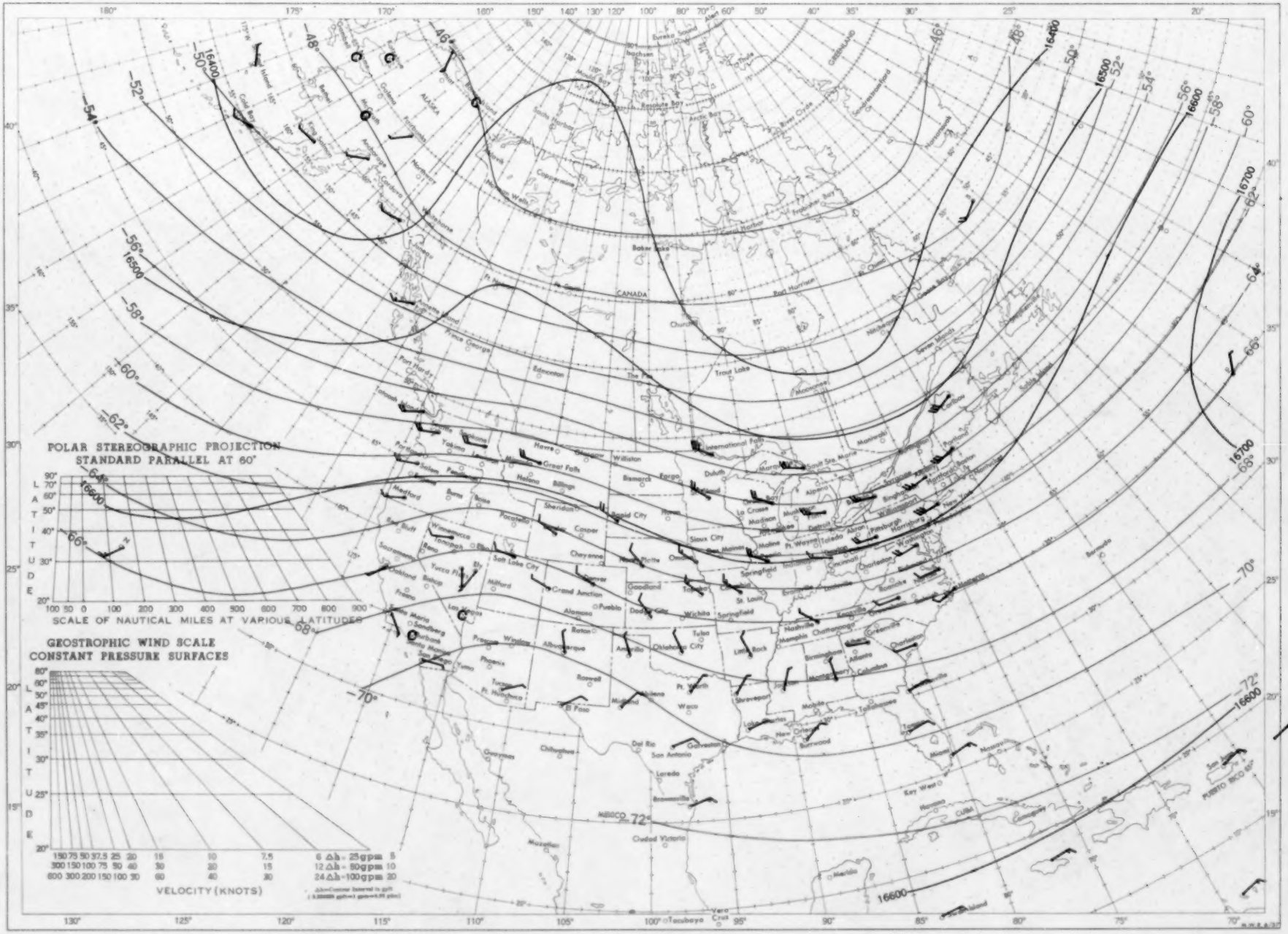

AUGUST 1958

See Chart XII for explanation of map.